General Disclaimer

One or more of the Following Statements may affect this Document

- This document has been reproduced from the best copy furnished by the organizational source. It is being released in the interest of making available as much information as possible.

- This document may contain data, which exceeds the sheet parameters. It was furnished in this condition by the organizational source and is the best copy available.

- This document may contain tone-on-tone or color graphs, charts and/or pictures, which have been reproduced in black and white.

- This document is paginated as submitted by the original source.

- Portions of this document are not fully legible due to the historical nature of some of the material. However, it is the best reproduction available from the original submission.

Issued: 7 February 1970

FINAL REPORT

AN ANALYSIS OF AIRBORNE MICROWAVE RADIOMETRIC DATA

Contract NAS 5-11685

Prepared by

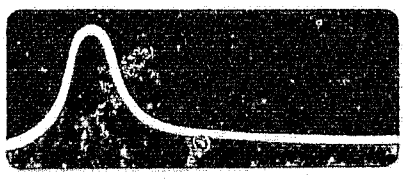

Radiometric Technology, INC.
179 FIFTH STREET o CAMBRIDGE, MASSACHUSETTS 02141

Prepared for

GODDARD SPACE FLIGHT CENTER
Greenbelt, Maryland

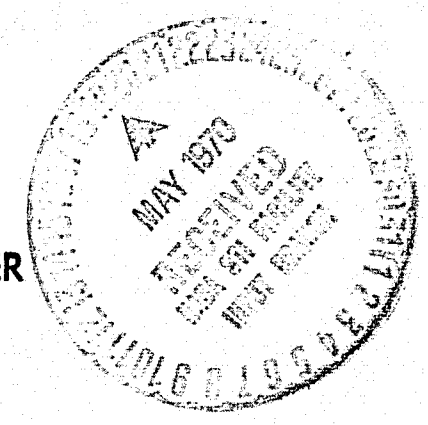

Final Report

AN ANALYSIS OF AIRBORNE MICROWAVE RADIOMETRIC DATA

7 February 1970

Contract NAS 5-11685

Goddard Space Flight Center

Contracting Officer: J.C. Comstock

Technical Monitor: A. Conaway

Prepared by

RADIOMETRIC TECHNOLOGY, INC.
179 - Fifth Street
Cambridge, Massachusetts 02141

Project Manager: Ronald A. Porter

for

GODDARD SPACE FLIGHT CENTER
Greenbelt, Maryland

ABSTRACT

Data from measurements taken in 1967, 1968, and 1969 over ocean and land areas by a 19.35 GHz phased-array scanner aboard the NASA Convair 990 are analyzed. Of particular interest are data which relate to the radiation emitted and affected by clouds. Other data from sensors measuring energy at IR wavelengths, temperature *in situ*, and, for the flights in 1969, energy at 9.3 GHz, are utilized to reconstruct atmospheric, surface and cloud characteristics. Theoretical brightness temperatures derived from cloud models, consistent with the physical data available, are in general agreement with the brightness temperatures observed over ocean areas. Although a somewhat limited effect is evidenced by clouds over dry bare soil and vegetation areas, a reasonably pronounced effect appears possible over moist soils. Analysis of those cases in which computed brightness temperatures do not match the observed brightness temperatures indicates either: (1) the existence of cloud droplets larger than can be treated successfully by the simple Rayleigh theory utilized; or (2) the incompleteness of the cloud models themselves. A simplified technique for converting brightness temperature to liquid water content in the clouds is presented and examples given.

ACKNOWLEDGEMENTS

The cooperation and assistance of the following individuals, who made valuable contributions to this study, is gratefully acknowledged:

Dr. N.E. Gaut and Dr. E.C. Reifenstein,III (Environmental Research & Technology, Inc.)	- for performing an important portion of the study, dealing with atmospheric properties.
Mr. D.K. Agrawal	- for analysis of surface characteristics and certain atmospheric effects.
Dr. A. Conaway (NASA-GSFC)	- for assistance with selection of raw data and for valuable briefings during the project.
Mr. A. Holland (NASA-ERC)	- for information on properties of the atmosphere.

TABLE OF CONTENTS

TABLE OF CONTENTS (Continued)

ILLUSTRATIONS

ILLUSTRATIONS (Continued)

ILLUSTRATIONS (Continued)

LIST OF TABLES

I. INTRODUCTION

The purpose of this report is to analyze selected radiometric data, taken at a frequency of 19.35 GHz over ocean and land surfaces, by the NASA-Goddard Convair 990 aircraft and to infer information about clouds from recorded data. Significant emission and absorption from the atmosphere at 19.35 GHz is produced by three constituents: water vapor, oxygen, and clouds. The observation frequency is close enough to the lowest frequency rotational spectral line of water (22.235 GHz) for the observed brightness temperature to strongly depend upon the water vapor content of the atmosphere. Oxygen absorption at this frequency is normally more steady than absorption by water vapor and is usually less important. However, for dry, cloudless atmospheres, oxygen is the dominant absorbing species.

Radiation passing through, and emitted by, clouds is more difficult to treat in its general form than is radiation affected by water vapor and oxygen. Scattering can be significant in clouds. When it is, the theoretical treatment of the radiation fields can be very complex. At 19.35 GHz, however, the radiation affected by most clouds can be treated satisfactorily by very simple approximations to the complete Mie scattering theory normally required in the general case. When the simpler approach is used, the identification of clouds which can be thus treated becomes an important problem.

In addition to atmospheric effects on the radiation fields, an important complication is introduced to measurements at 19.35 GHz, when the radiometer views the surface of the earth. Even over the chemically simple ocean surface, the angle of view, surface roughness and temperature of the water greatly complicate the specification of its contribution to the radiation field.

To accurately infer some characteristic of one of the contributors to the brightness temperature at 19.35 GHz, one must be able to satisfactorily estimate and compensate for the influence of all other contributors. To use measurements at 19.35 GHz for inferring the integrated condensed water in the antenna beam, for instance, one must remove the contributions of water vapor, oxygen, and the surface. To accomplish this satisfactorily, fairly complex modeling associated with other data, usually taken during the Convair 990 aircraft flights, is required.

This report concerns itself with modeling of the radiational environment in order to isolate the effects of clouds and, from these effects, infer some cloud parameter.

The organization of the report is straightforward: the airborne data utilized is reviewed; models of the environment used for calculations are presented; the results of calculations and their interpretation follow; some simple inversion schemes for integrated condensed water are outlined; various conclusions arrived at; and recommendations for future experiments are presented.

II. OBSERVED DATA PRESENTATION

A. DATA AVAILABLE FOR ANALYSIS

Data from flights made in 1967 (Gulf of Mexico), 1968 (Pacific Ocean west of California), 1968 (a Central California valley) and in 1969 (Atlantic Ocean west of Ireland) were available for analysis. Subsets of the data from each flight were chosen to illustrate several different and diverse characteristics of the measurements. Eight types of information were potentially available from the flights. They were:

1) 19.35 GHz brightness temperature
2) 9.3 GHz brightness temperature
3) 10-12 μ band temperature] -From MRIR
4) 6.3 μ temperature]
5) Aircraft altitude
6) Ambient air temperature
7) Photographs in the visual
8) Comments by aircraft occupants concerning cloud structure, surface conditions and unusual phenomena.

Useful data for the analysis carried out were mostly restricted to the information in categories (1), (3), (5), (6), (8) and sometimes (2).

B. DISCUSSION OF THE DATA CHOSEN FOR ANALYSIS

Of the 1967 flights, Flight 13 was singled out for analysis. The subset of data chosen for detailed study is given in Figures 1 and 2. The clouds of interest were cumulonimbus buildups over the Gulf of Mexico and represented moderate sized clouds of this type. Points of interest taken for further study are indicated by vertical arrows and identified as Case 1, Case 2, and Case 3 in Figure 1. In Figure 2, Case 4 is identified.

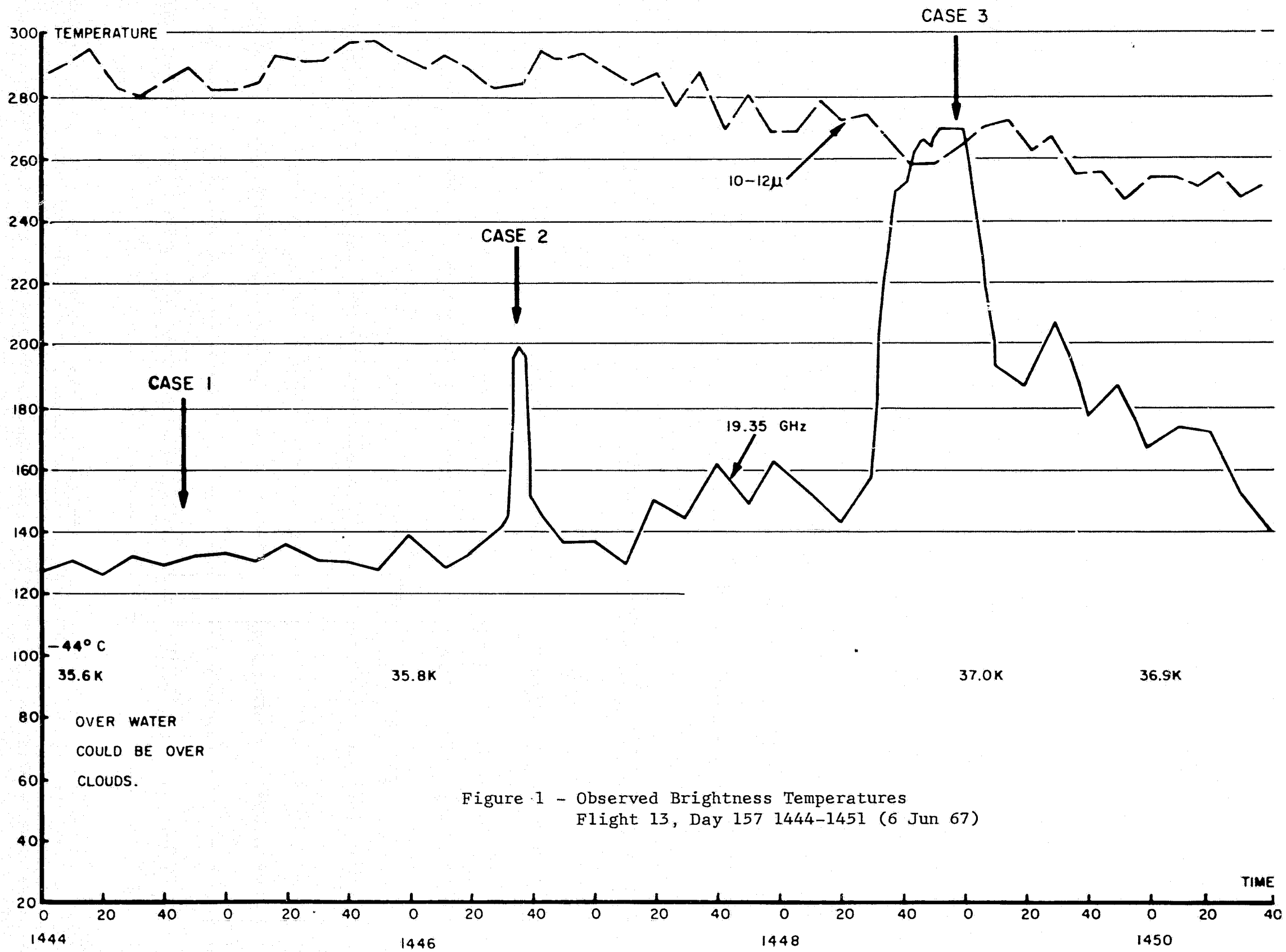

Figure 1 - Observed Brightness Temperatures
Flight 13, Day 157 1444-1451 (6 Jun 67)

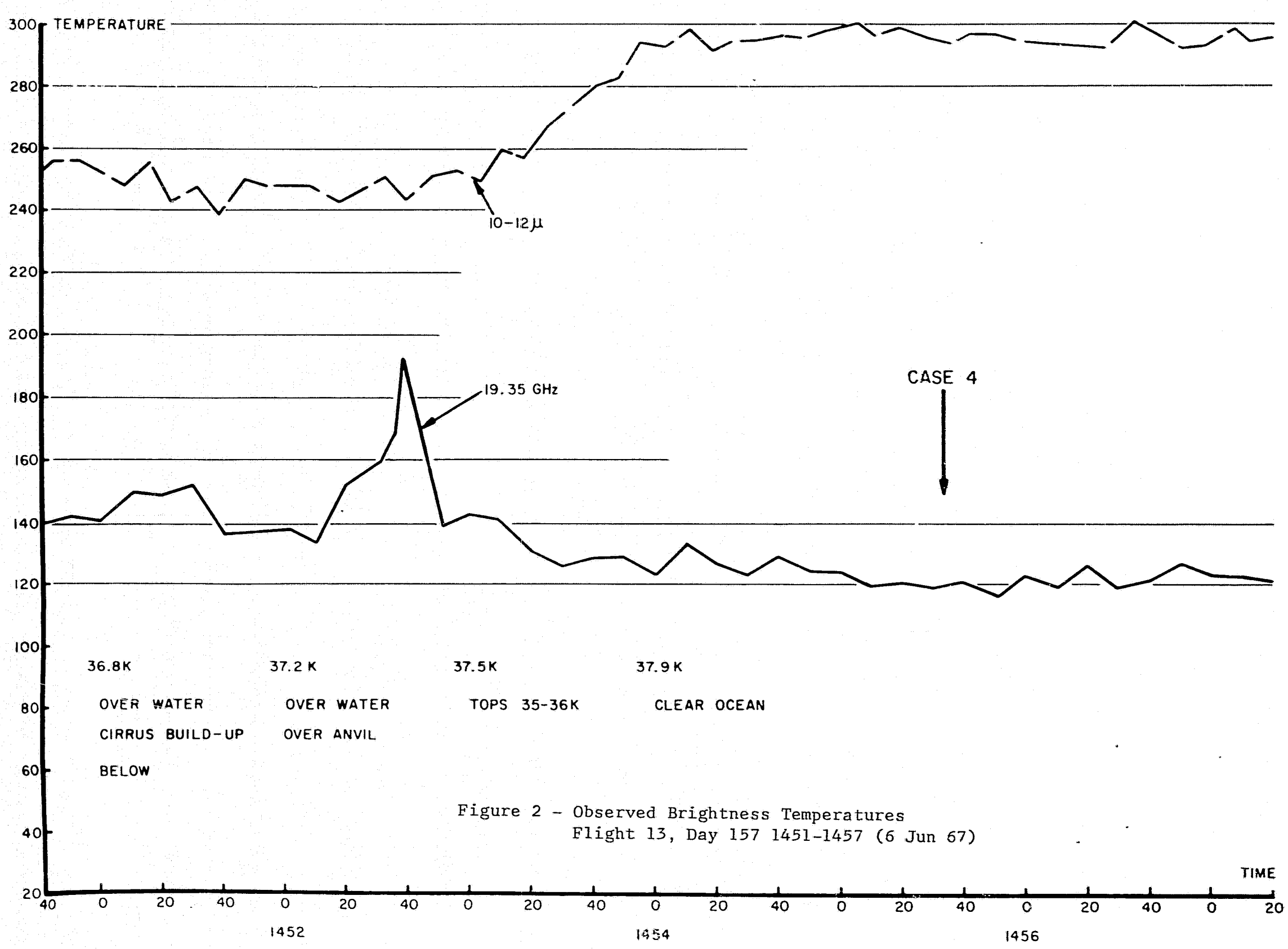

Figure 2 - Observed Brightness Temperatures
Flight 13, Day 157 1451-1457 (6 Jun 67)

Case 1 (1444:50) was chosen because it represented stratocumulus conditions often found over oceanic regions. Case 2 (1446:36) must represent a tower rapidly building toward full maturity as a tropical cumulonimbus cell.

Case 3 (1449:00) apparently represents a fully developed, extensive, cumunonimbus cell probably close to maximum water density, maximum number of large water droplets, and maximum vertical penetration of condensed water. The 10-12 μ channel of the MRIR data shows that for Case 3, if it is assumed cloud top height is correlated with the temperature measured in this band, the maximum height of the cirrus appears at somewhat of a distance from the core of the cloud. This can be seen as a minimum IR temperature removed in time from the maximum microwave temperature. Visual observations indicated that intense rain was falling out of the mature cell and probably from the maturing cell of Case 2.

Case 4 was chosen to define the atmosphere clear of clouds. It is used for various calibration procedures with respect to surface temperature, surface relectivity, and clear air atmospheric water vapor.

In 1968, Flight 9 was chosen as affording interesting examples of clouds. The portions of the flight analyzed are illustrated in Figures 3, 4, and 5. Four cases were again chosen for detailed analysis. Cases 1 and 2 are both clear air examples and are presented because they indicate a dilemma of sorts. They represent segments of continuous records near the beginning of the flight and near the end of the flight. Conditions in each case showed a clear atmosphere over what appeared to be a fairly calm ocean. However, there is a marked difference between the average brightness temperatures observed. For the part of the flight going away from the coast, the observed temperature is nearly 20° lower than that observed as the airplane was returning to the San Francisco area. The two points are spatially separated by approximately 300 nautical miles, but the temperature difference holds over most of the outgoing and incoming parts of the flight. The contribution by 13,500 feet of clear atmosphere is considered to be negligible since this "layer" was above an altitude of 26,000 feet.

Cases 3 and 4 are taken from portions of Flight 9 in 1968 when the airplane

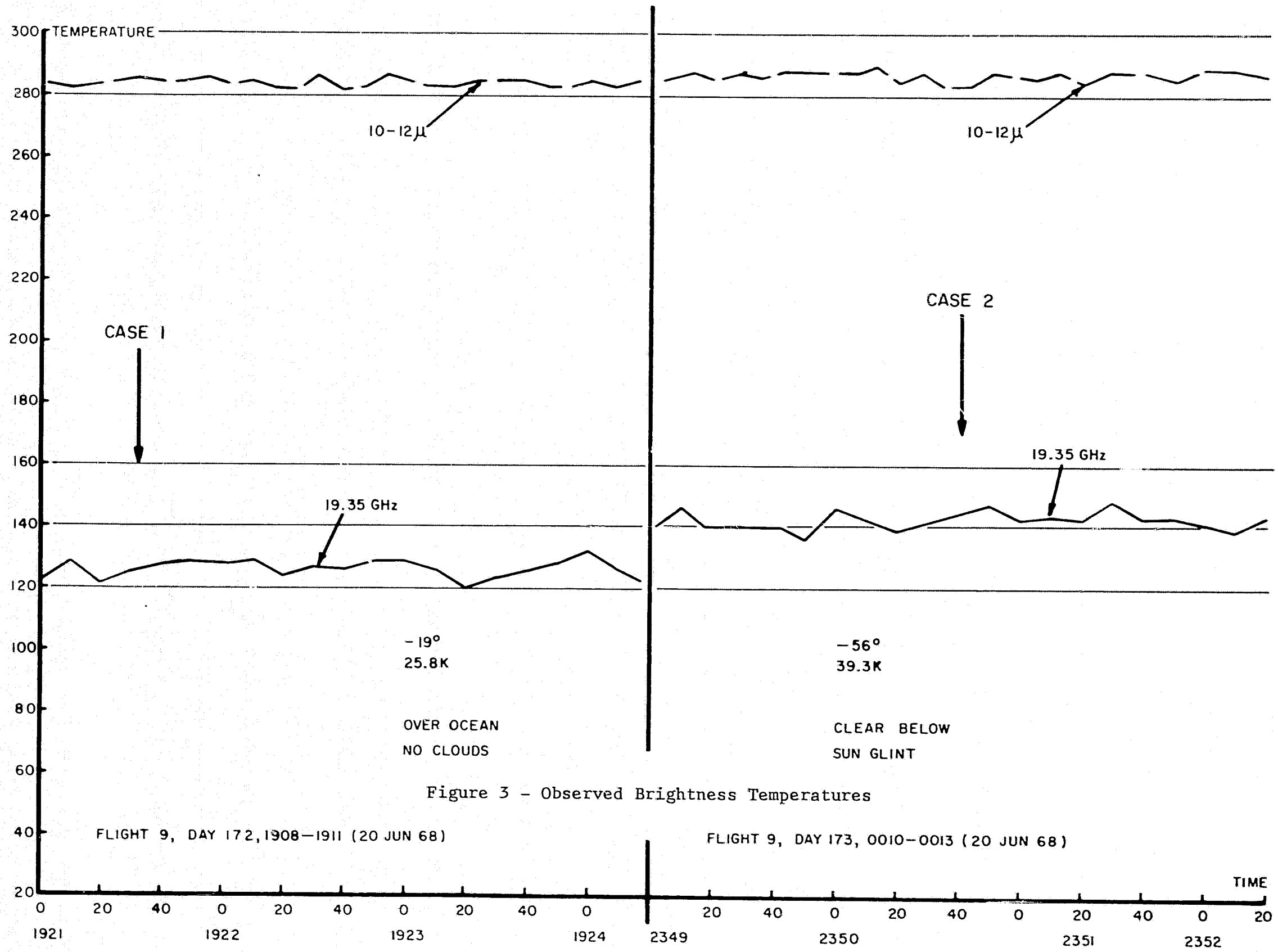

Figure 3 - Observed Brightness Temperatures

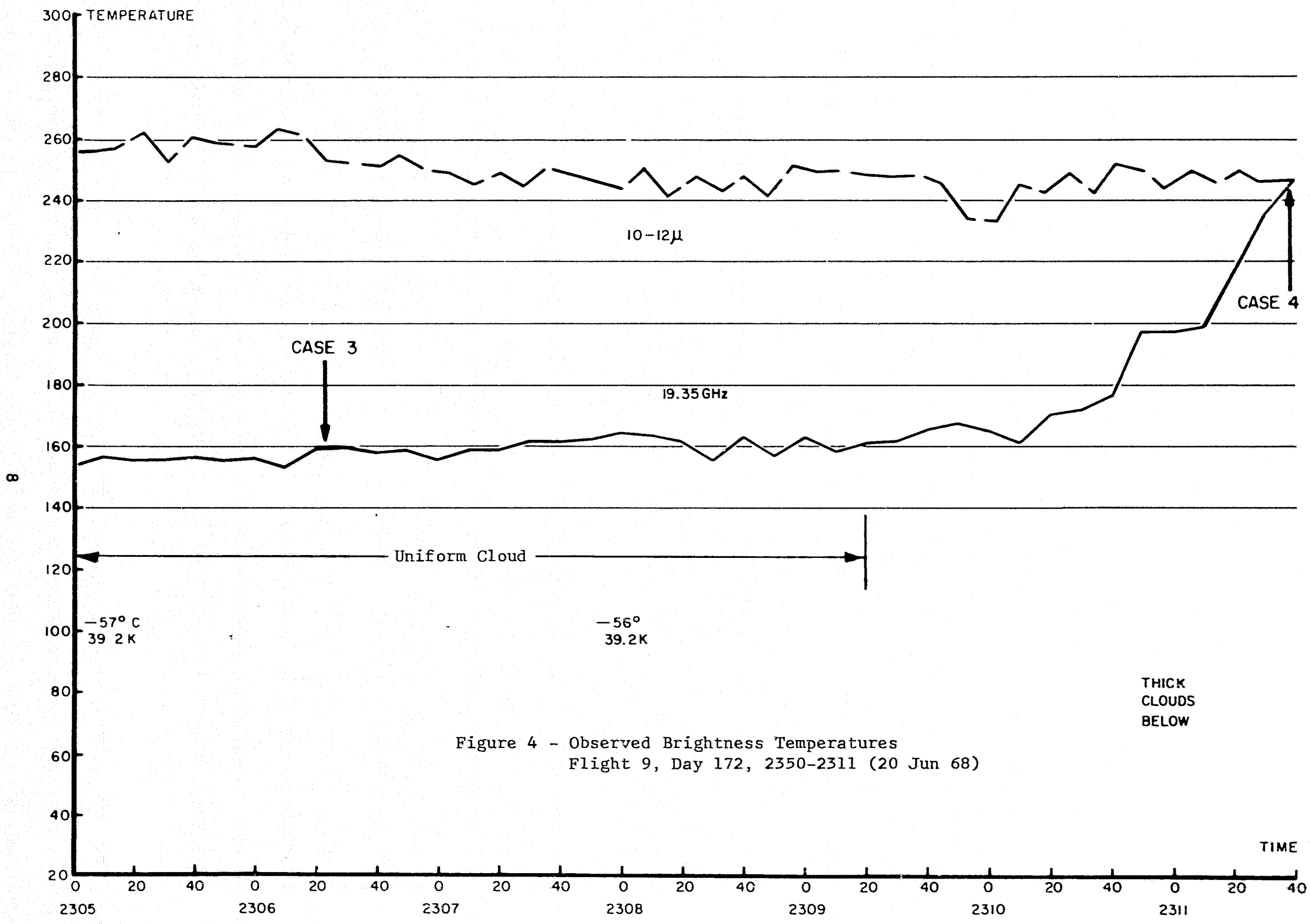

Figure 4 - Observed Brightness Temperatures
Flight 9, Day 172, 2350-2311 (20 Jun 68)

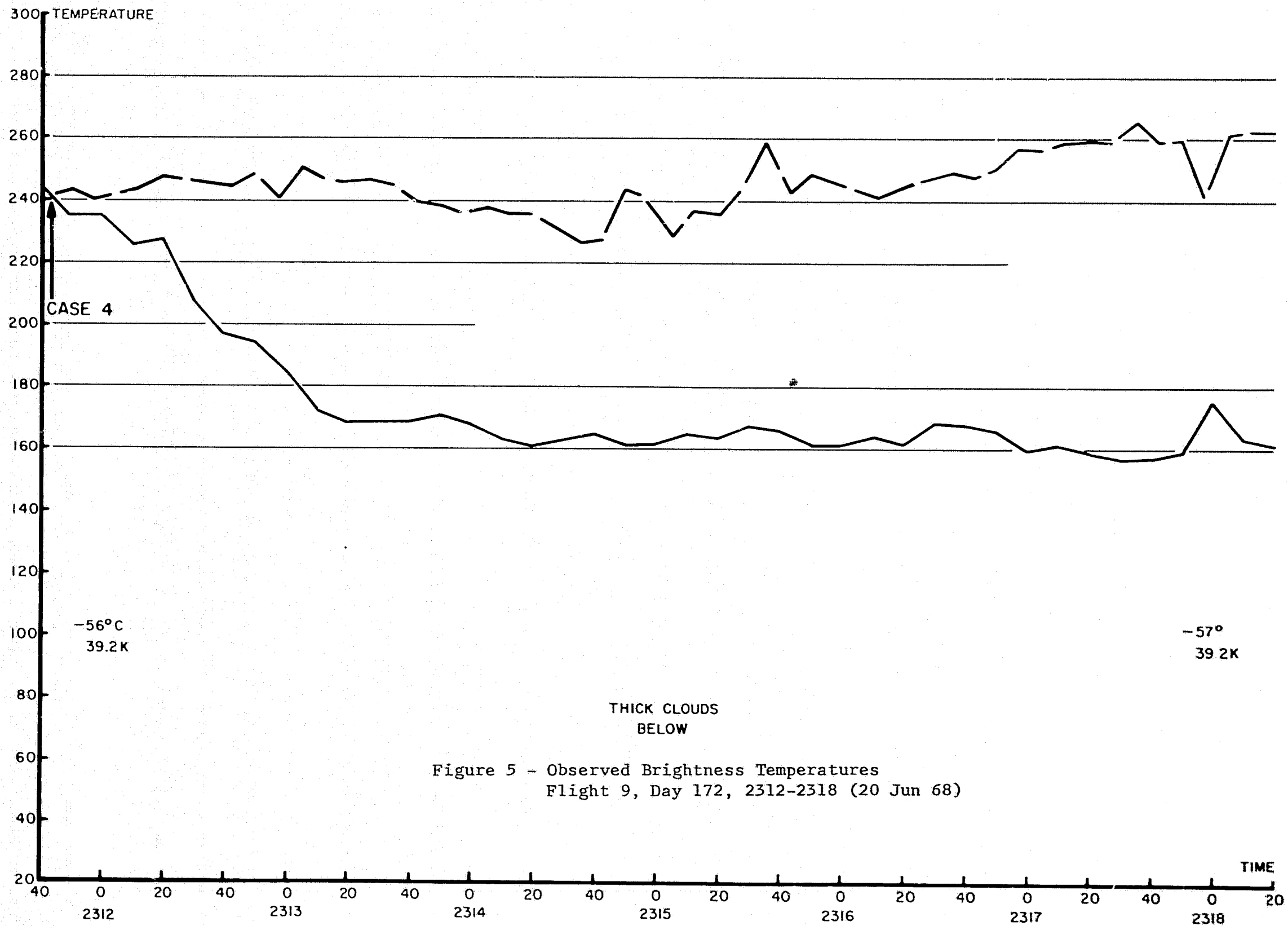

Figure 5 - Observed Brightness Temperatures
Flight 9, Day 172, 2312-2318 (20 Jun 68)

was over thick clouds for a considerable period of time. The data used for these two cases are taken from the information plotted on Figures 4 and 5. Case 3 is representative of uniform clouds; Case 4 is taken as an apparent embedded cell of considerable opacity. Case 4 appears on the edge of both Figures 4 and 5.

A segment of Flight 2, made in 1968, was chosen to indicate the effects of clouds over uniform land areas. This portion of the Flight covered the track shown in Figure 6 and included both bare desert areas and vegetation-covered soil. Figures 7, 8, and 9 show enlarged topographic views of portions of the flight track.

The last flight chosen for analysis was flown in 1969, and was the 8th of a series over the North Atlantic and Irish Sea. Figures 10 through 14 display subsets of the data taken on this flight which include four Cases studied in detail. Radiometer data, characteristic of land and sea, are included in this series.

Figure 10 represents a trace of the brightness temperatures as the airplane left Shannon, Ireland. The airplane passed over a river, clouds and rain, then over land for several minutes, then headed out over the open ocean. At the far right of Figure 10 the land-ocean boundary can be seen to represent a change of nearly 150°K in brightness temperature.

Figure 11 represents data taken at low altitude ($\approx$ 6 thousand feet) over a calm ocean surface. The mean 19.35 GHz brightness temperature was measured to be near 120°K and the recorded 10-12 μ temperature was near 275°K. 9.3 GHz data is also plotted in this Figure.

Figure 12 shows data taken while flying over some clouds and embedded cells: Case 2 is chosen at a point in time where both the 19.35 and 9.3 GHz temperatures show a maximum value.

Figure 13 is included only to show the effect of viewing off the nadir. For this polarization (electric field aligned along the axis of the airplane's fuselage) the emissivity of the ocean's surface decreases away from the nadir and therefore lower brightness temperatures are recorded.

Case 3 of Flight 8 is shown in Figure 14. It was chosen because it

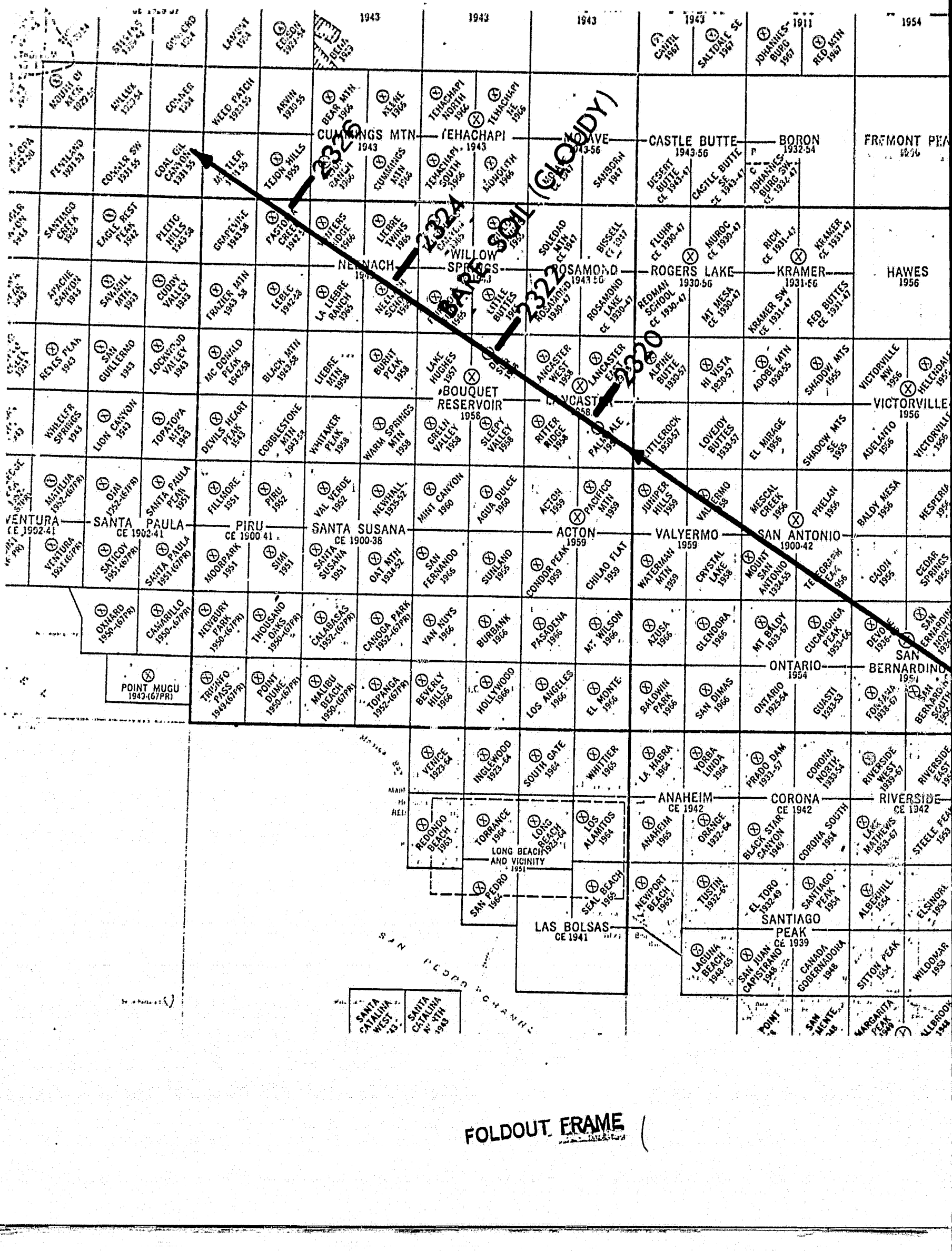

FOLDOUT FRAME

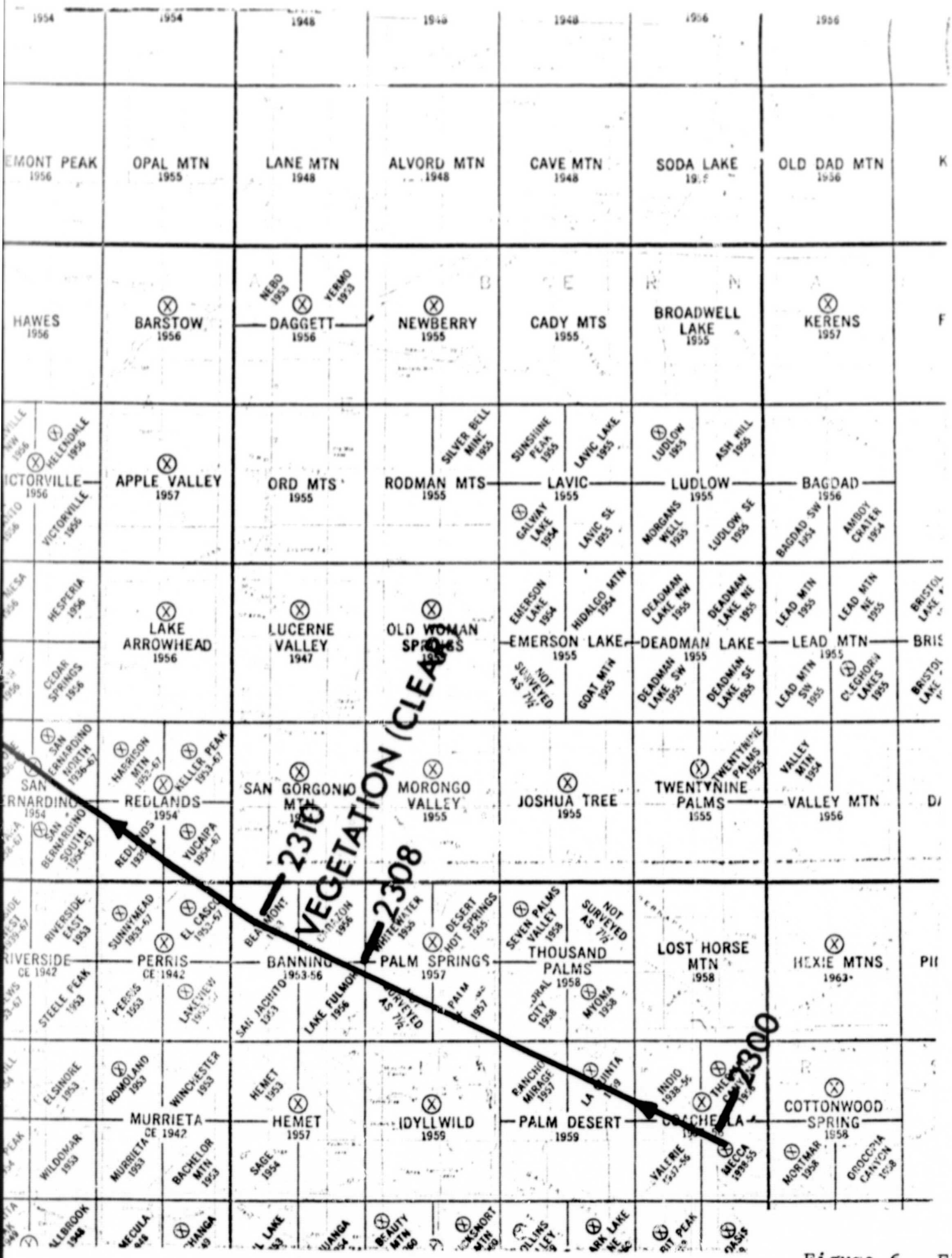

Figure 6 - Flight 2, 1968,
portion of Flight Track
Time: 2300 - 2327 hrs.

FOLDOUT FRAME 2

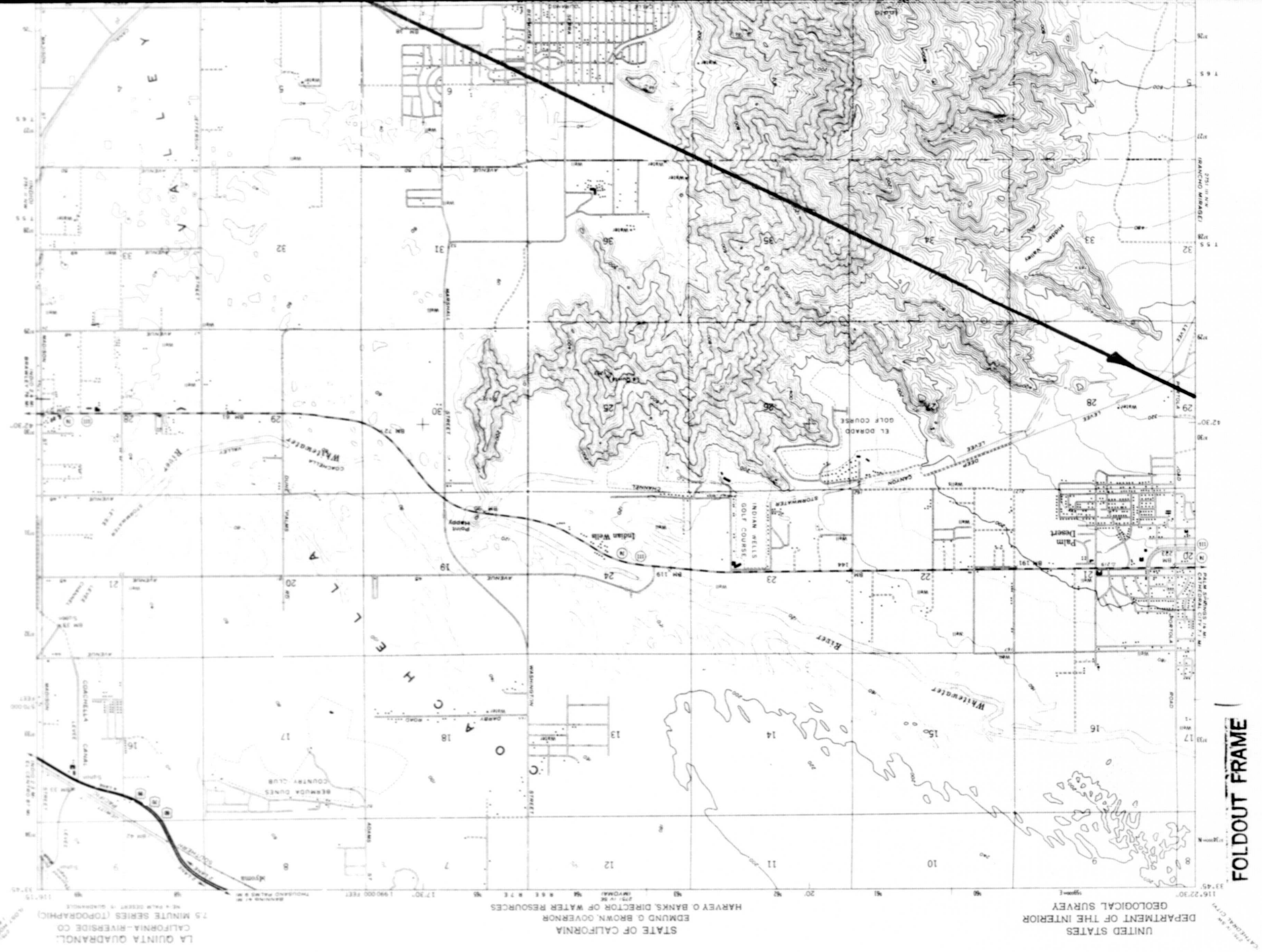
UNITED STATES
DEPARTMENT OF THE INTERIOR
GEOLOGICAL SURVEY
STATE OF CALIFORNIA
EDMUND G. BROWN, GOVERNOR
HARVEY O. BANKS, DIRECTOR OF WATER RESOURCES
LA QUINTA QUADRANGLE
CALIFORNIA-RIVERSIDE CO
7.5 MINUTE SERIES (TOPOGRAPHIC)
FOLDOUT FRAME

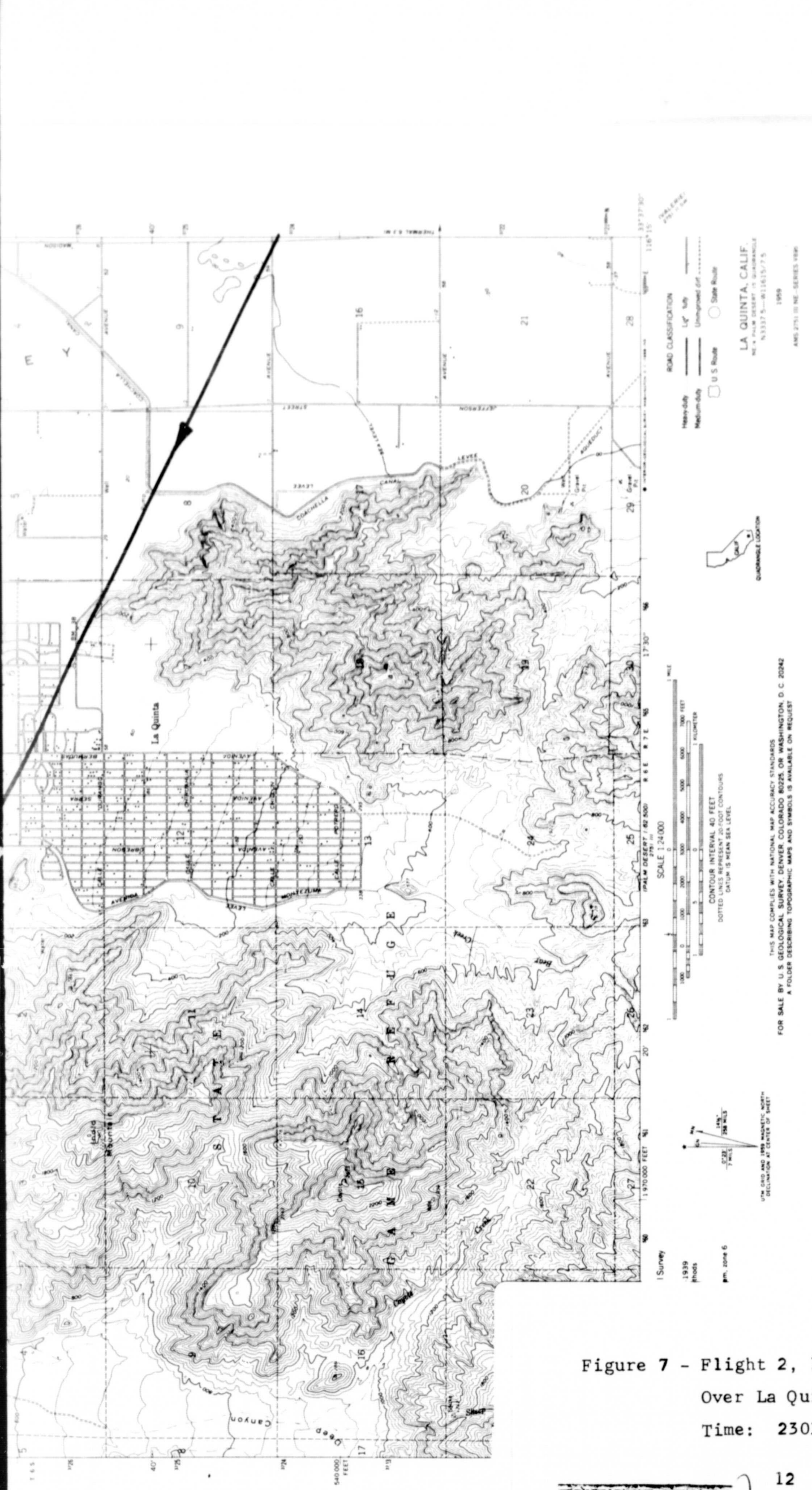

Figure 7 - Flight 2, 1968, Track
Over La Quinta, California
Time: 2303 hrs.

FOLDOUT FRAME 2

FOLDOUT FRAME

UNITED STATES
DEPARTMENT OF THE INTERIOR
GEOLOGICAL SURVEY

STATE OF CALIFORNIA
DEPARTMENT OF WATER RESOURCES

CABAZON QUADRANGLE
CALIFORNIA—RIVERSIDE CO
7.5 MINUTE SERIES (TOPOGRAPHIC)
NE ¼ BANNING 15' QUADRANGLE

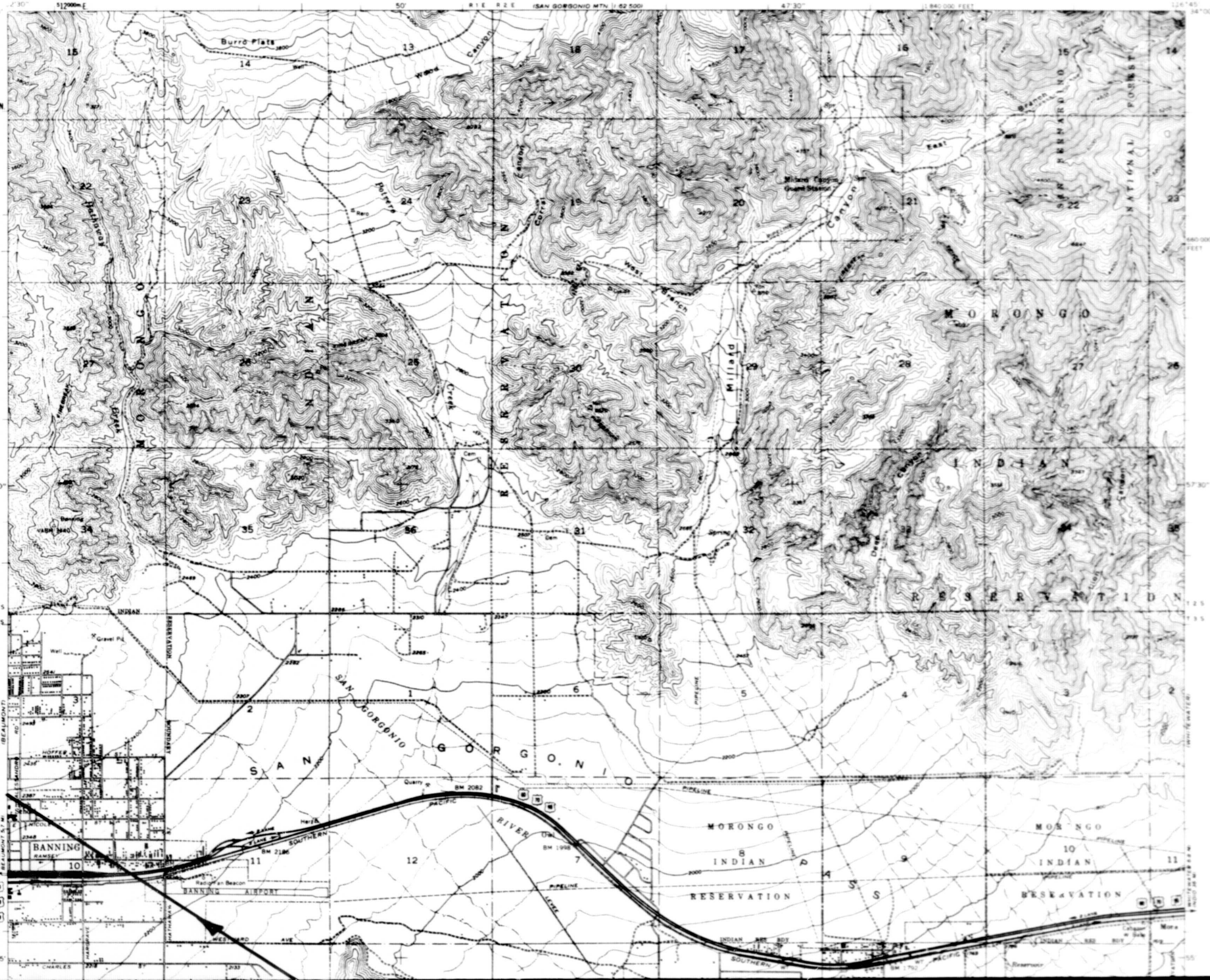

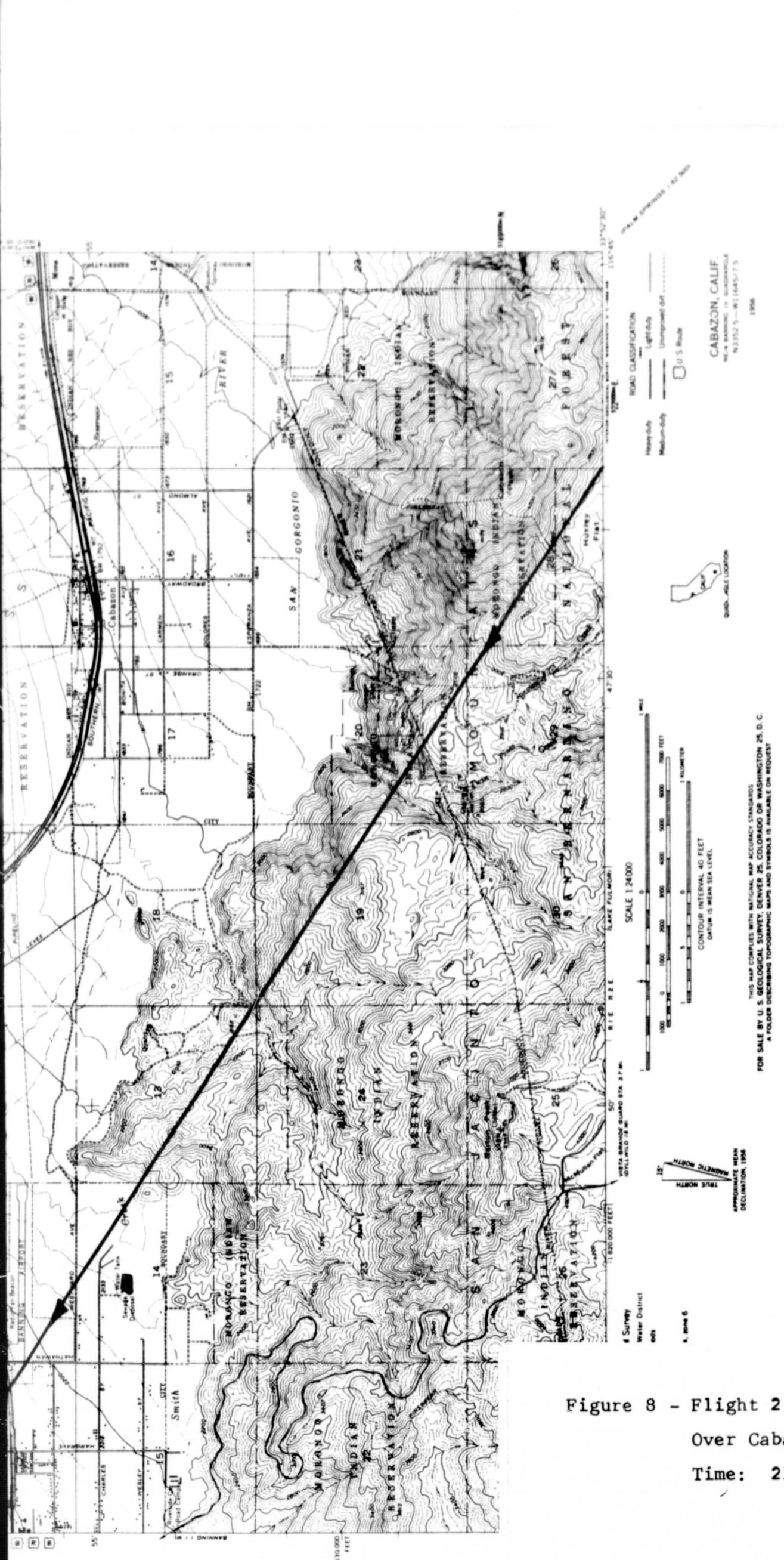

Figure 8 - Flight 2, 1968, Track
Over Cabazon, California
Time: 2309 hrs.

FOLDOUT FRAME 2

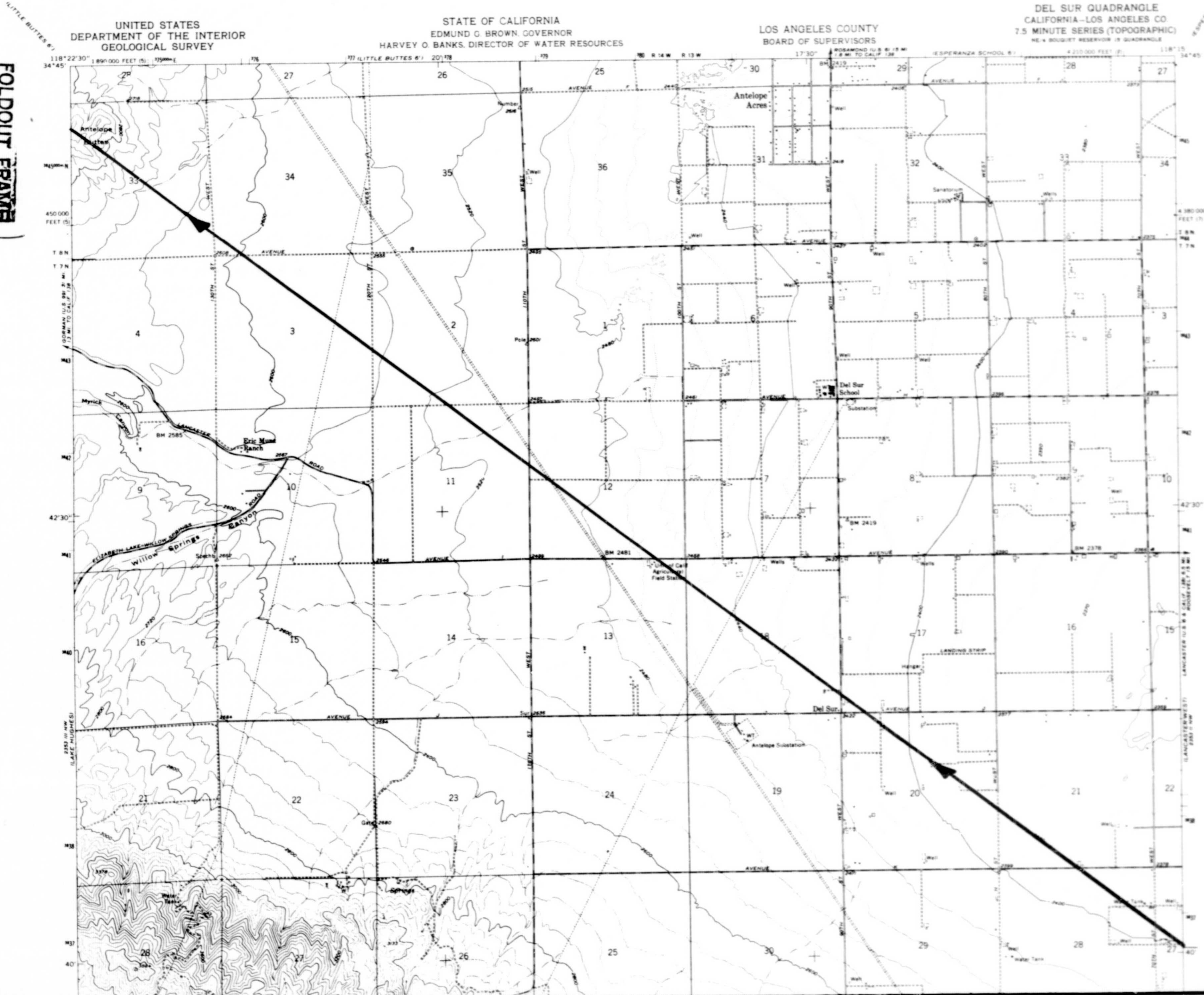

FOLDOUT FRAME

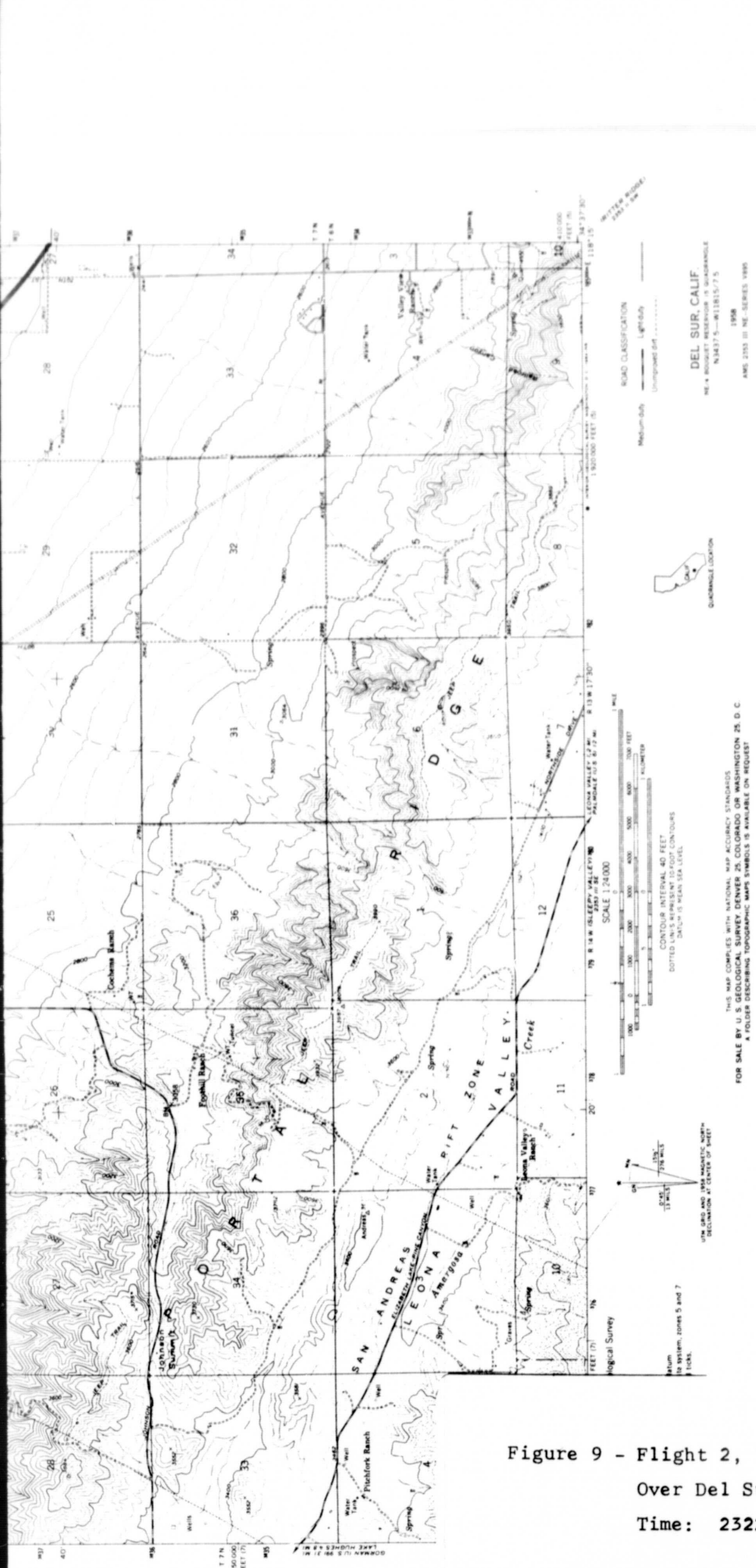

Figure 9 - Flight 2, 1968, Track
Over Del Sur, California
Time: 2322 hrs.

FOLDOUT FRAME 2

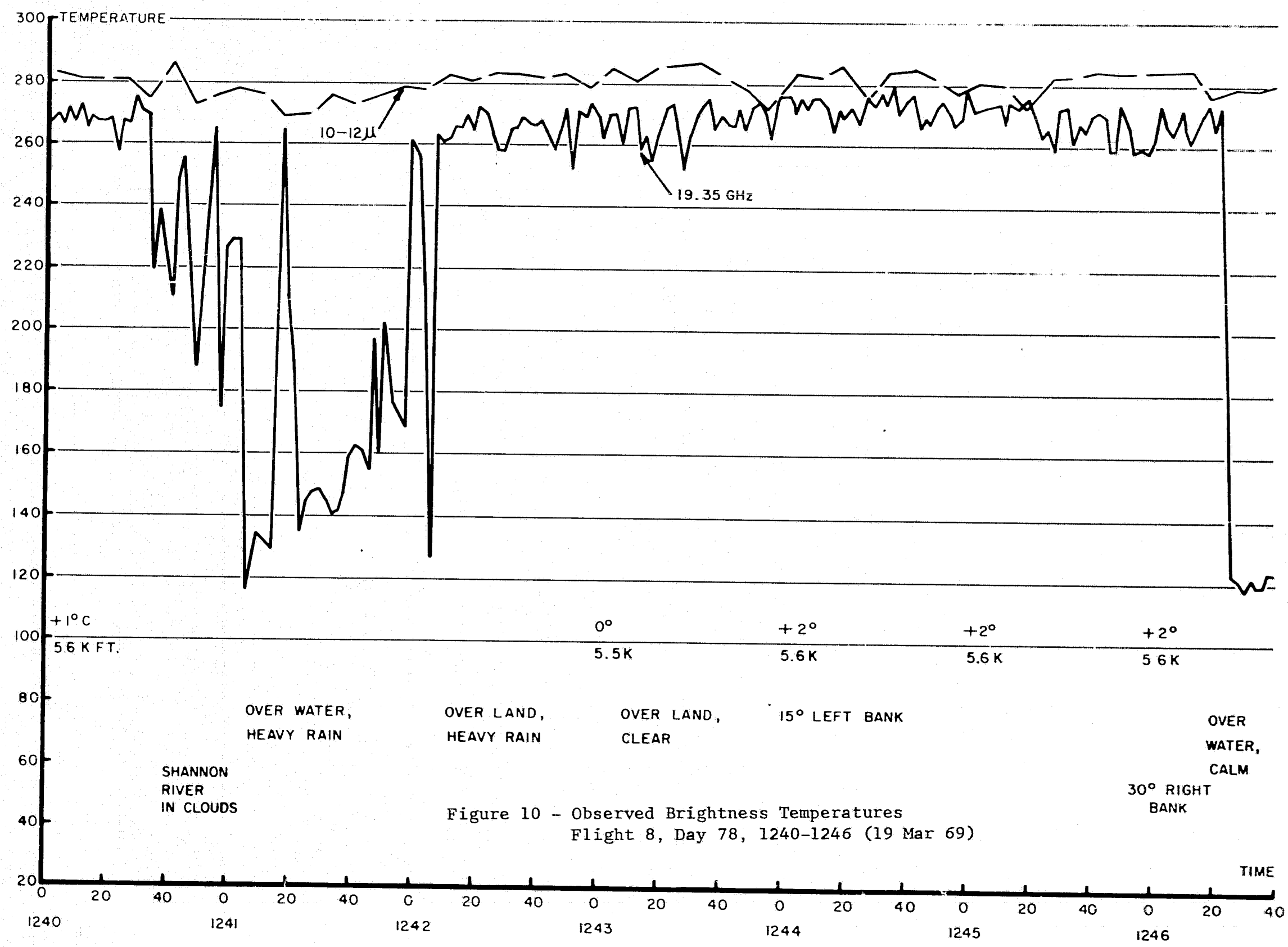

Figure 10 - Observed Brightness Temperatures
Flight 8, Day 78, 1240-1246 (19 Mar 69)

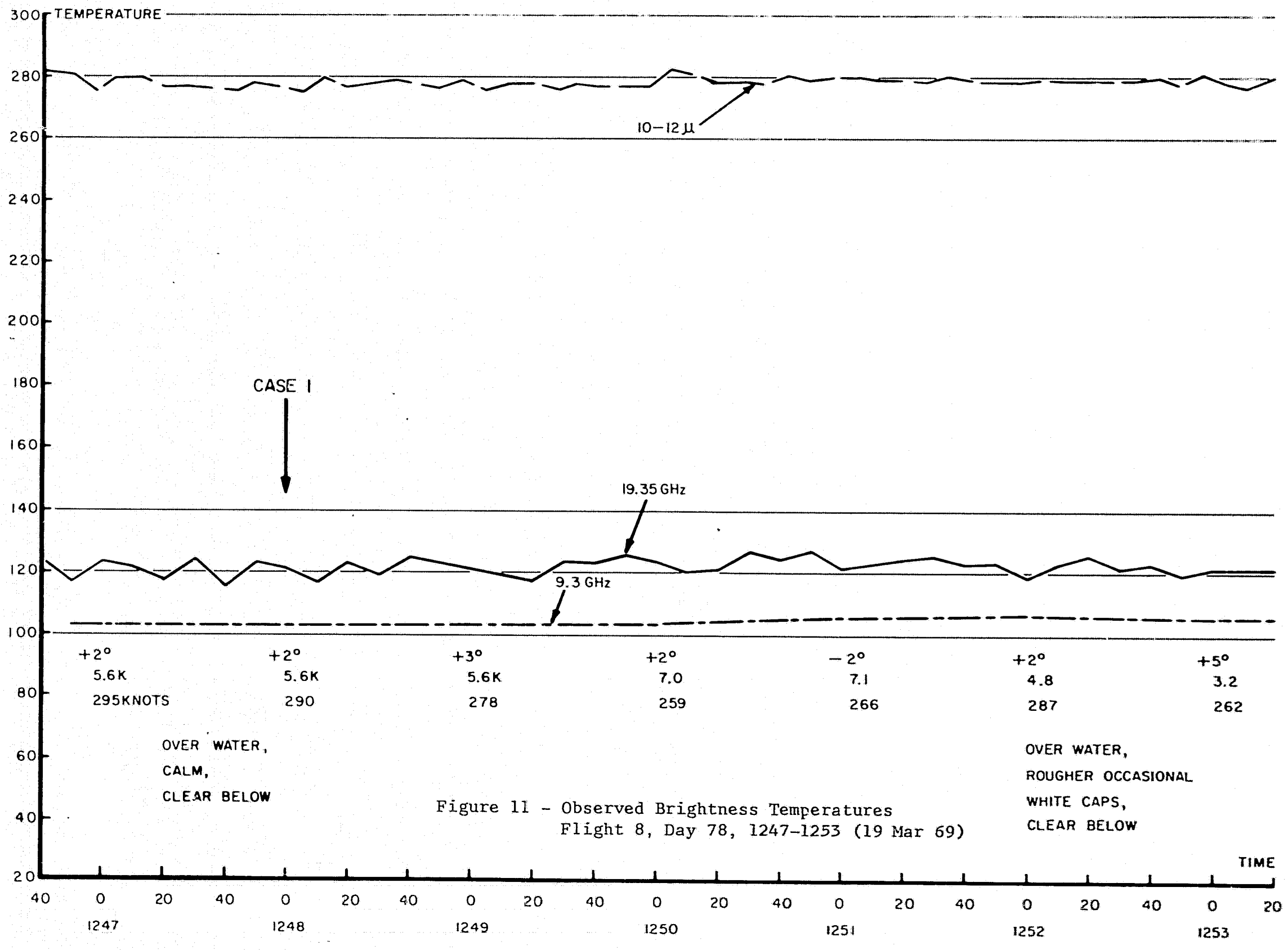

Figure 11 - Observed Brightness Temperatures
Flight 8, Day 78, 1247–1253 (19 Mar 69)

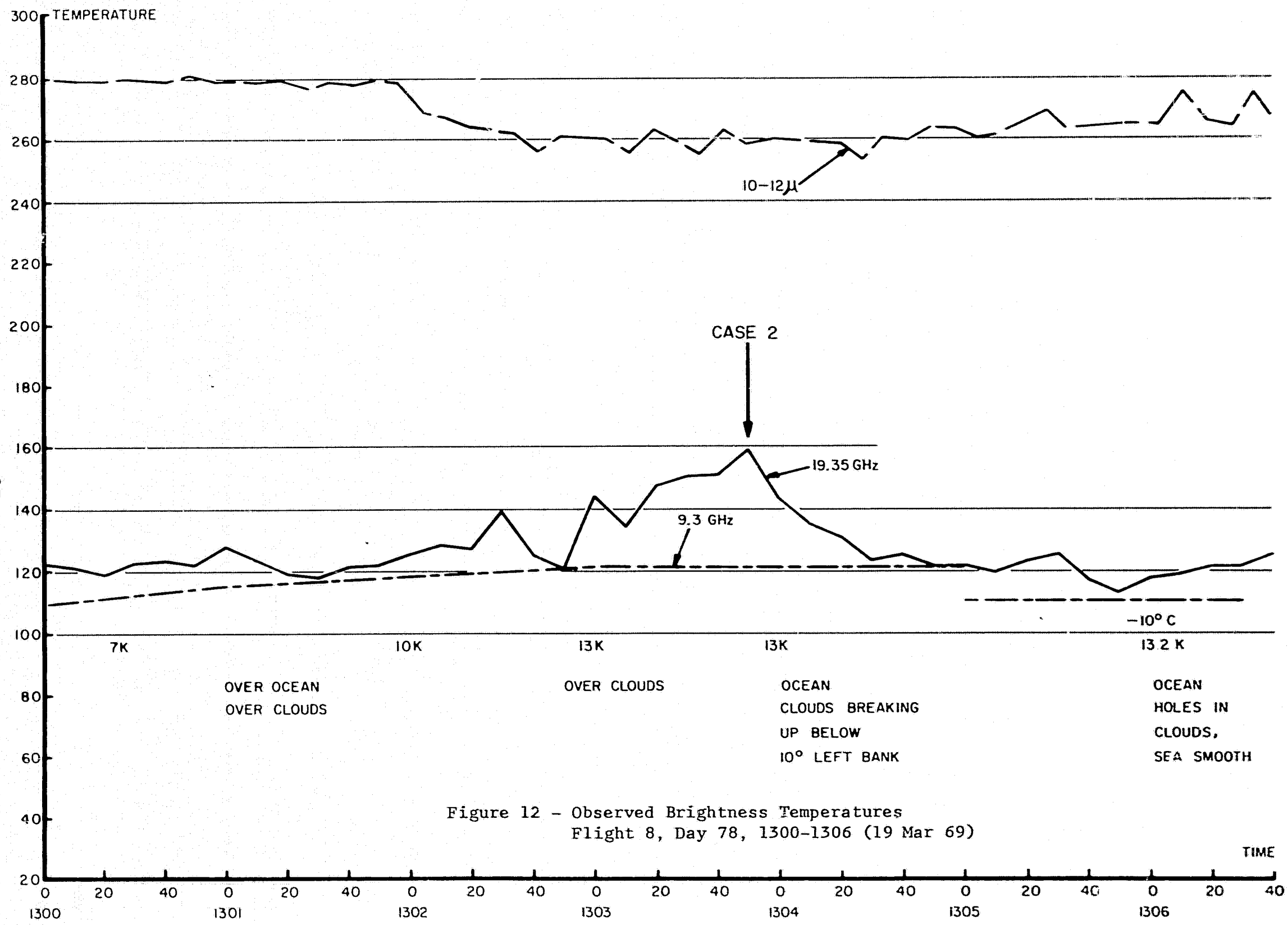

Figure 12 - Observed Brightness Temperatures
Flight 8, Day 78, 1300-1306 (19 Mar 69)

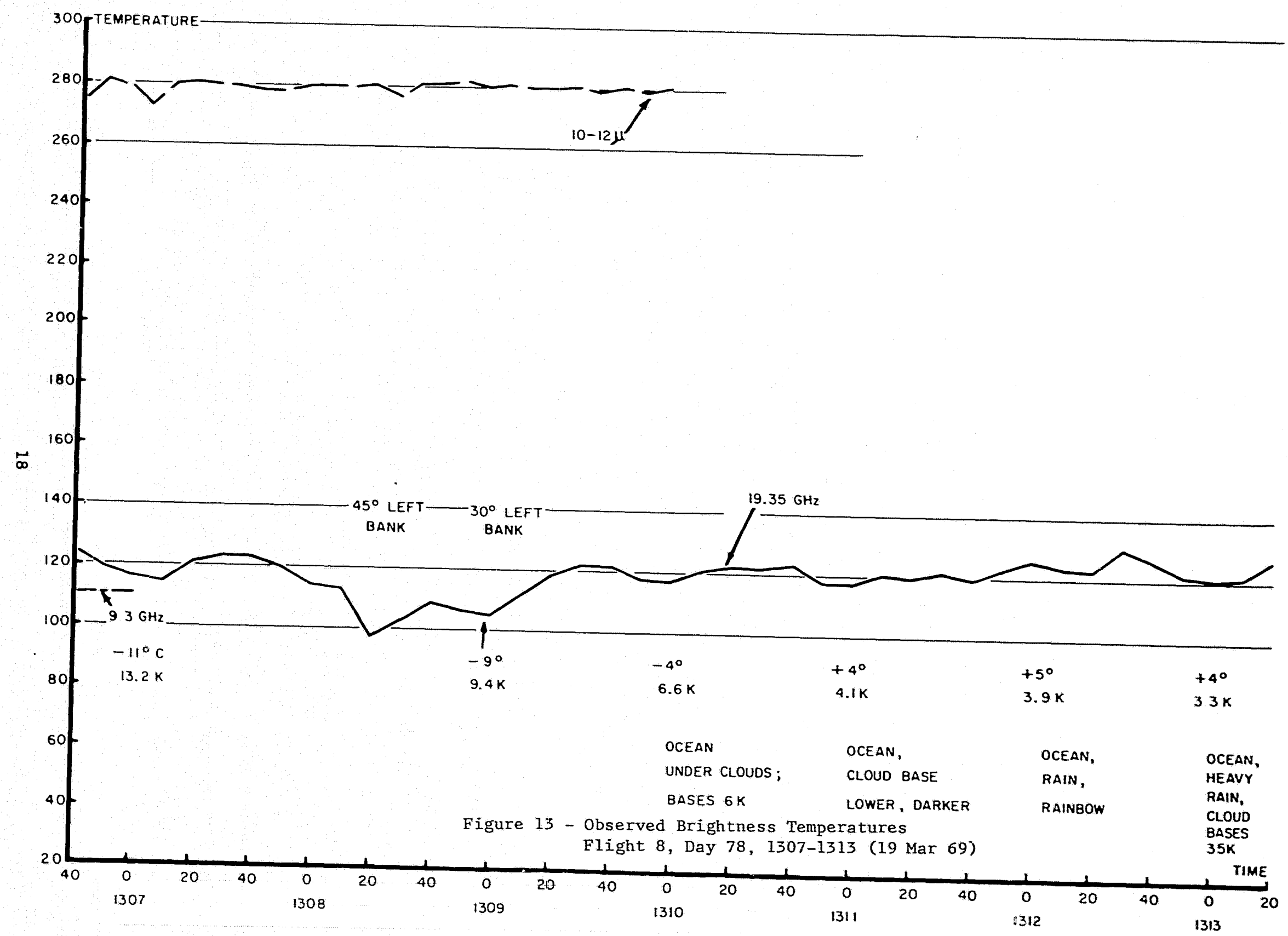

Figure 13 - Observed Brightness Temperatures
Flight 8, Day 78, 1307-1313 (19 Mar 69)

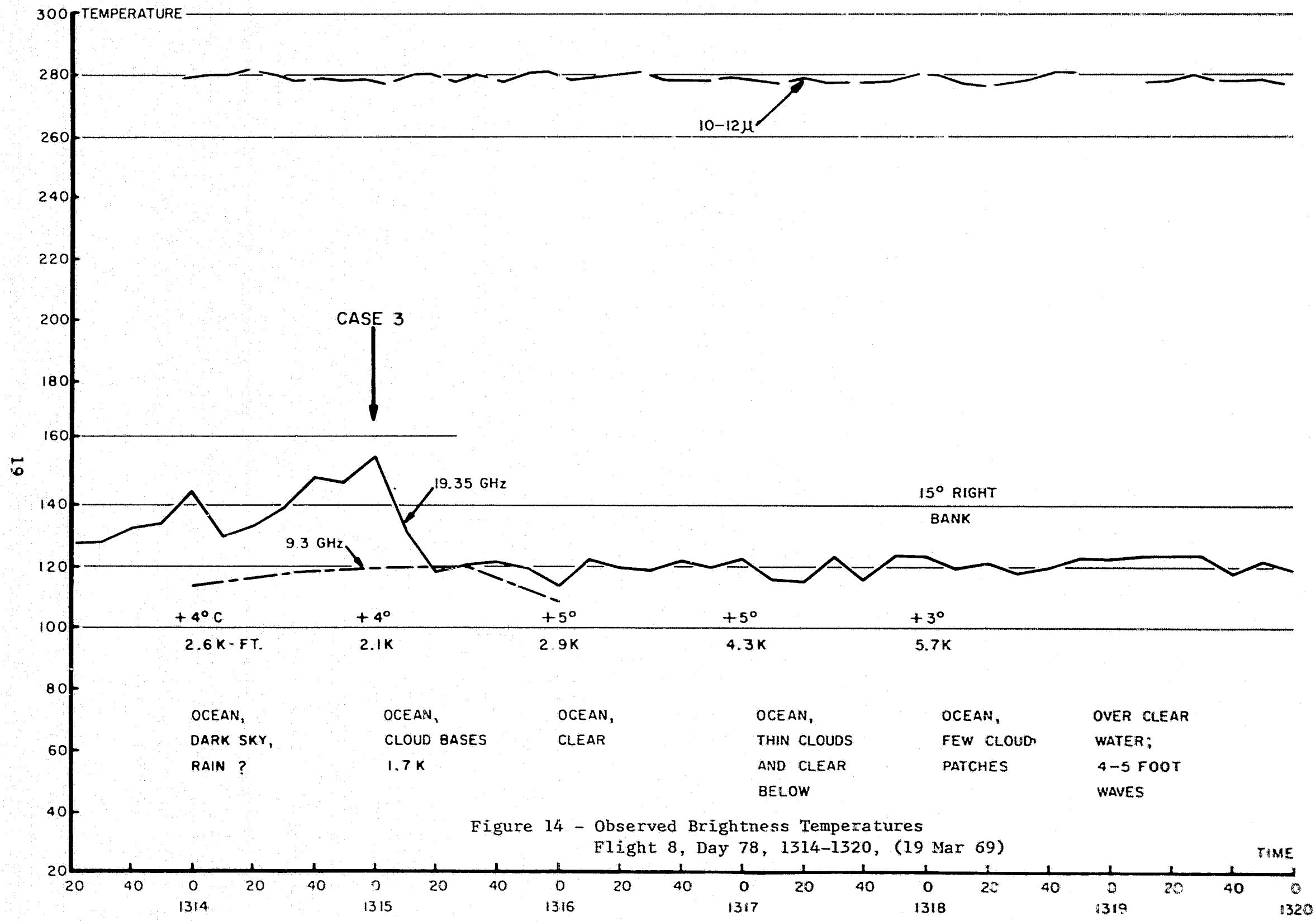

Figure 14 - Observed Brightness Temperatures
Flight 8, Day 78, 1314-1320, (19 Mar 69)

represents the same cloud of Case 2, except that the data was recorded while the airplane was flying below the cloud. It affords a unique opportunity to study the effects of reflected energy from below a moderately opaque cloud.

For convenience, the pertinent data represented by the eleven cases, studied in detail over oceanic regions, have been condensed and presented in tabular form in Table II-1. The Table also includes four Cases involving land areas overflown in a Central California valley.

TABLE II-1

CASES FOR DETAILED STUDY OF FOUR FLIGHTS

FLIGHT and CASE NO.	TIME	T_B(9.35)	T_B(19.35)	T_B(IR)	ALT(kft)	NOTE
FLIGHT 13	Gulf of Mexico (June, 1967)					
Case 1.	14:44:50		132	287	36	8000' tops
2.	14:46:36		200	283	37	Cell,5400' top
3.	14:49:00		269	262	37	T Cu, tops 22500'
4.	14:55:30		120	296	38	Clear
FLIGHT 9	Pacific Ocean (July, 1968)					
Case 1.	19:21:30		125	284	26	Clear
2.	23:50:40		145	286	39	Clear
3.	23:06:20		160	252	39	Tops 26,000' Over Clouds
4.	23:11:40		247	246	39	Tops 29,000' Over Clouds
FLIGHT 8	Atlantic Ocean west of Ireland (March, 1969)					
Case 1.	12:48:00	102	120	276	5.6	Clear
2.	13:03:50	122	159	259	13.0	Tops 13,000' Over Clouds
3.	13:15:00	119	156	278	2.1	Under Clouds Bottom 2,000'
FLIGHT 2	Central California Valley (June, 1968)					
Case 1.	23:25:06		276.3	306.7	39.2	Clear — Dry Soil
2.	23:04:14		278.0	269.0	39.2	Str. Cu. — Dry Soil
3.	Same as Case (1), except Moist Soil.					
4.	Same as Case (2), except Moist Soil.					
5.	Theoretical data only.				39.2	Clear — Vegetation
6.	23:08:06		267.1	268.2	39.2	Str. Cu. — Vegetation

III. DERIVED DATA PRESENTATION

Some data for example the 19.35 GHz brightness temperatures, are taken for this analysis as observed quantities. Other data are derived indirectly from the information collected on the flights. Examples of indirect or derived data are: the temperature profile, water vapor profile, dimensions and types of clouds observed, and the properties of the surface being observed. In this Section, the information which was not directly observed, but which is essential to the analysis, is simulated or reconstructed from the available information.

A. CLEAR ATMOSPHERE MODELS

To compute the absorption and emission caused by constituents of the clear atmosphere at wavelengths in the vicinity of 1 to 3 centimeters, the temperature and water vapor within the antenna field of view need to be known as a function of pressure. The temperature profiles for each flight are therefore derived from measurements taken in situ by instruments in the Convair 990 aircraft. The only exception is the surface temperature plotted for the atmosphere corresponding to Flight 8 flown in 1969. This value was obtained from Weathership J. The profiles are actually composites of the temperatures which are closest, in time, to the observations analyzed. Sufficient points are included so that the profiles extend from close to the surface to the aircraft altitude. Some of the points recorded on Figures 15 through 18 could have been taken hundreds of miles from the actual point of an analyzed observation, and removed in time by up to one hour.

Figure 15 portrays the temperature profile inferred from the data taken over the Gulf of Mexico in June 1967. No attempt was made to check for unusual gradients or other self-consistencies. The profile is approximate but is, no doubt, much better (barring systematic errors in the instrument recording the temperature) than climatological temperature profiles. The profile is fairly typical of tropical regions. Temperatures are warm at the surface, cold at altitude. It shows two stable regions, one near the

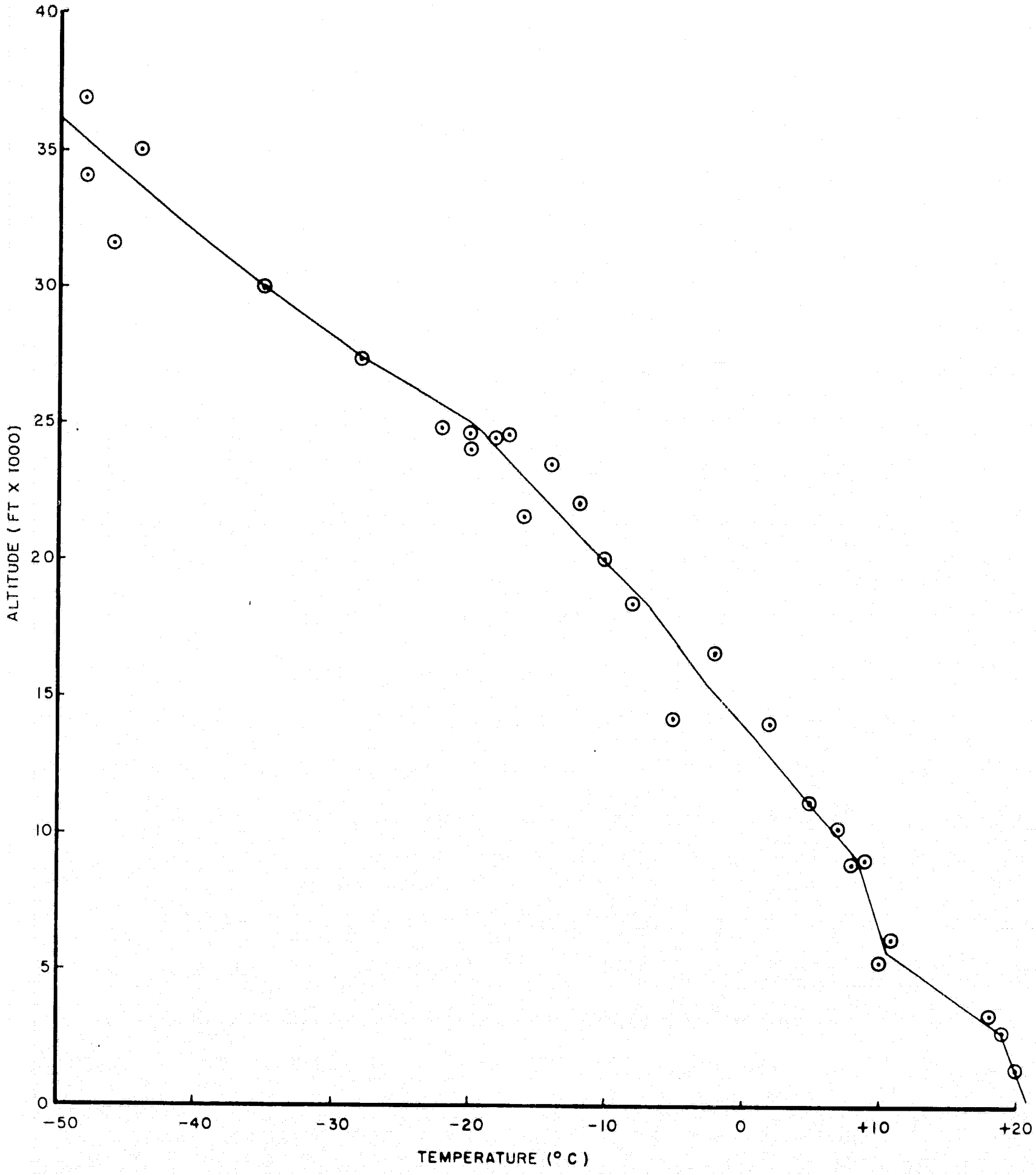

Figure 15 - Temperature Profile Inferred from
Flight 15, Day 157 (6 Jun 67) (Gulf of Mexico)

surface, and the other starting at about 7,000 feet. The tropopause is not clearly evident unless the low temperature at 32,000 feet is construed to be representative and marking the base of the stratosphere. If one were to differentiate between points taken as the aircraft ascended and those taken as it descended, a systematic separation of the two sets of points would be evident. Temperatures would appear warmer than the average as the airplane ascended and cooler than the average as it descended.

Flight 9, flown in June 1968 over the Pacific Ocean west of San Francisco, recorded a number of temperature readings above 9,000 feet but none below, except on takeoff and landing. The temperature distribution is shown in Figure 16. The general shape of the curve was retained below the level of measurement and extrapolated to the ground.

Flight 8, flown over the Atlantic Ocean west of Ireland in 1969, was fortunate enough to be close to Weathership J which recorded surface conditions appropriate to the general area. The mean temperature of the region, as may be noticed from Figure 17, was easily the coldest of the four analyzed. At 25,000 feet, for example, the temperature was already $-40^{o}C$, as opposed to approximately $-20^{o}C$, at 25,000 feet over the Pacific Ocean on Flight 9, of 1968, and about $-20^{0}C$, also at 25,000 feet, for the Gulf of Mexico Flight in 1967.

For analysis of the radiation from certain land areas in central California, the temperature profile relevant to Flight 2, of the series carried out in 1968, is shown in Figure 18.

Figure 19 presents a set of curves which represent the assumed water vapor distributions corresponding to the four temperature profiles discussed above. The atmosphere presumed to be most moist is that over the Gulf of Mexico. The curve represents a plot of the following exponential function:

$$e\ (z) = e\ (0)\ \exp\ (-z/H)$$

where,

H = scale height
e (z) = water vapor partial pressure at height z
e (0) = surface water vapor partial pressure.

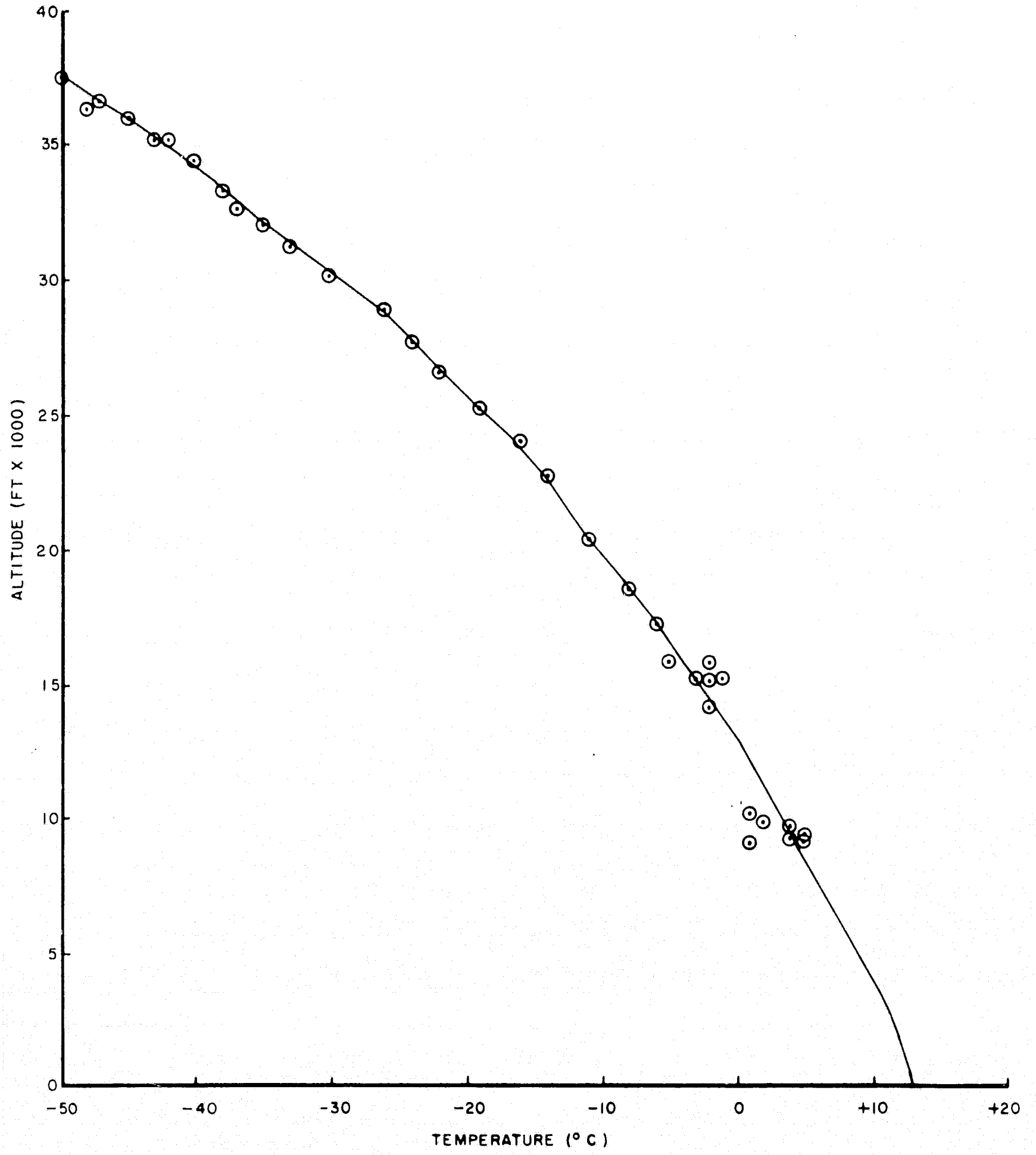

Figure 16 - Temperature Profile Inferred from Flight 9, Day 172, (20 Jun 68) (Pacific Ocean off Calif. Coast)

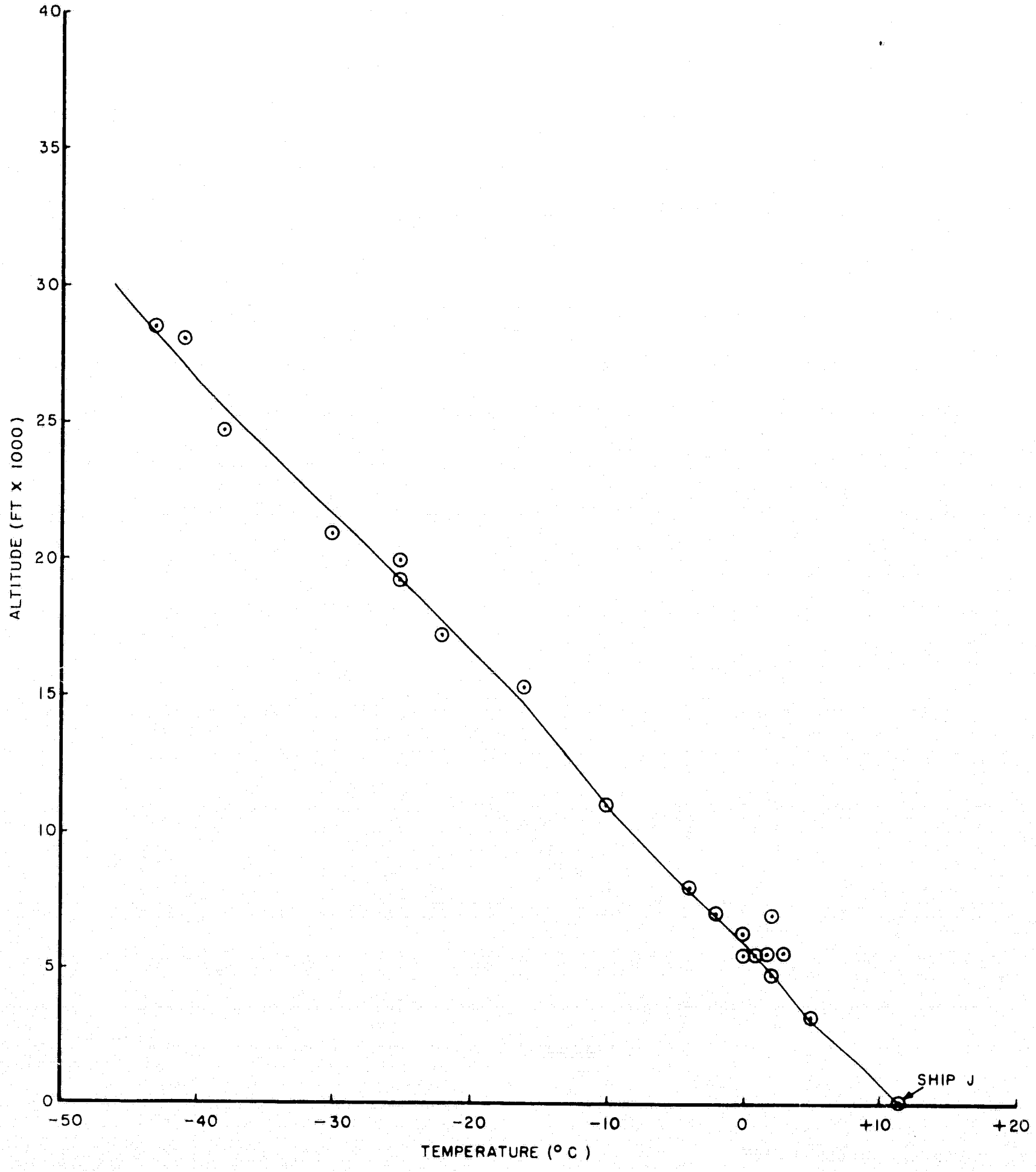

Figure 17 - Temperature Profile Inferred from Flight 8, Day 78 (19 Mar 69) (Irish Sea)

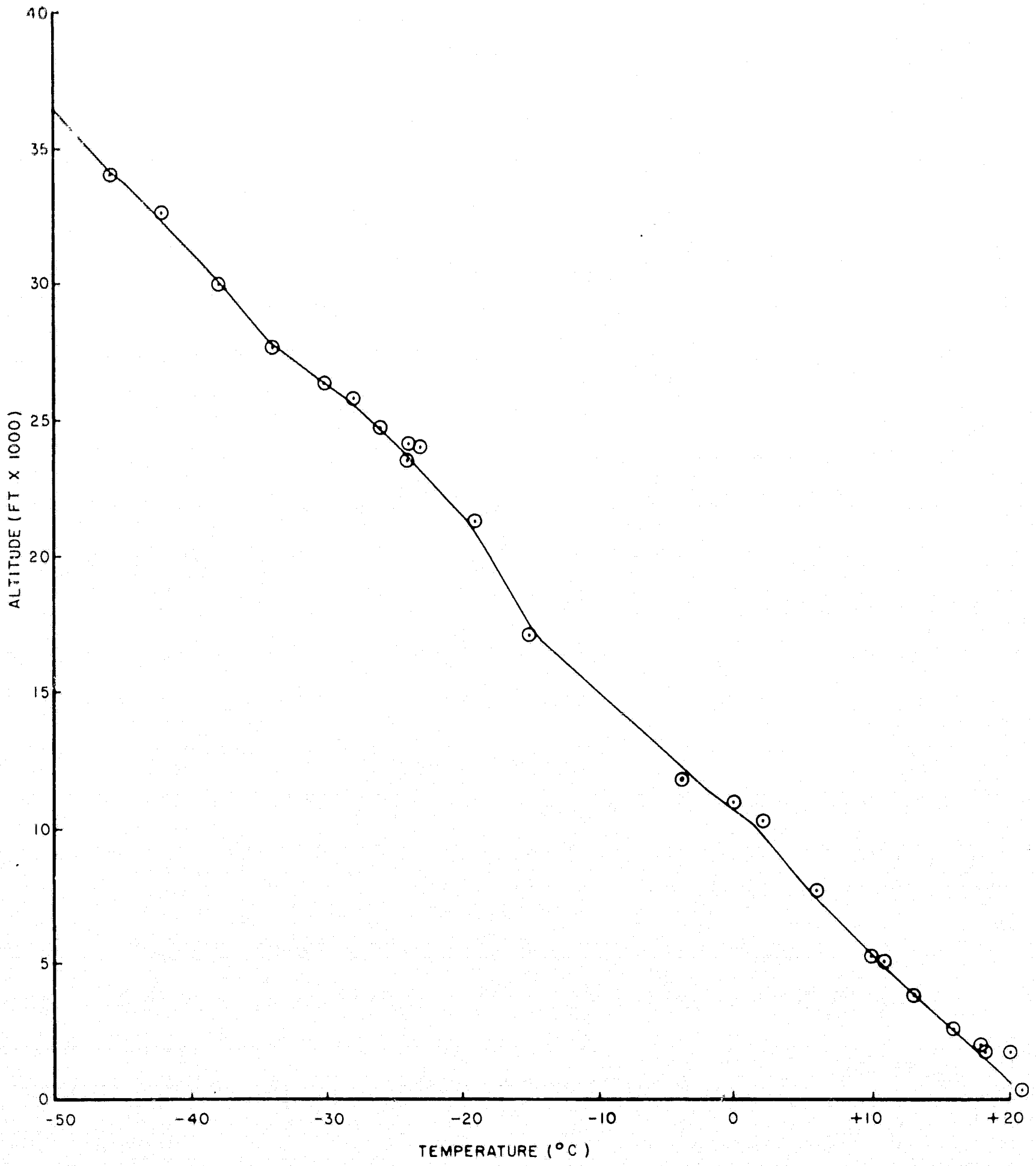

Figure 18 - Temperature Profile Inferred from
Flight 2, Day 159 (7 Jun 68), (Central Calif. Valley)

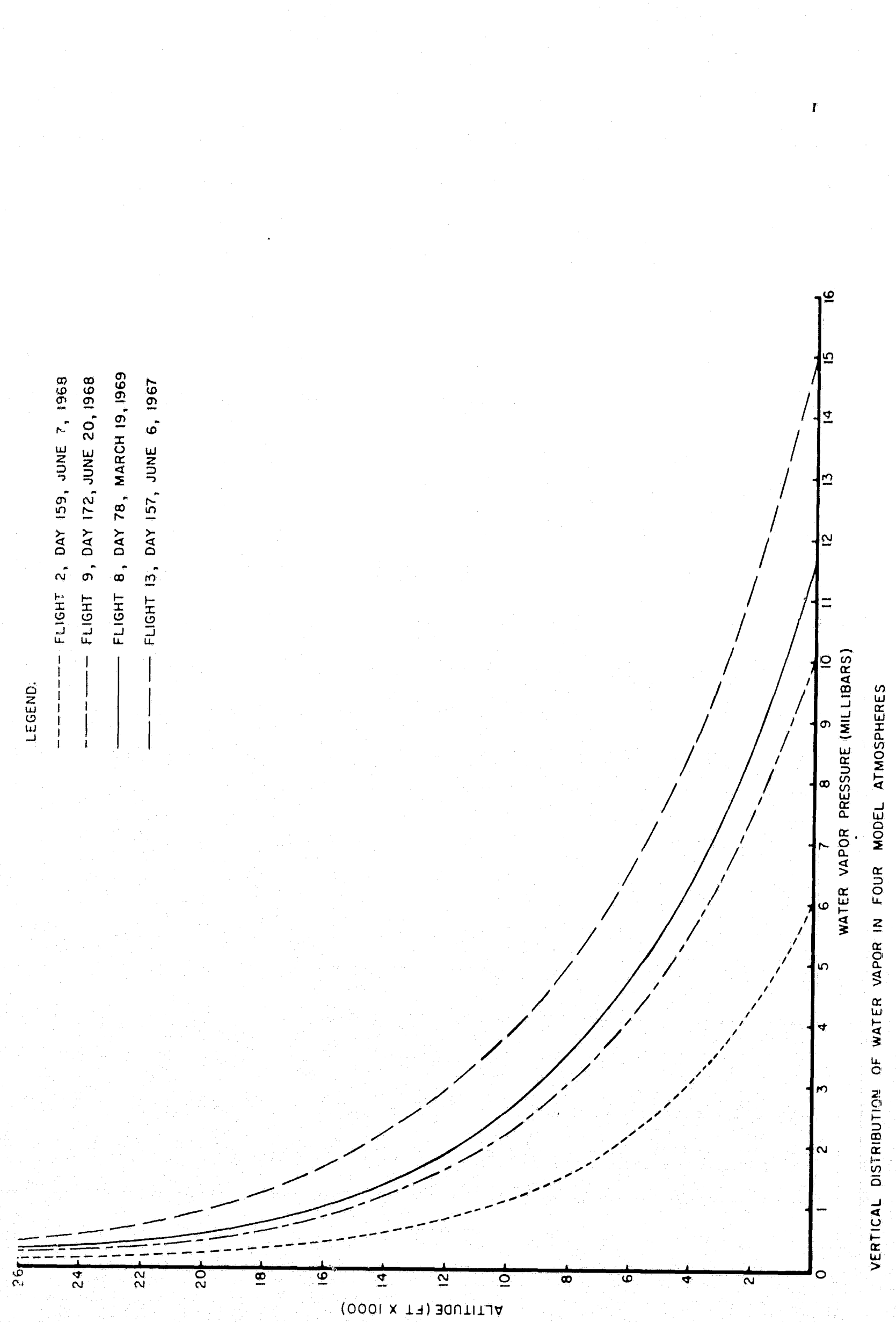

Figure 19 - Assumed Water Vapor Distributions for Data Shown in Figures 15, 16, 17 and 18.

The parameters characterizing the water vapor in the clear atmosphere in each of the four flights analyzed are summarized in Table III-1. The integrated water vapor, surface values of the partial pressure, and the scale heights for the water vapor in each atmosphere are tabulated. Only Flight 8, over the Atlantic Ocean, uses other than a guess for the surface value of the water vapor partial pressure. For this flight, the dew point temperature at Ship J was used as the surface data point.

B. CLOUD MODELS CONSTRUCTED FOR THE SELECTED DATA POINTS

Since the object of the study was to analyze the effects that clouds have upon observed brightness temperatures at 19.35 GHz, observation periods were chosen from each flight during which some interesting cloud was being monitored. From the adjunctive data, cloud models were deduced which seemed to best fit the circumstances of the selected observation. These cloud models are presented in Figures 20 through 26.

Cloud top heights were assumed to be correlated to the 10-12 μ MRIR temperature recorded at the point in time of observational interest. The 10-12 μ temperatures were referred to the temperature profile of that day's flight. Cloud tops were assumed to be at the altitude corresponding to the measured temperature.

The bases of the clouds were simply estimated unless the aircraft flew sufficiently low to permit direct measurement or estimation by the flight crew.

Figure 20 portrays the first case studied from Flight 13 of 1967. This was believed to be a stratocumulus deck with occasional clouds above. The lower layer was thought to have bases typical of ocean stratocumulus or near 2,000 feet. MRIR temperatures were somewhat erratic but it was felt 286^{o}K probably marked the temperature of the top of the lower cloud deck. This temperature corresponds roughly to 5 - 6,000 feet in the temperature profile, leading to a choice of 5,600 feet for the top of the cloud. (Since the condensed water density is one of the derived parameters of the microwave data, each model cloud graphed in Figures 20 thru' 26 shows only a relative condensed water density scale. The maximum density of each cloud model is labeled 1.0 gm/m^{3}.

Table III-1 - Parameters of Surfaces and Atmospheres of Four Flights

FLIGHT →	FLIGHT 13	FLIGHT 2	FLIGHT 9	FLIGHT 8
DAY NUMBER	157	159	172	78
DATE OF FLIGHT	June 6, 1967	June 7, 1968	June 20, 1968	March 18, 1969
SURFACE TYPE	Sea	Land	Sea	Sea
LOCATION	Gulf of Mexico	California	Pacific Ocean	Atlantic Ocean west of Ireland
SURFACE TEMP. (^{o}K)	296.0 (MRIR)	300.0(Bare Soil) 287.3(Vegetation)	285.0 (MRIR)	276.0 (MRIR)
SURFACE PRESS. (mB)	(1000.0)	(1000.0)	(1000.0)	(1000.0)
SURFACE WATER Vp. (mB)	15.0	6.0	10.0	11.6
SCALE HEIGHT (kft)	7.20 (2.2 km)	5.90 (1.8 km)	6.55 (2.0 km)	6.55 (2.0 km)
TOTAL WATER CONTENT IN VAPOR FORM (CLEAR ATMOSPHERE) g/cm^{2}	2.49	0.82	1.54	1.84

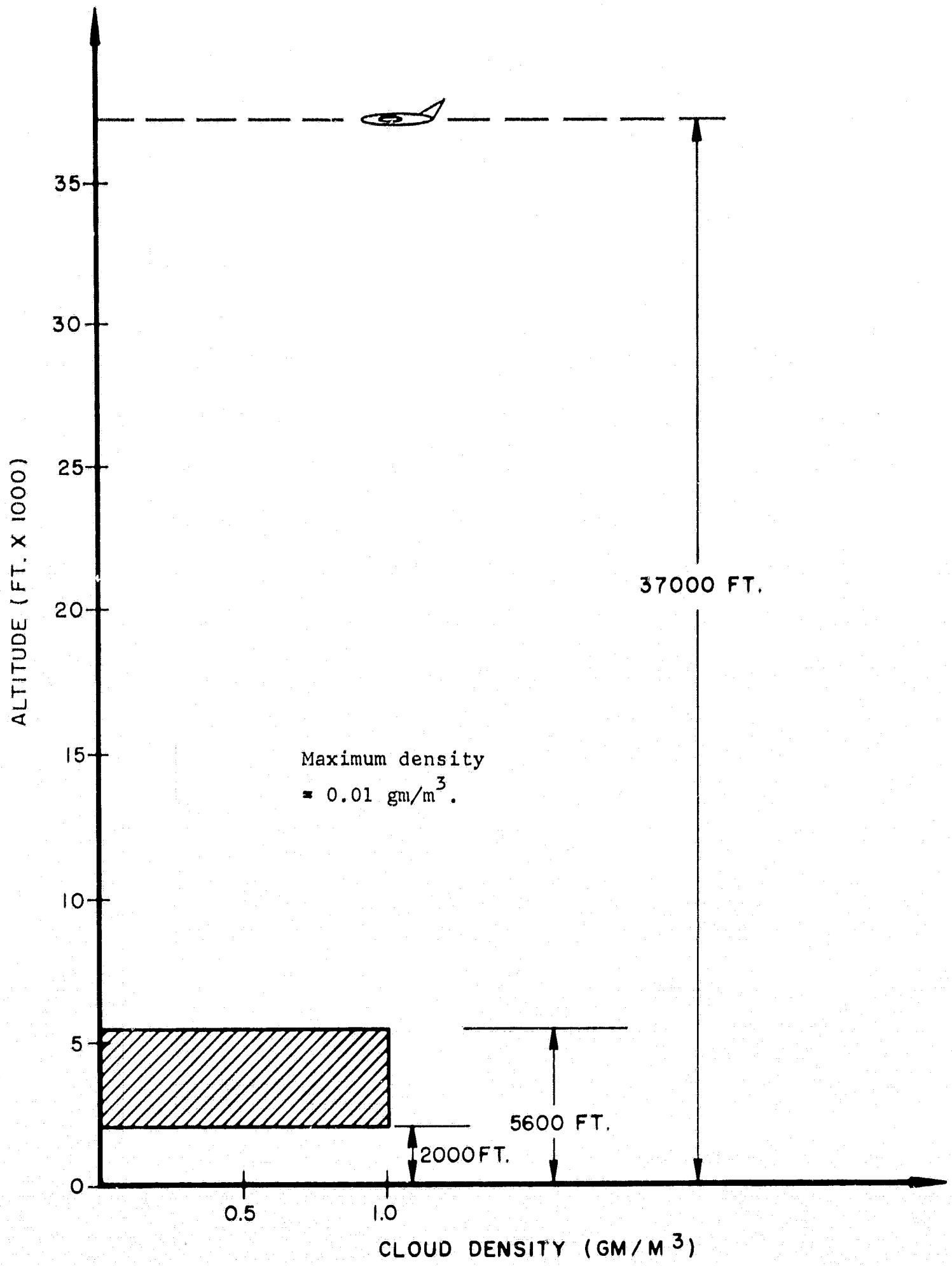

Figure 20 - Stratocumulus Deck
Flight 13, Day 157, June 6, 1967 Case 1
[14:44:50]

Therefore, to derive the absolute densities which were inferred from the microwave data, each relative scale must be multiplied by the maximum density, as indicated in each Figure.

Figure 21 represents schematically the cloud model chosen for Case 2 of Flight 13. The data suggest that it is an intense, small, rain shower. Tops of the cloud were indicated to be near 9,000 feet. Bases were estimated again to be near 2,000 feet. This last estimate could be high.

Case 3 of Flight 13, shown in Figure 22, is a full fledged cumulonimbus with a hard core which was reported to extend to 22,500 feet. The MRIR temperature indicated that the tops were near 20,000 feet. The cloud model was broken up into a number of layers to roughly correspond to models of cumulonimbus which have been postulated (see Mason, 1957). The most dense part of the cloud was assumed to be near the bottom. (No attempt was made to model the rise in density from base to core). The cloud probably consisted of water drops mainly because the top of the cloud was still above $-20^{\circ}C$. The size of the cloud, and the intensity of the rain falling from it, mean that it was probably close to the maximum possible condensed water density and that it most likely contained the maximum number of large water droplets which it could produce.

Flight 9 in 1968 produced two clear atmosphere cases of interest and two cloudy cases. Case 3 was the first cloudy case and is depicted in Figure 23. MRIR data indicated tops near 24,000 feet. Two layers were postulated. The clouds were fairly opaque at 19.35 GHz and therefore the lower layer was estimated to extend to 14,800 feet with a, more or less, homogeneous density distribution. The cirrus layer was postulated to have a density of one-half the lower layer and to extend only 3,000 feet vertically.

Case 4 of Flight 9 was apparently another large cumulus with a high probability of rain beneath it. The structure of the cloud, as envisioned for analysis, is shown in Figure 24. Three densities are assumed. The lowest part of the cloud extends over the same vertical extent as the lower layer in Case 2, but this time is more dense. A middle region of one-half the lower layer density is capped by a cirrus layer of very low density.

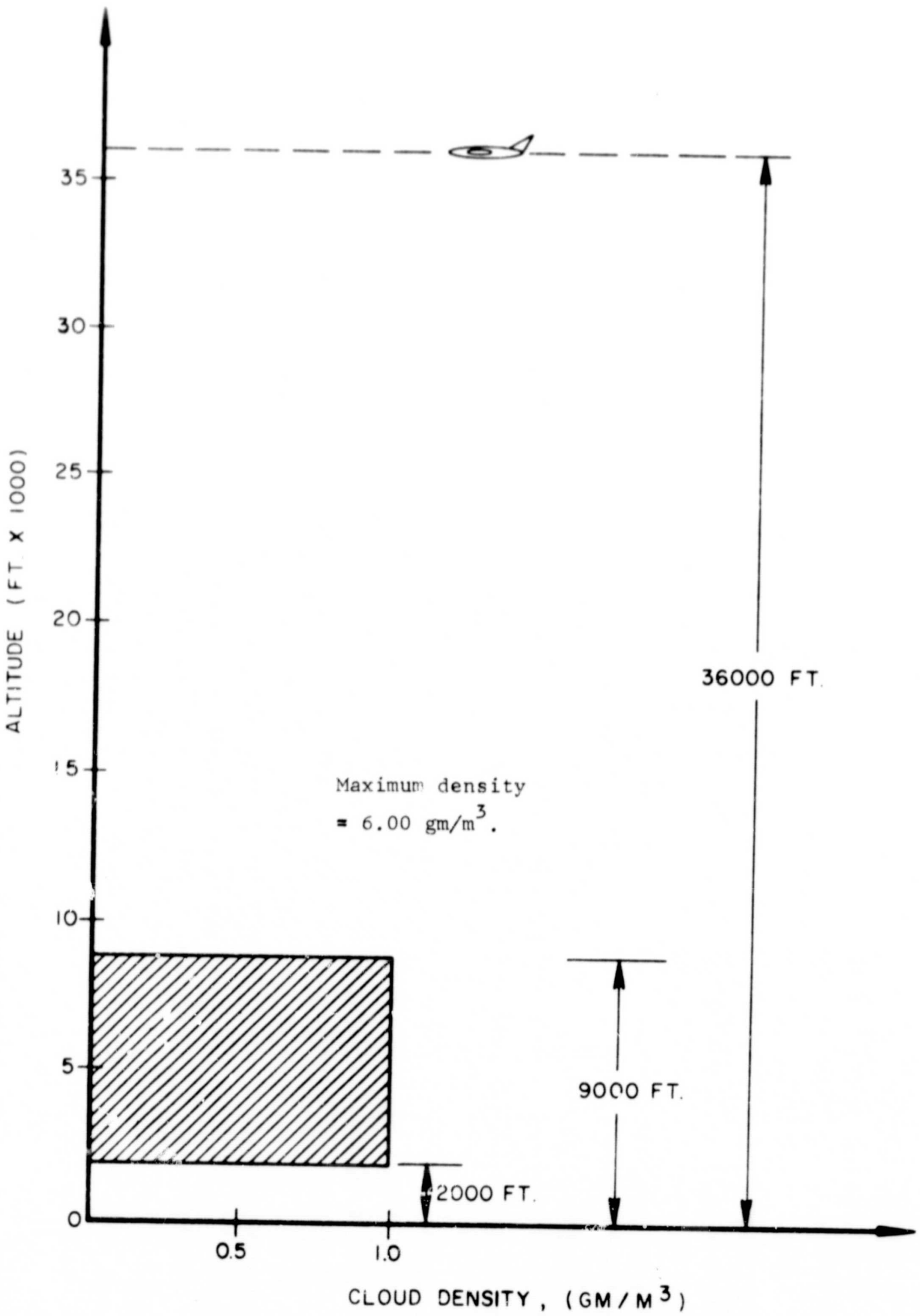

Figure 21 - Small Rain Cloud
Flight 13, Day 157, June 6, 1967 Case 2
[14:46:36]

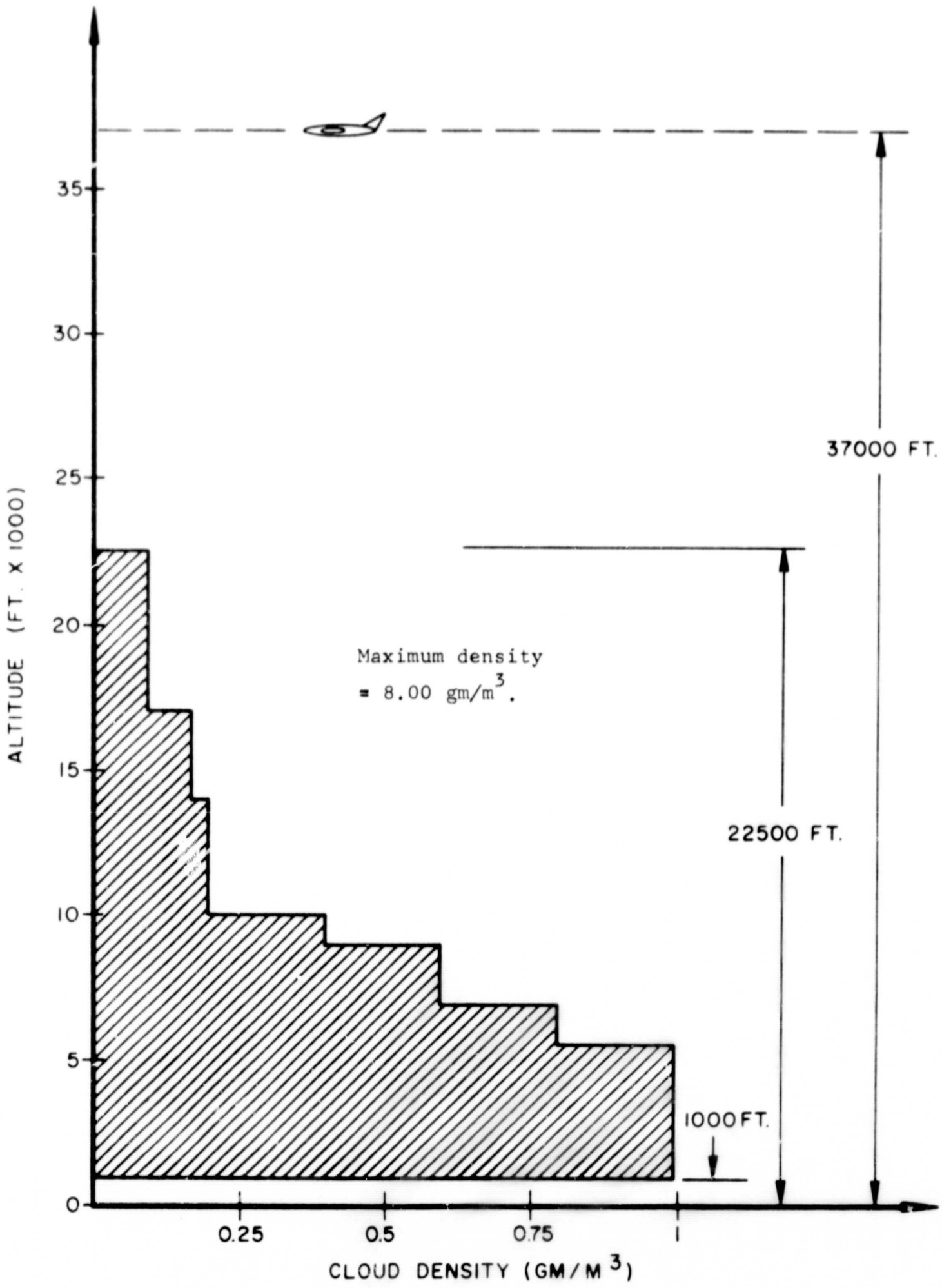

Figure 22 - Full Cumulonimbus Rain Cloud
Flight 13, Day 157, June 6, 1967 Case 3 [14:46:36]

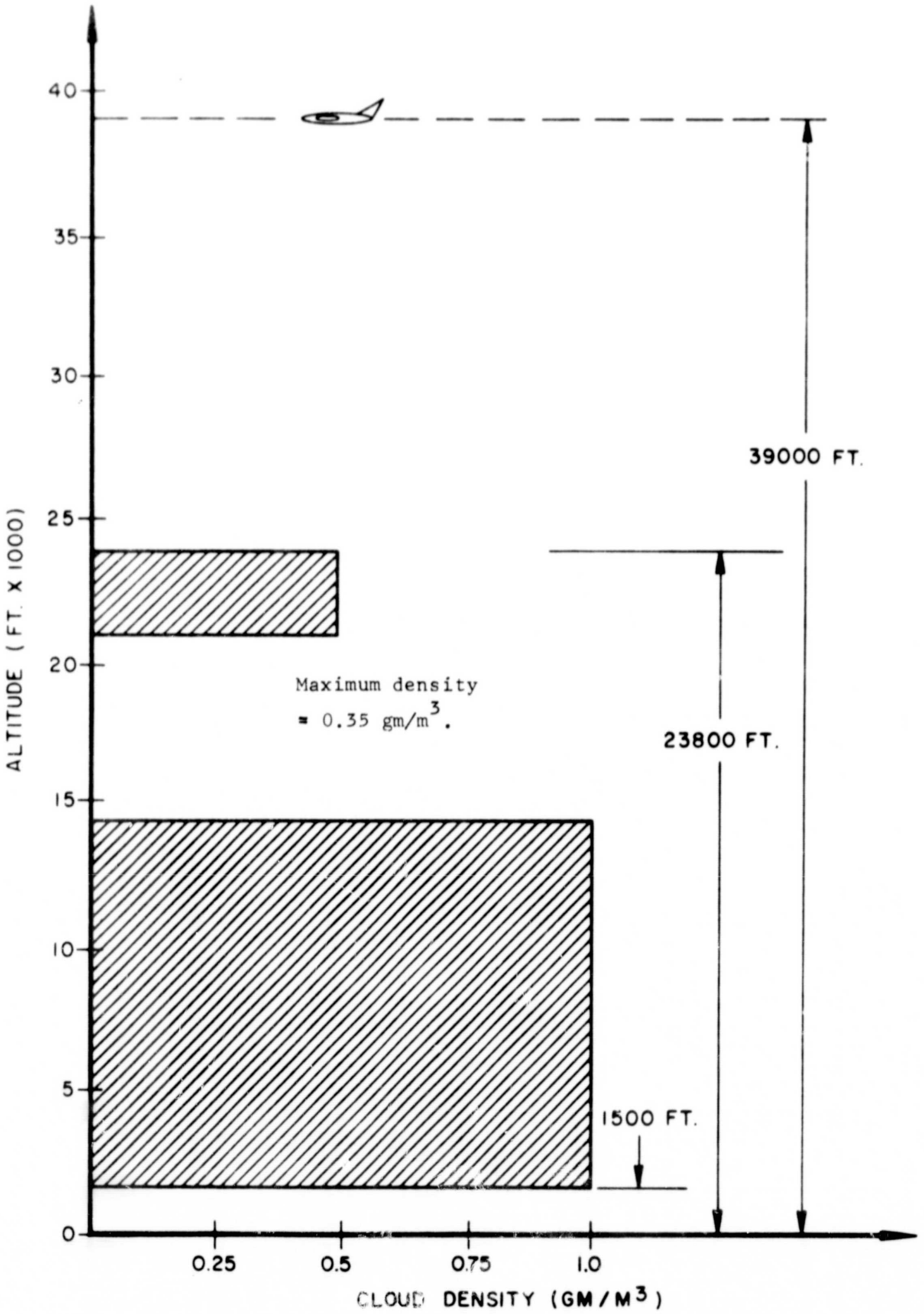

Figure 23 - Layered Clouds
Flight 9, Day 172, June 20, 1968 Case 3
[23:06:20]

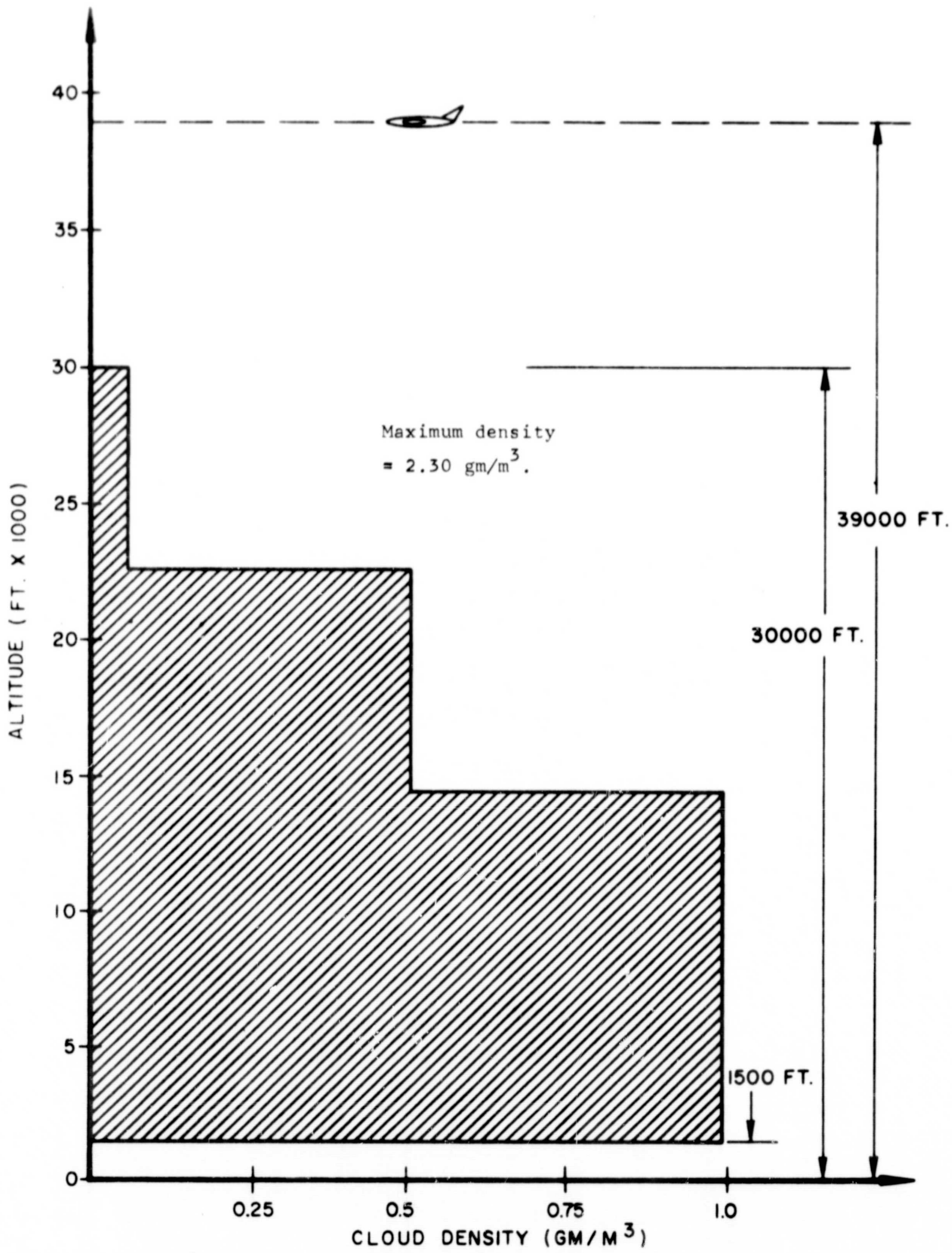

Figure 24 - Large Cumulus Cloud
Flight 9, Day 172, June 20, 1968 Case 4
[23:11:40]

Flight 8 of 1969 brought up quite a unique set of data. The aircraft flew above and below the same cloud. Excellent data on the vertical extent, altitude of the base, and general characteristics of the cloud were gathered. Some uncertainty, however, existed as to the extent of rain beneath the cloud. The over-cloud flight is shown in Figure 25. The under-cloud flight is depicted in Figure 26.

C. SURFACE TEMPERATURE

The temperature recorded in the 10-12 μ channel of the MRIR sensor, looking down in a clear atmosphere at the ocean's surface, is the mean temperature of a thin surface film, at least to within several degrees. For this report, the 10-12 μ temperature is taken to be the surface temperature, under conditions of a clear atmosphere.

In every flight, some clear areas were reported such that the MRIR data could be used to establish the surface temperature. These temperatures are reported in Table III-1. The clear areas were obviously not where the clouds were, but most were reasonably close. If they were not close, (as was the case for Flight 9), they were used, in any event, as the best estimate of the surface temperature at the cloud position.

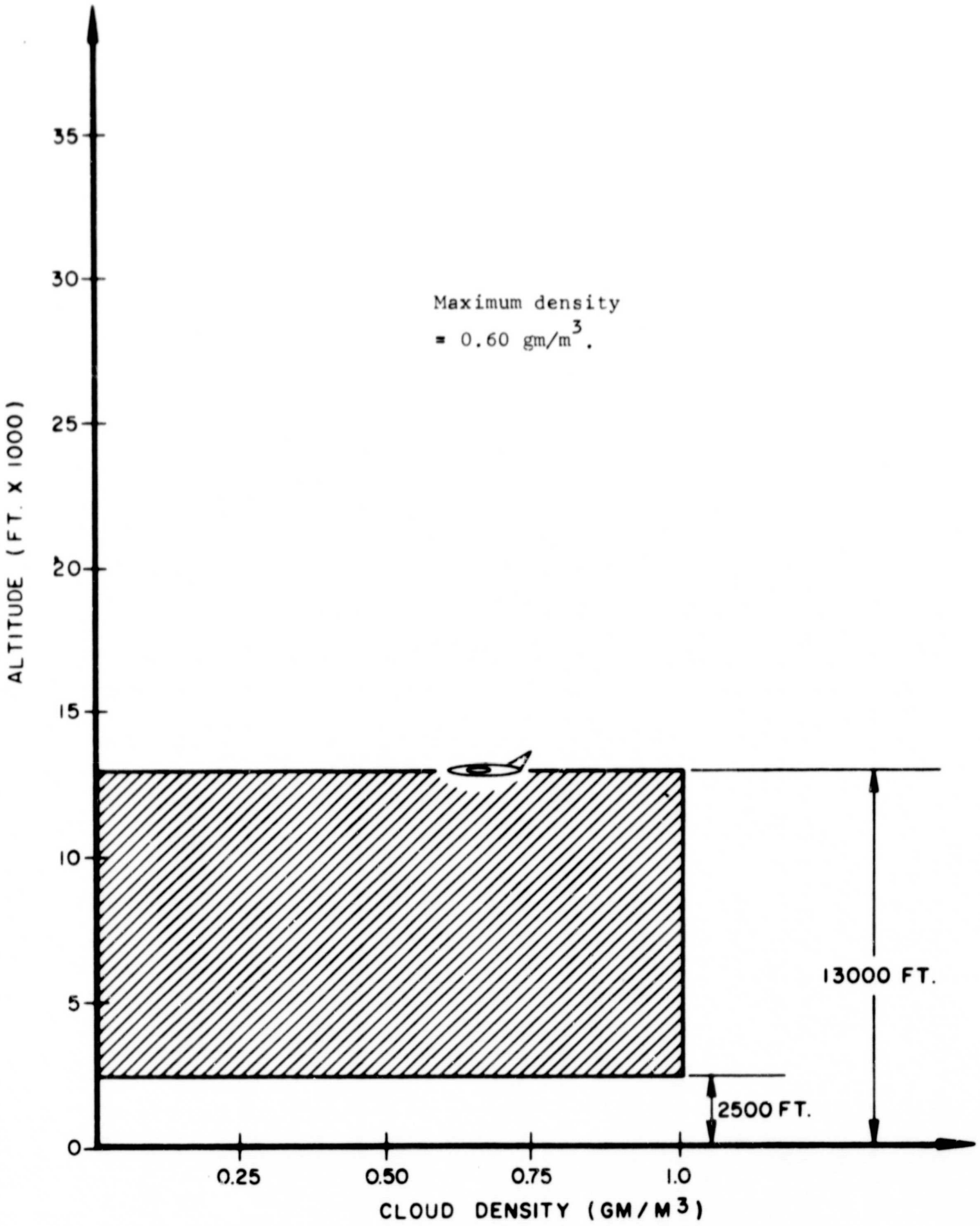

Figure 25 - Cloud Without Rain
Flight 8, Day 78, March 19, 1969 Case 2
[13:03:50]

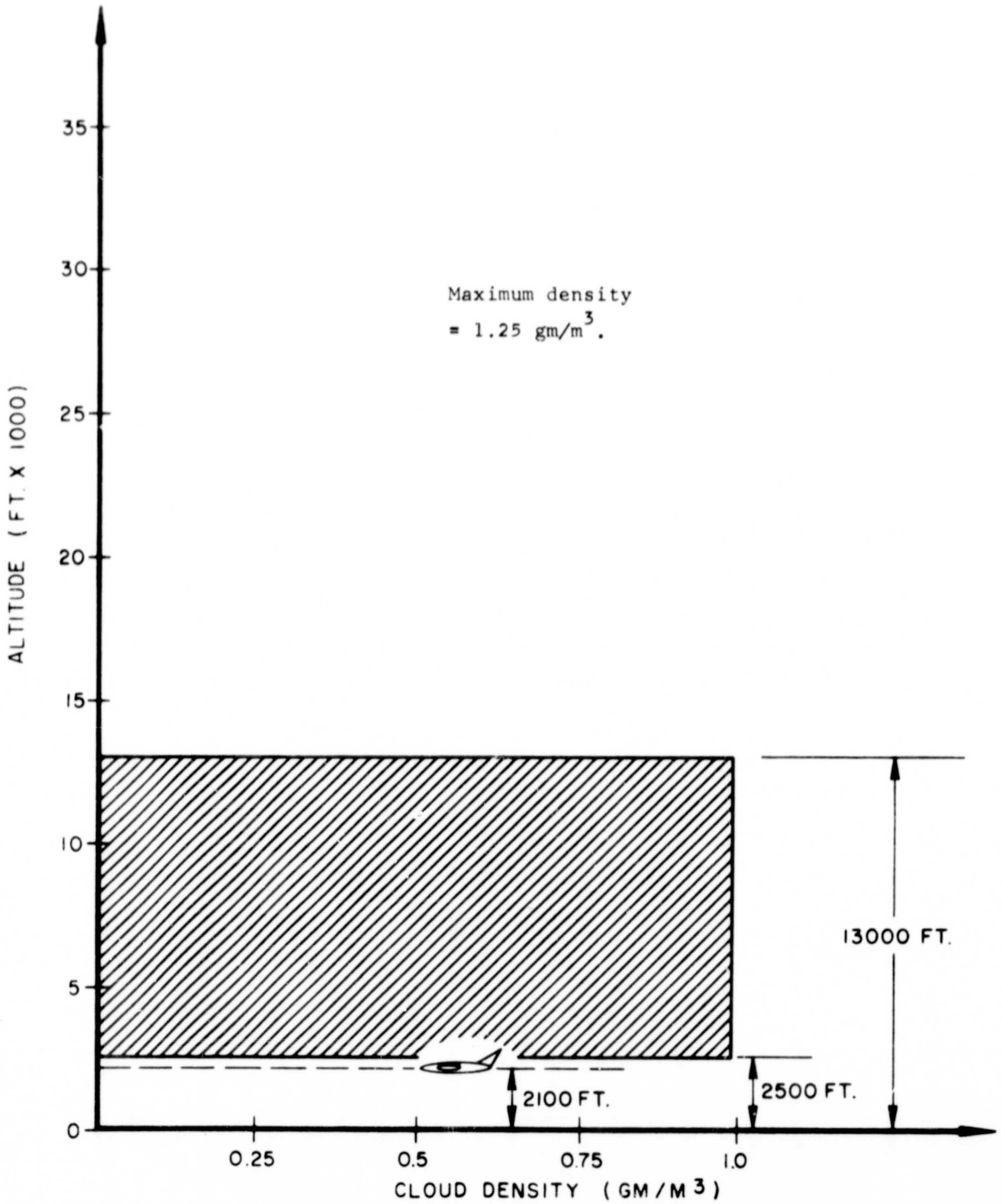

Figure 26 - Cloud Without Rain
Flight 8, Day 78, March 19. 1969 Case 3
[13:15:00]

IV. THEORY OF RADIATIVE TRANSFER

A. GENERAL

The fundamental relation describing the interaction of thermal radiation with the medium through which it passes is the equation of radiative transfer. (See Chandrasekhar, 1950, and Samuelson, 1967). At a given point in the medium, which is characterized by an extinction coefficient, γ_ν, and an emission coefficient, j_ν, the elemental change in intensity, $I_\nu(\mu, \varphi)$, as it traverses a distance, ds, in the direction (μ, φ) where, $\mu = \cos\varphi$, is given by,

$$\frac{d I_\nu (\mu, \varphi)}{ds} = -\gamma_\nu I_\nu (\mu, \varphi) + j_\nu (\mu, \varphi) \qquad (1)$$

The first term on the right-hand side of Equation (1) represents the loss of radiation by both absorption and scattering, and the second the total gained by thermal emission and scattering into the direction(μ, φ).

The emission coefficient may be expanded in the form

$$j_\nu (\mu, \varphi) = j_\nu^A (\mu, \varphi) + j_\nu^s (\mu, \varphi) \qquad (2)$$

where,

j_ν^A refers to the process of thermal emission and j_ν^s refers to the energy scattering into the direction of interest.

j_ν^A can be written for a medium in thermal equilibrium, using Kirchoff's Law, as

$$j_\nu^A (\mu, \varphi) = \gamma_\nu^A B_\nu (T) \qquad (3)$$

in which, γ_ν^A is the absorption coefficient and $B_\nu (T)$ is the Planck function given by

$$B_\nu (T) = \frac{2h \nu^3}{c^2} \frac{1}{\left(e^{-h\nu/kT} - 1\right)} \qquad (4)$$

where,

h is Planck's constant

ν is the frequency of radiation

c is the velocity of light in a vacuum

k is Boltzmann's constant, and

T is the absolute temperature of the medium.

The scattering term of Equation (2) may be written in terms of a scattering function such that

$$j_\nu^s(\mu, \varphi) = \gamma_\nu^s \mathcal{J}_\nu(\mu, \varphi) \tag{5}$$

where,

γ_ν^s is the scattering coefficient at that point in the medium

$\mathcal{J}_\nu(\mu, \varphi)$ is a function dependent upon the scattering characteristics of the medium.

The extinction coefficient γ_ν is related to the absorption and scattering coefficient as

$$\gamma_\nu = \gamma_\nu^s + \gamma_\nu^A \tag{6}$$

A scattering albedo can be defined as

$$\tilde{\omega}_o = \gamma_\nu^s / \gamma_\nu \tag{7}$$

and the optical depth as

$$d\tau = -\gamma_\nu \, ds \tag{8}$$

such that Equation (1) can be written as

$$\frac{d\, I_\nu(\mu, \varphi)}{d\tau} = I_\nu(\mu, \varphi) - (1 - \tilde{\omega}_o)\, B_\nu(T) - \tilde{\omega}_o \mathcal{J}_\nu(\mu, \varphi) \tag{9}$$

At microwave frequencies, where $h\nu \ll kt$, the Rayleigh-Jeans approximation may be made and Equation (9) may be integrated to give

$$T_B(\mu, \varphi, \tau) = T_B(\mu, \varphi, 0)e^{-\tau_{max}} + \int^{\tau_{max}} T_{eff}(\mu, \varphi, \tau)e^{-\tau}\, d\tau \qquad (10)$$

in which,

$$T_{eff}(\mu, \varphi, \tau) = (1 - \tilde{\omega}_o(\tau))\, T_m(\tau) + \tilde{\omega}_o(\tau)\, T_{sc}(\mu, \varphi, \tau). \qquad (11)$$

$T_m(\tau)$ is the radiation temperature associated with the medium and equals the kinetic temperature in the case of thermodynamic equilibrium. $T_{sc}(\mu, \varphi, \tau)$ is a temperature associated with the energy scattered from all directions in the direction (μ, φ).

The two limiting forms of Equation (11) are defined when $\tilde{\omega}_o \to 0$ to give the scatter-free limit, and when $\tilde{\omega}_o \to 1$ to give the conservative limit. T_{eff}, in the first case, becomes the medium radiation temperature and, in the second case, T_{eff} becomes the local brightness temperature averaged over 4π steradians, weighted by the so-called normalized phase function $\rho_o(\mu, \varphi; \mu', \varphi')$ which describes the effectiveness of the scattering process from all directions into the direction (μ, φ).

B. ABSORPTION COEFFICIENTS FOR GASEOUS CONSTITUENTS AND SMALL WATER DROPLETS

In order to compute $T(\mu, \varphi, \tau)$ in Equation (10) for the scatter-free case, γ_ν^A must be known. Three constituents of the atmosphere contribute to γ_ν^A: water vapor, oxygen, and condensed water in the form of clouds and rain. The expansion of the total absorption coefficient may be written as

$$\gamma_\nu^A = \gamma_{H_2O} + \gamma_{O_2} + \gamma_{CL} \qquad (12)$$

where,

γ_{H_2O}, γ_{O_2} and γ_{CL} are the absorption coefficients for water vapor, oxygen and clouds, respectively. Since each of these absorbers are important at 19.35 GHz their complete expression in terms of environmental parameters will be given.

The expression for the absorption by water vapor is an adaptation by Gaut (1968) of an expression first presented in Barrett and Chung (1962). It is given as follows:

$$\gamma_{H_2O} = 1.57 \times 10^{-6} \rho \frac{\nu^2}{T^{3/2}} \left[\frac{\exp(-642/T)}{T} f(\nu, \nu_{1.35}, \Delta\nu_{1.35}) + 7.07 \times 10^{-24} \Delta\nu_{1.35} \right] \text{ dB/km} \quad (13)$$

where,

γ_{H_2O} = absorption coefficient for water vapor in dB/km

ρ = water vapor density, in g/m^3

ν = frequency, in Hertz

$\nu_{1.35}$ = 22.235 GHz (equivalent to λ = 1.35 cm)

T = kinetic temperature, in ^oK

$$\Delta\nu_{1.35} = 2.62 \times 10^9 \left(\frac{P}{1013.25}\right) \left(\frac{318}{T}\right)^{0.625} \left(1 + 0.015 \frac{\rho T}{P}\right) \text{ Hertz} \quad (14)$$

P = atmospheric pressure in millibars

$$f(\nu, \nu_{1.35}, \Delta\nu_{1.35}) = \frac{\Delta\nu_{1.35}}{(\nu_{1.35} - \nu)^2 + \Delta\nu_{1.35}^2} + \frac{\Delta\nu_{1.35}}{(\nu_{1.35} + \nu)^2 + \Delta\nu_{1.35}^2} \quad (15)$$

The expression used for the oxygen absorption coefficient, γ_{02}, is the one given by Meeks and Lilley (1963). It can be written as follows:

$$\gamma_{O_2} = 2.0057 \times \left(10^{-9}\, P T^{-3}\, \nu^2\right) \times$$

$$\sum_{N\ \text{odd}} \left[g_N^{+}\, f\left(\nu,\ \nu_{N+},\ \Delta\nu_{O_2}\right) + g_N^{-}\, f\left(\nu,\ \nu_{N-},\ \Delta\nu_{O_2}\right) \right.$$

$$\left. + g_N^{o}\ f\left(\nu,\ 0,\ \Delta\nu_{O_2}\right) \right] \exp\left[-2.0684\ N(N+1)/T\right] \qquad (16)$$

dB/km

in which,

P = pressure, in millibars

T = temperature, in ^{o}K

ν = frequency, in Hertz

$$g_N^{+} = \frac{N\ (2N+3)}{N+1} \qquad g_N^{-} = \frac{(N+1)(2N-1)}{N}$$

$$g_N^{o} = \frac{(N^2 + N + 1)(2N+1)}{N\ (N+1)} \qquad (17)$$

$$f\left(\nu,\ \nu_{N+N-},\ \Delta\nu_{O_2}\right) = \frac{\Delta\nu_{O_2}}{(\nu_o - \nu)^2 + \Delta\nu_{O_2}^2} + \frac{\Delta\nu_{O_2}}{(\nu_o + \nu)^2 + \Delta\nu_{O_2}^2} \qquad (18)$$

and the general line-width is given by,

$$\Delta\nu_{O_2} = 1.976 \times 10^{9} \left(\frac{P}{1013.25}\right)\left(\frac{300}{T}\right)^{0.85} \left(0.21 + 0.78\beta\right) \qquad (19)$$

where,

$$\beta = \begin{cases} 0.25 \ ; & \text{For } Z < H_1 \ (P > 356 \text{ mb}) \\ 0.25 + 0.50\ (Z - H_1)/(H_2 - H_1) \ ; & \text{for } H_1 \leq Z \leq H_2 \\ 0.25 \ ; & \text{For } Z > H_2 \ (P < 25.3 \text{ mb}) \end{cases} \qquad (20)$$

In the atmosphere, assemblages of more or less spherical water droplets are suspended in the form of clouds, fogs and rains. If the wavelength of the radiation which passes through such an assemblage is much greater than the size of the largest drops, then significant energy can be absorbed while scattering remains negligible for the path lengths corresponding to clouds. The expression for the absorption coefficient due to clouds is taken from Staelin (1966) and can be written as follows:

$$\gamma_{CL} = \frac{M \times 10^{[0.0122(291 - T) - 6]}}{\lambda^2} \text{ nepers/cm} \qquad (21)$$

where,

M = liquid water content in g/m^3

λ = wavelength in centimeters

T = temperature in degrees Kelvin

The above expression is a derivative of the analysis by Mie of the radiational properties of a dielectric sphere and the temperature dependence of the complex dielectric constant for water.

C. SCATTERING IN CLOUDS AND RAIN

The solution of Equation (10), for even the simplest cases in which scattering exists, is formidable due to the fact that every point in the medium depends on every other point through the relationship given in Equation (11). Certain simplifying assumptions can be made, however, which enables one to: (i) estimate the validity of assuming a scatter-free medium; and (ii) estimate the lowest order correction due to scattering effects.

It is particularly important, at microwave frequencies, to define the limitations of the simple case, because the approximate theory is accurate in most, but certainly not all, cloud situations.

$$\chi_j(\tilde{n}, \alpha, r) = Q_j(\tilde{n}, \alpha)\, \pi r^2 \qquad j = S, A, E$$

$$\alpha = 2\pi r/\lambda \tag{23}$$

where,

χ_j is the appropriate cross-section, r the radius of the drop, and Q_j the corresponding "efficiency factor", which is a function of the dimensionless scattering parameter, α, and the complex index of refraction, $\tilde{n}$.

The efficiency factors are obtained by solving the electromagnetic field equations for a dielectric sphere of complex index of refraction, with the solutions taking the form of multipole expansions in Legendre polynomials. The complex coefficients a_ℓ and b_ℓ of the multipoles are expressed in terms of the Ricatti-Bessel functions

$$\psi_\ell(x) = \chi\, j_\ell(x)$$

$$\zeta_\ell(x) = \chi\, h_\ell^{(2)}(x) \tag{24}$$

and their derivative. Here $j_\ell(x)$ and $h_\ell^{(2)}(x)$ are the spherical Bessel and Hankel functions of the complex argument x. The expressions for the efficiency factors are

$$Q_S = \frac{2}{\alpha^2} \sum_{\ell=1}^{\infty} (2\ell + 1) \left(|a_\ell|^2 + |b_\ell|^2 \right) \tag{25}$$

$$Q_E = \frac{2}{\alpha^2} \sum_{\ell=1}^{\infty} (2\ell + 1)\, R_e\, (a_\ell + b_\ell) \tag{26}$$

$$Q_A = Q_E - Q_S \tag{27}$$

The determination of γ_S and $\tilde{\omega}_c$ for the medium requires the assumption of a drop-size distribution, N(r), from which

$$\gamma_j = \int_0^{\infty} N(r)\, \chi_j(r)\, dr \qquad j = S, A, E \tag{28}$$

A necessary condition for neglect of the effects of scattering is that the effective mean free path for a scattering event be large compared to the scale length of the medium itself. One may formalize this criterion (See Crane 1969) by noting that an error of $\sim$ 0.1 neper in the opacity τ (due to neglect of scattering terms) leads to an error of $\sim$10% in the evaluation of $e^{-\tau}$. The error $\Delta\tau$ in τ, made in traversing a distance d in a uniform medium is:

$$\left|\Delta\tau\right| = (\gamma_E - \gamma_A)\, d = \gamma_s d = \tilde{\omega}_o\, \tau \qquad (22)$$

in which, γ_E is the extinction coefficient.

Hence, an error of 0.1 neper occurs in a "penetration distance" d_s such $\gamma_s\, d_s = 0.1$.

The dependence upon the scattering albedo $\tilde{\omega}_o$ is clear from Equation (10) and (11); insertion of (11) into (10) leads to an infinite series of integrals in successive orders of $\tilde{\omega}_o$, with terms linear in $\tilde{\omega}_o$ representing single scattering, $\tilde{\omega}_o^2$ double scattering, and so on. Hence an error of $\sim \tilde{\omega}_o$ is made in the determination of T_{eff} due to omission of (single) scattering, $\sim \tilde{\omega}_o^2$ due to consideration of single scattering but neglect of double scattering, and so forth.

With these criteria in mind, it is apparent that the validity of omission of scattering terms in the radiative transfer equation depends upon the scattering coefficient, γ_s, and the scattering albedo, $\tilde{\omega}_o$, as determined from a full Mie-scattering treatment of the medium under study. A sufficient condition for omission of scattering terms is that at every point along the path, $\tilde{\omega}_o$ is small, and that the "scattering depth", d_s, is everywhere large compared to the physical dimensions involved.

The full development of the Mie theory will not be given here, as excellent discussions are found in many texts, notably Chandrasekhar (1950), Samuelson (1967) and others. The Mie efficiency factors for scattering, absorption and extinction are defined such that,

$$N_o = \int_0^\infty N(r)\, dr \tag{29}$$

in which, N_o is the total number density at the point in the medium. In the present study it was found convenient to use the distribution of Deirmendjian (1964), which characterizes the ensemble in terms of four parameters A, B, C1 and C2. It is given by

$$N(r) = Ar^{C1} e^{-Br^{C2}} \tag{30}$$

The distribution has the advantages of: (1) easy representation of a wide variety of cloud types by proper choice of parameters; and (2), straightforward computation over a wide range of radii. Moreover, the availability of published results, using this distribution for infrared scattering problems (see for examples, Deirmendjian, 1964, and Bauer, 1964) has been useful for verification of the computational procedure.

V. COMPUTATIONAL MODELS

A. COMPUTER PROGRAM GABTAWF

To understand the radiational environment observed from the Convair 990, a computational scheme was employed which estimated the radiation field anywhere in the atmosphere, if certain facts are furnished about the thermodynamic properties of the atmosphere and surface. The computer program embodying the scheme, and which utilizes the absorption coefficients summarized in the previous Section, is called GABTAWF, an acronym standing for Generalized Absorption, Brightness Temperature And Weighting Function. It represents the complete model of the radiational environment box shown in Figure 27. Figure 27 represents a general approach to data interpretation.

GABTAWF provides a variety of information. The central computation solves the scatter-free equation of radiative transfer for the geometries illustrated in Figure 28 and the quantities illustrated in Figure 29.

The formation of the numerical equivalent to Equation (10), for a radiometer viewing at an angle φ, using the notation of Figure 28, is as follows:

$$T_B(H) = T_{back} \exp\left(-\sum_{i=1}^{N-1} \gamma_i \sec\varphi \, \Delta Z_i\right) + \sum_{n=1}^{N-1} T_{air_n} \gamma_n \exp\left(-\sum_{j=n+1}^{N-1} \gamma_j \sec\varphi \, \Delta Z_j\right) \sec\varphi \, \Delta Z_n \tag{31}$$

where, for a radiometer looking at the earth,

$$T_{back} = T_s (1 - R) + R\left[\sum_{n=1}^{N-1} T_{air_n} \gamma_n \exp\left(-\sum_{i=n-1}^{N-2} \gamma_i \sec\varphi \, \Delta Z_i\right) \sec\varphi \, \Delta Z_i + T_{sky} \exp\left(-\sum_{i=1}^{N-1} \gamma_i \sec\varphi \, \Delta Z_i\right)\right] \tag{32}$$

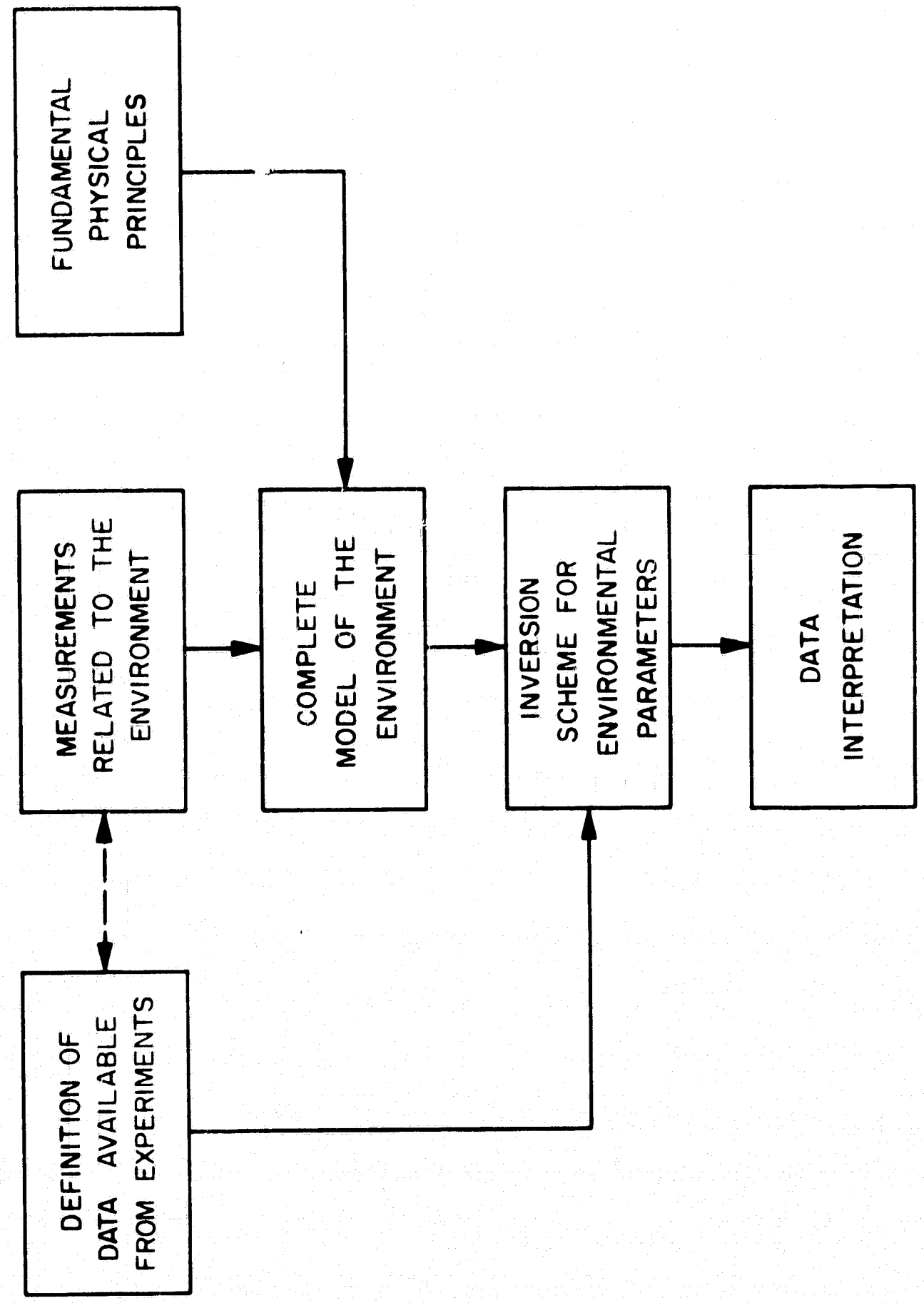

Figure 27 - General Data Interpretation Flow Chart

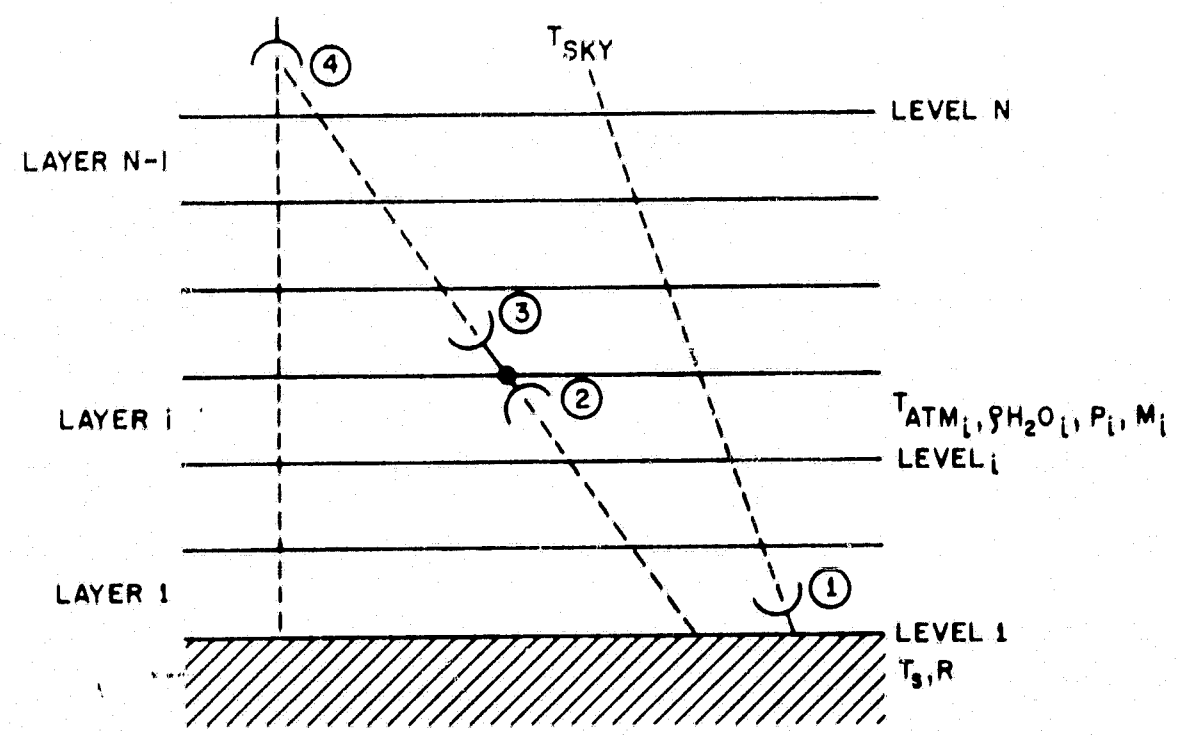

Figure 28 - The Geometries for which GABTAWF Solves the Equation of Radiative Transfer.

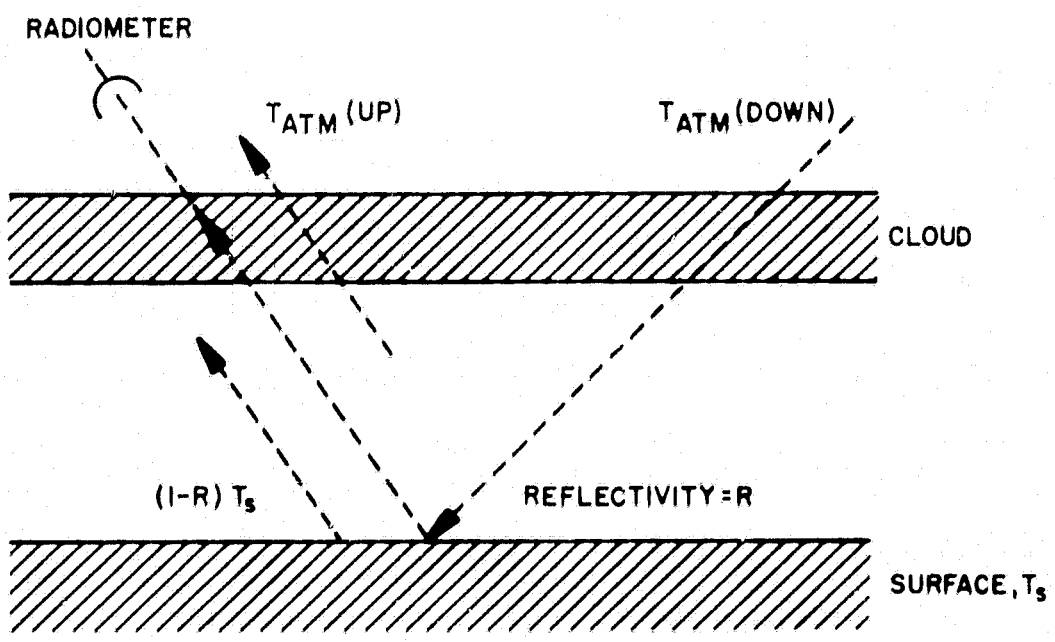

Figure 29 - Various Contributions which Make Up the Signal Measured by a Radiometer from Space.

$\gamma_o \sec \theta \Delta Z_o \equiv 0$

γ_i = mean absorption coefficient for layer i

ΔZ_i = thickness of layer i

T_s = temperature of the surface

R = reflectivity of the surface = (1-ϵ) where, ϵ is the emissivity.

T_{air_i} = mean temperature of layer i

T_{sky} = background radiation from space

$T_B(\nu)$ = brightness temperature observed by the radiometer.

The observing radiometer can be located at the surface looking up, or at some intermediate level looking up or down, or above the atmosphere where it can view the earth from space. It can simulate any angle (plane parallel atmosphere assumed), and it provides the following information as output:

1) Brightness temperature observed by the radiometer.
2) Opacity of the atmosphere as a whole.
3) Opacity of the atmosphere above and below the radiometer.
4) Opacity of every layer.
5) Opacity weighting function for water vapor, oxygen and clouds.
6) Cumulative opacity from the surface (or from space) to the radiometer.
7) Brightness temperature of the energy emitted by each layer.
8) Contribution of each layer to the brightness temperature observed at the radiometer.
9) Brightness temperature of the surface and its contribution to the brightness temperature observed at the radiometer.

GABTAWF allows control over all important inputs and the amount, detail and format of the output. Its completeness and versatility is important to the ease of interpreting the data.

B. COMPUTER PROGRAM RASP

RASP stands for Radiation Scattering Program. Three goals were set for RASP when it was originally conceived:

1) To permit computation and plotting of the Mie efficiency factors for spherical dielectric drops for absorption, scattering and extinction.

2) To compute certain physical parameters which describe a unit volume cloud with an arbitrary drop size distribution.

3) To permit the use of drop size distribution parameters from (2) and the single particle efficiency factors from (1). To compute and plot integrated absorption, scattering and extinction properties for the droplet assemblage.

Each of the goals is fulfilled by the final program.

RASP solves the following equation:

$$\gamma_j(\lambda) = \int_0^\infty N(r)\, \chi_j(r, \lambda)\, dr \qquad (33)$$

where,

j = S, A, E (scattering absorption, or extinction)

γ_j = Coefficient of scattering, absorption or extinction, in nepers m^{-1}.

$N(r)$ = particle distribution function in particles, $cm^{-3}\ \mu^{-1}$.

χ_j = Single particle cross-section for S, A, E, in cm^2.

The cross-sections χ_j are obtained from the expression,

$$\chi_j(r, \lambda) = Q_j(r, \lambda)\, \pi r^2 \qquad (34)$$

with the constraint,

$$\chi_E = \chi_A + \chi_s \qquad (35)$$

The Mie efficiency factors are given by the Q_j's and represent the ratio of the scattering, absorption of extinction cross-sections to the geometrical cross-section.

The droplet size distribution used is that conceived by Deirmendjian (1964) and is given by,

$$N(r) = Ar^{C1} e^{-Br^{C2}} \text{ cm}^{-3} \mu^{-1} \tag{36}$$

where, C_1 and C_2 are chosen to control the distribution shape, and A and B are constants to be determined.

The constraints from which A and B may be determined are as follows:

$$1) \quad \text{Require } M = \int_0^\infty N(r)\, 4/3\, \pi\, r^3\, dr \text{ g/m}^3 \tag{37}$$

where, M is the liquid water density.

Solving for A gives,

$$A = \frac{MC1B^{\left(\frac{C1+4}{C2}\right)}}{(4/3\,\pi \times 10^{-6})\left(\frac{C1+4}{C2}\right)} \tag{38}$$

$$2) \quad \text{Require} \quad \left.\frac{dN(r)}{dr}\right|_{r = r_c} = 0 \tag{39}$$

where, r_c defines the modal drop radius.

From the result, B can be found by evaluating the following equation:

$$B = \frac{C1}{C1\ r_c^{C2}} \tag{40}$$

The results of calculations performed by RASP are presented in Table VI-2.

C. EMISSIVITIES OF SURFACE MATERIALS

It is considered worthwhile to compare observed values of brightness temperatures with theoretical and semi-empirical values, to facilitate data interpretation. The methods used in generating the necessary emissivities are presented in the following paragraphs.

1. Dielectric Permittivities and Emissivities of Sea Water

From information given in Hasted, Ritson and Collie (1948) and Paris (1969) the real and imaginary parts of the dielectric permittivity are given by,

$$e' = e_\infty + \frac{e_s - e_\infty}{1 + \left(\frac{\lambda_s}{\lambda}\right)^2} \tag{41}$$

$$e'' = \frac{(e_s - e_\infty)(\lambda_{s/\lambda})}{1 + \left(\frac{\lambda_s}{\lambda}\right)^2} + \frac{1.8\sigma}{f} \tag{42}$$

where,

e_s = static permittivity

λ_s = relaxation wavelength

e_∞ = high frequency limit of the permittivity

λ = wavelength

σ = static conductivity in units of 10^3 mho/cm

and, f = frequency, GHz.

The conductivity varies with temperature according to,

$$\sigma(T) = .59\ [80.625714 + 1.702\Delta t + 0.0075714286\Delta t^2] \tag{43}$$

where, $\Delta t = T - 293$

in which T is in degrees Kelvin.

Hasted, Ritson, and Collie made measurements to determine the dielectric constants of various water-salt solutions for several normalities and temperatures at wavelengths of 10 cm, 3 cm and 1.25 cm. The relaxation wavelength, λ_s, has been computed as a function of normality, N, in a NaCl solution at 21°C. The results are shown in Figure 30. A linear relationship obtains with a slope of -0.16 cm/N.

It should be noted here that sea water can be represented quite accurately by a 0.578N NaCl solution, as discussed in Porter (1969). Such a solution exhibits, in many ways, the characteristics of sea water in the Pacific Ocean. Measured salinities, obtained during the course of work described in Porter, showed a mean value of 33.664 parts per thousand. Assuming that the specific gravity of a normal solution of NaCl is unity, there are 58.45 grams of sodium chloride in 1000 grams of solution (see Paris (1969)). Thus, the salinity, S, may be expressed as,

$$S = 58.45N \text{ o/oo} \tag{44}$$

Thus, the above-mentioned salinity corresponds to a 0.578N NaCl solution.

Hasted, Ritson and Collie also furnished data on the variation of the relaxation wavelength with temperature for a 0.66N NaCl solution. A correction has been applied to these values, to correspond to a 0.578N solution. The results appearing in Figure 31 show a fairly rapid variation of λ_s with temperature, particularly at low temperatures.

Calculated sea water permittivities are in reasonable agreement with measured values, as shown in Table V-1.

TABLE V-1

COMPARISON OF SEA WATER PERMITTIVITIES

Freq.: 14 GHz, T = 299.4°K

Item	Measured Value*	Calculated Value	Difference (%)
e'	43.0	47.6	+ 10.7
e''	31.4	36.6	+ 16.5

*Measured at Massachusetts Institute of Technology, Laboratory for Insulation Research

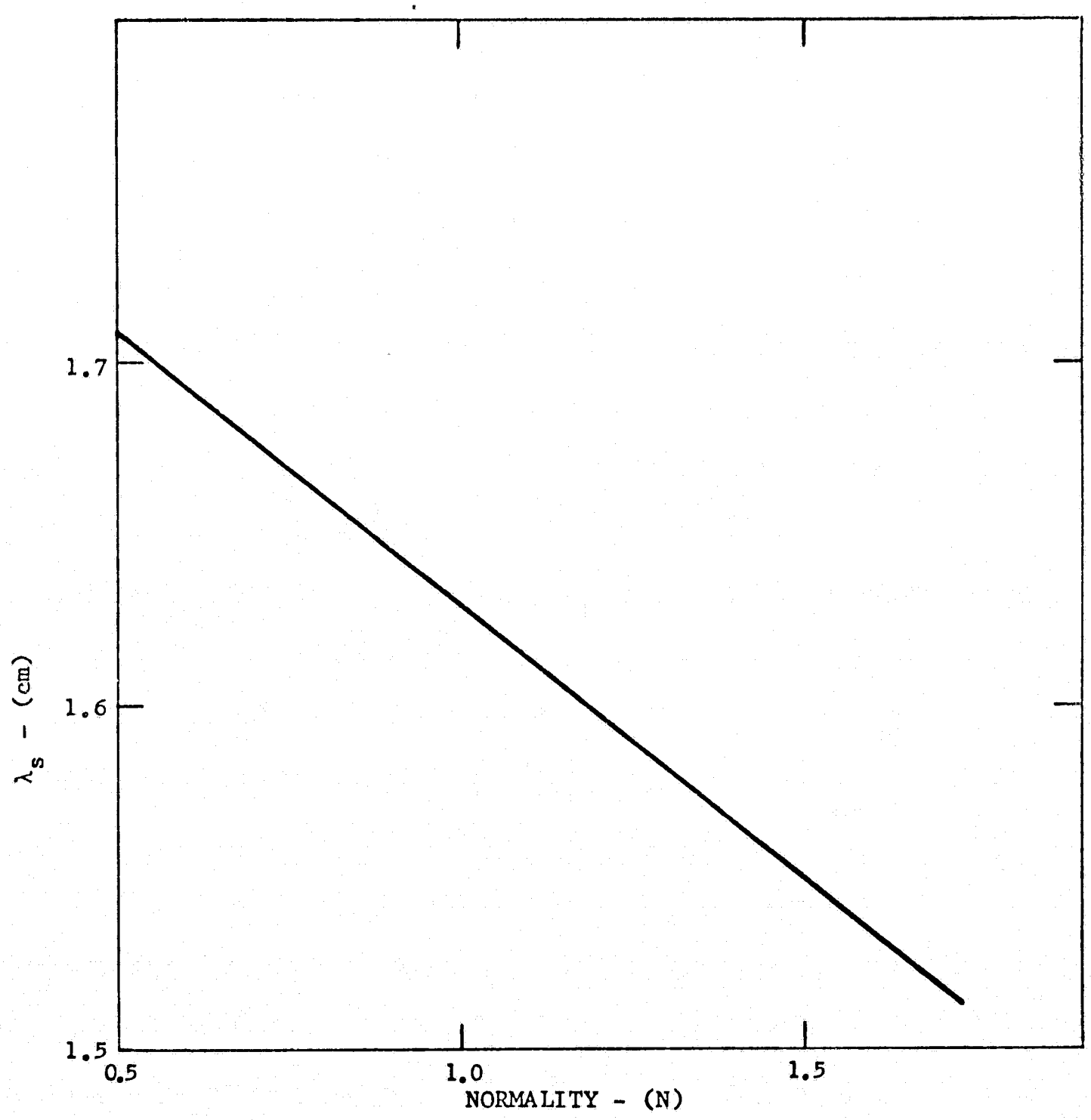

Figure 30 - Variation of λ_s with Normality for NaCl Solution at 21°C.

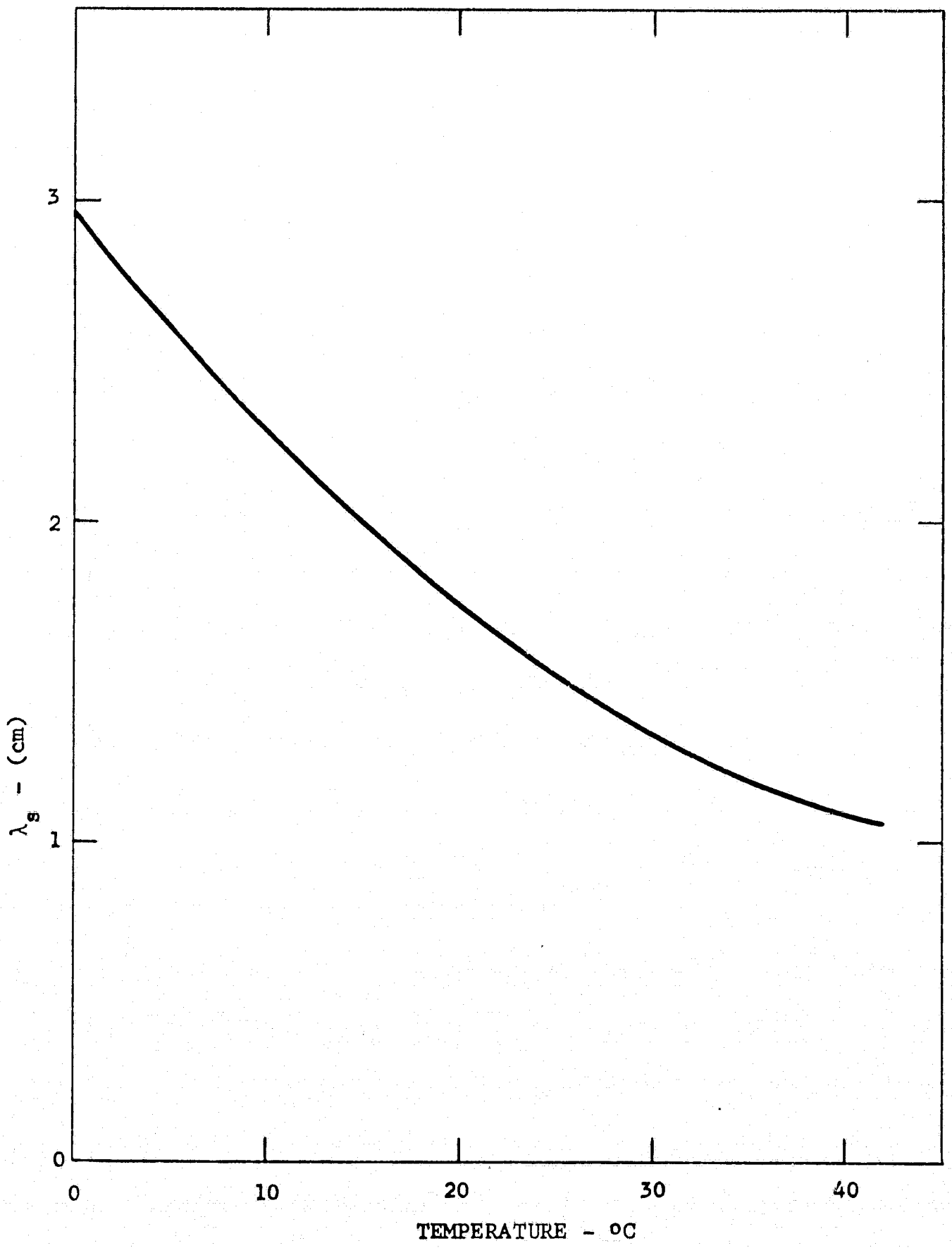

Figure 31 - Variation of λ_s with Temperature at 0.578N NaCl Solution.

The measurement errors in e' and e" are approximately ±15%; thus the above calculated values are considered to be reasonable.

Theoretical emissivities may be obtained with the aid of Equations (45) and (46) which stem from the Fresnel equations.

$$\epsilon_v = \frac{4\,(ae' + be'')\cos\varphi}{(e'\cos\varphi + a)^2 + (e''\cos\varphi + b)^2} \tag{45}$$

$$\epsilon_h = \frac{4a\cos\varphi}{(\cos\varphi + a)^2 + b^2} \tag{46}$$

In which,

$$a = r^{1/2}\cos\gamma \tag{47}$$

$$b = r^{1/2}\sin\gamma \tag{48}$$

$$r = [(e'-\sin^2\varphi)^2 + (e'')^2]^{1/2} \tag{49}$$

$$\gamma = 1/2\,\tan^{-1}\frac{e''}{(e' - \sin^2\varphi)} \tag{50}$$

and φ is the incidence angle.

Figure 32 shows the manner in which permittivity and emissivity vary with salinity, for a NaCl solution, at 19.35 GHz. It is clear that large variations in salinity have a very small effect on permittivity and emissivity.

Figure 33 shows the variation of e', e" and ϵ_h with temperature, at 19.35 GHz. Although e" does not exhibit much change, both e' and ϵ_h show considerable variation with temperature, with an inverse relationship applying to the emissivity data. This is also evident from an examination of vertical incidence emissivities in the plots appearing in Figures 34 thru' 36. The plots also show that the horizontally polarized component of emissivity is reduced by approximately 0.13 in the angular interval 0 - 50 degrees. At a surface temperature of 290°K, this would represent a reduction of approximately 38°K in brightness temperature, under clear sky conditions.

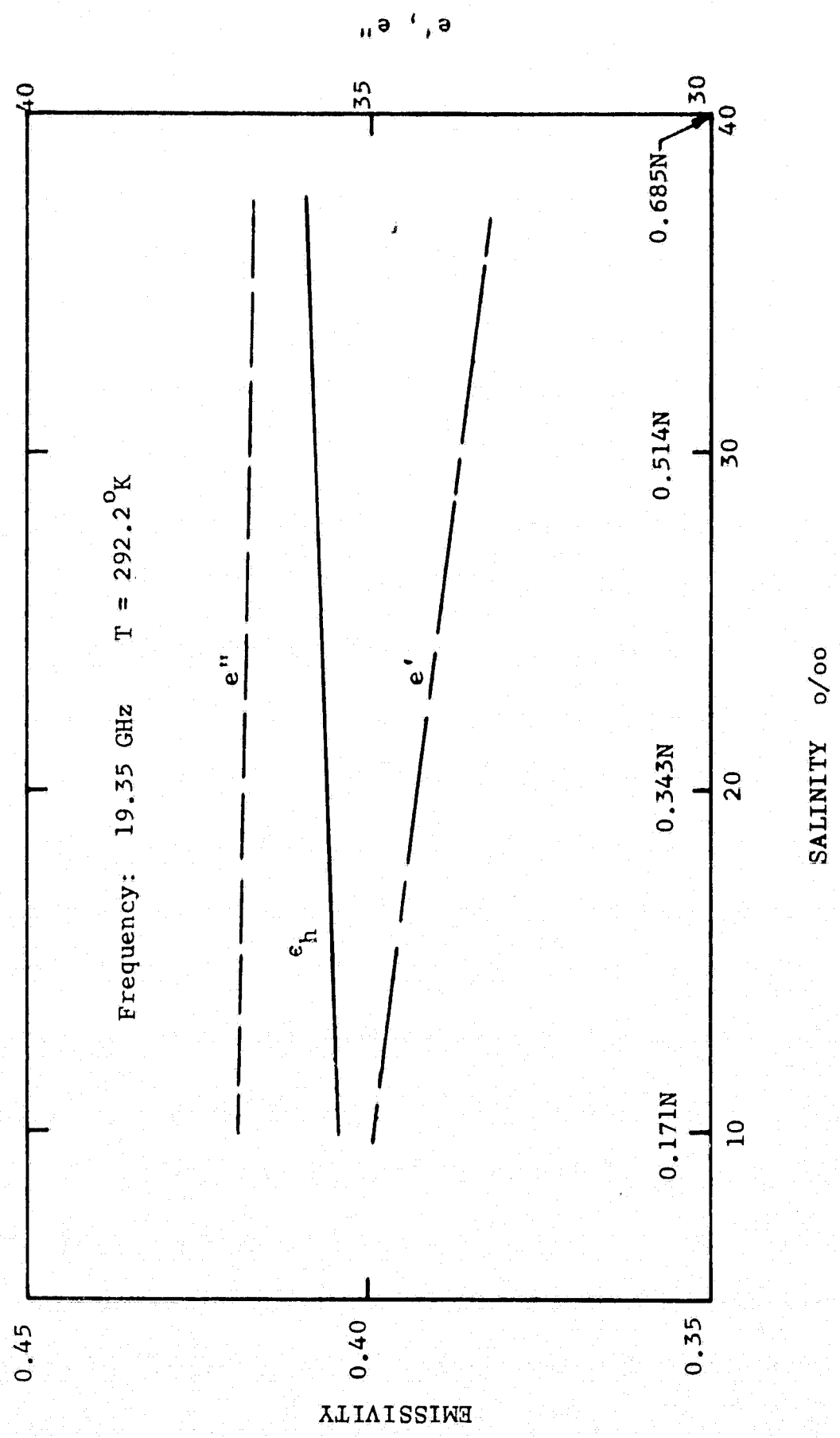

Figure 32 - Variation of Emissivity and Permittivity with Salinity for a NaCl Solution.

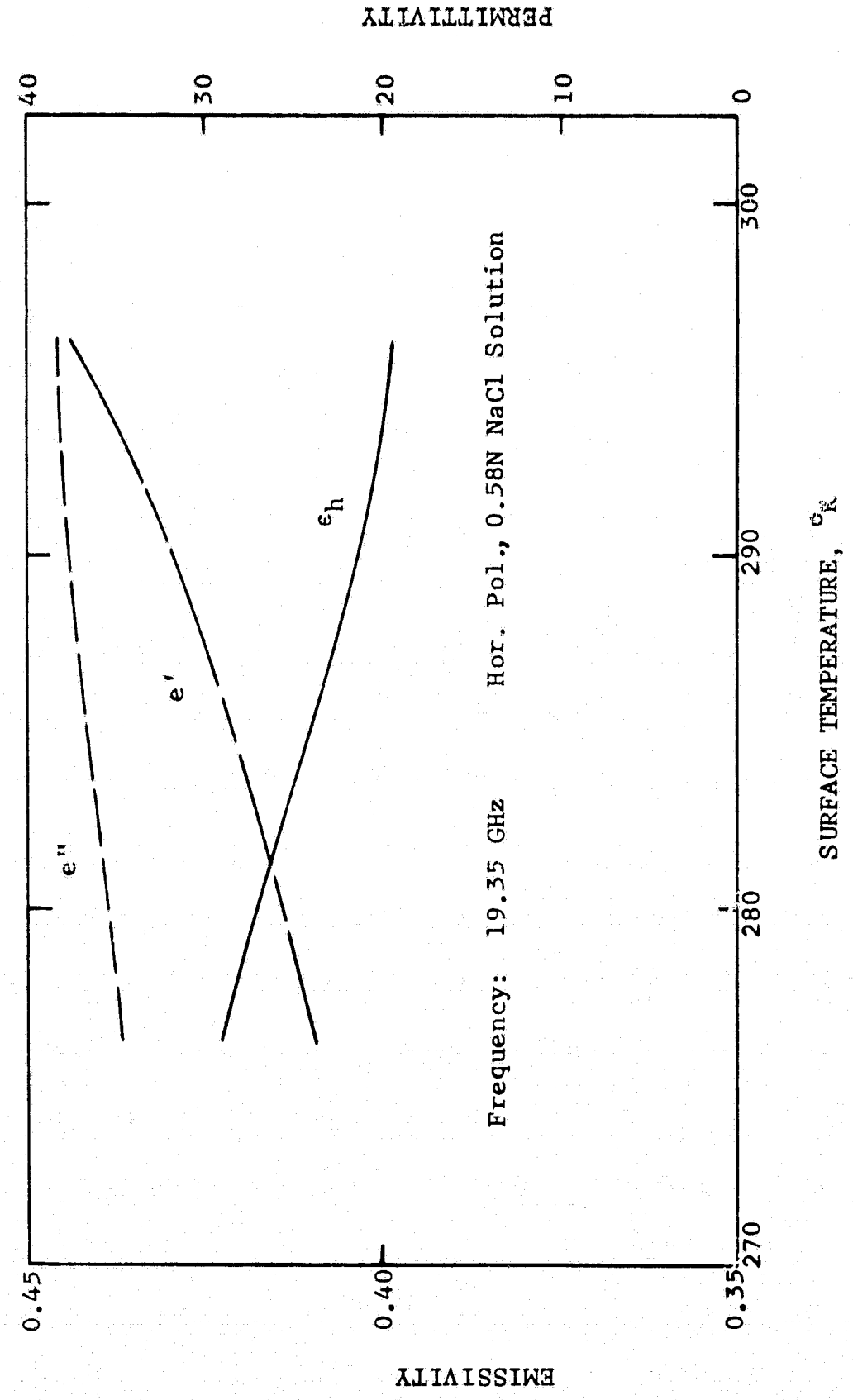

Figure 33 - Variation of Emissivity and Permittivity with Temperature.

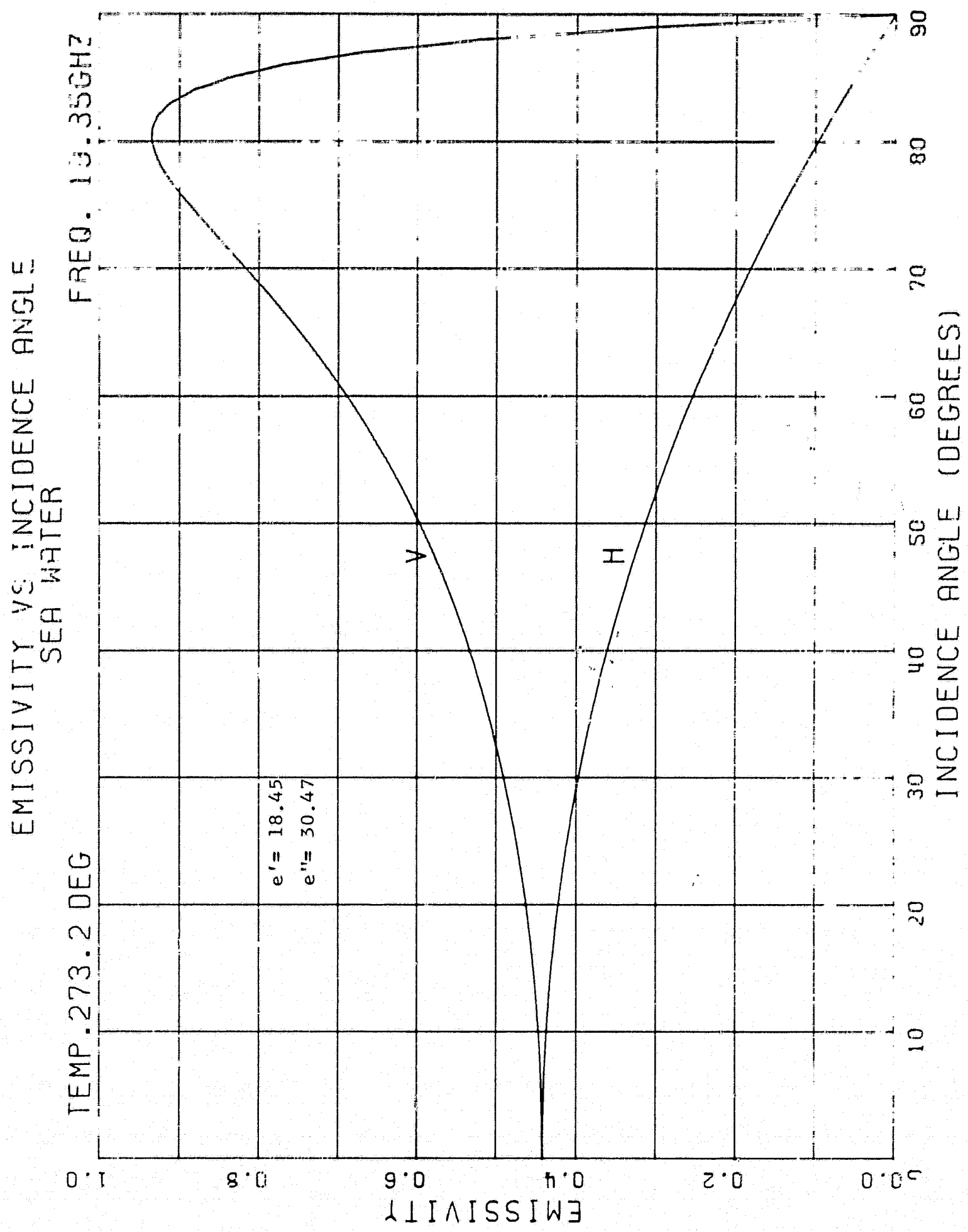

Figure 34 - Theoretical Emissivities of Sea Water at 19.35 GHz, T = 273.2 ^{o}K.

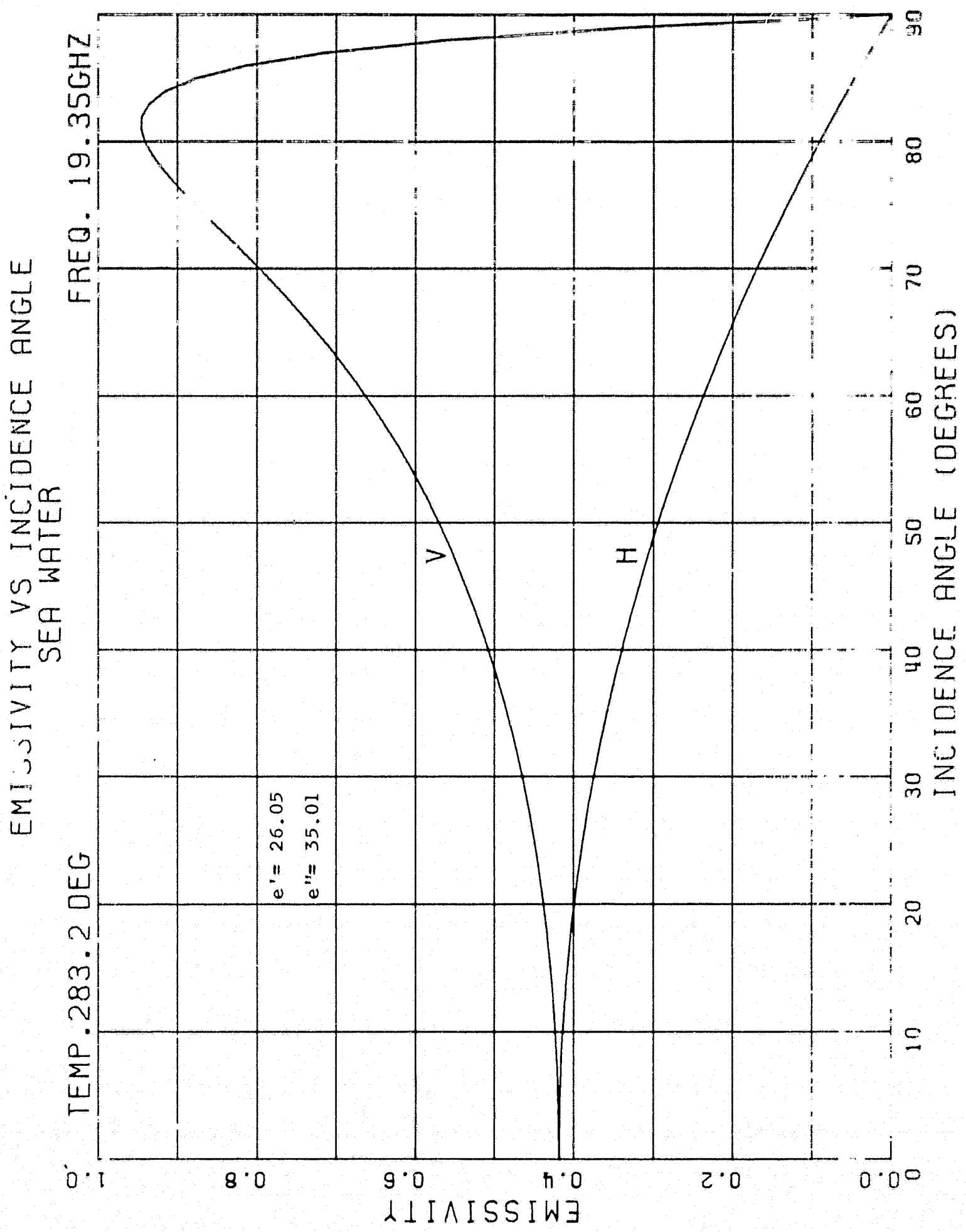

Figure 35 - Theoretical Emissivities of Sea Water at 19.35 GHz, T = 283.2°K.

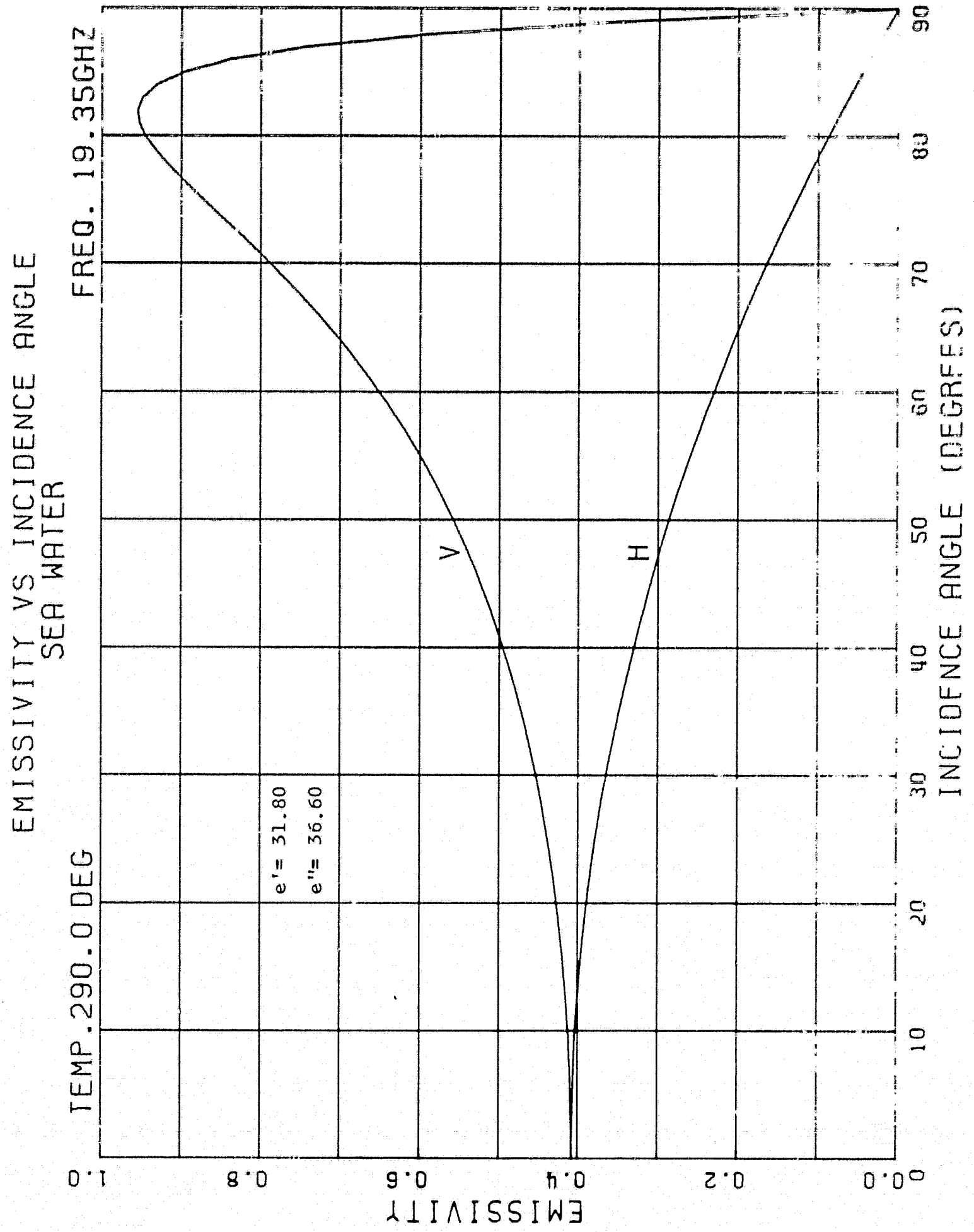

Figure 36 - Theoretical Emissivities of Sea Water at 19.35 GHz, T = 290.0°K.

2. Dielectric Permittivities and Emissivities of Solid Materials

An examination of topographic maps, covering the selected portion of Flight 2, shows that most of the flight track consists of bare desert, with a relatively small portion covered by vegetation (see Figures 7, 8 and 9). In the absence of specific information, it was assumed that the bare desert consists of a sandy soil. The emissivities of sandy soil have been calculated using the dielectric data of von Hippel (1954) at 25°C, relevant portions of which are given below.

Frequency ⟶	0.3 GHz	3 GHz	10 GHz
Real part of dielectric permittivity, e'	2.55	2.55	2.53
Loss tangent, tan δ	0.0100	0.0062	0.0036

The imaginary part of the dielectric permittivity may be obtained from the relation,

$$e'' = e' \tan \delta \qquad (51)$$

Extrapolation of the above data to 19.35 GHz, yields the following values: $e' = 2.50$ and $e'' = 0.0083$. The specular vertical and horizontal emissivities were calculated using Equations (45) and (46), respectively. Plots of these data are shown in Figure 37. At vertical incidence, the emissivity is quite high, having a value close to 0.95. Thus, the brightness temperatures, near vertical incidence, should lie close to the thermodynamic temperature.

Since soils exhibit wide variations in composition and, hence, permittivity, data was generated to show the relationship between emissivity and permittivity.

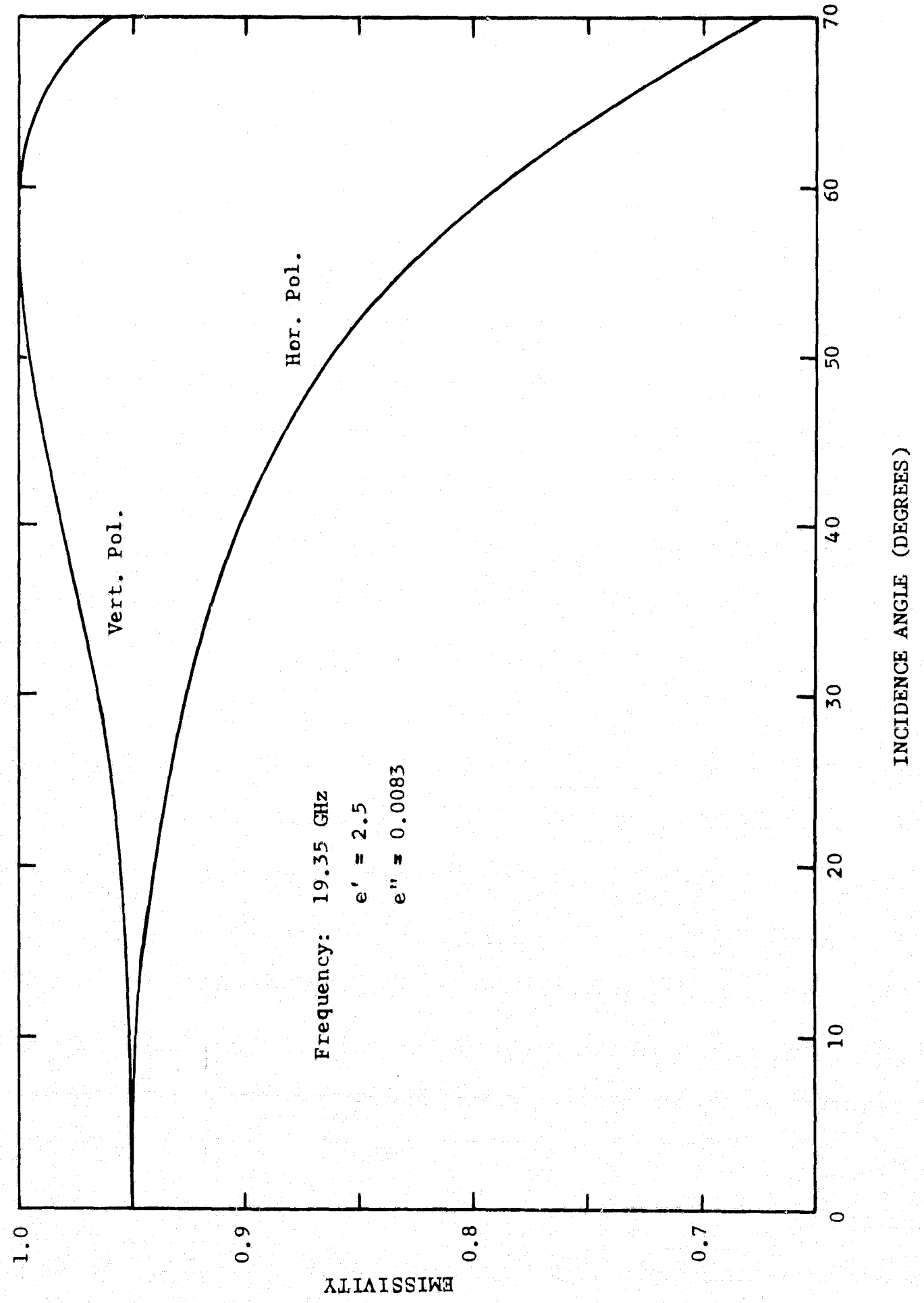

Figure 37 - Theoretical Emissivity Vs. Incidence Angle - Bare Dry Sandy Soil.

This is shown in Figure 38. It is clear that relatively small changes in e' can produce marked shifts in emissivity i.e., an increase in e' from 2.5 to 6.5 results in a reduction in ϵ from 0.95 to 0.80. At a temperature of 290°K, this would represent a reduction in brightness temperature of approximately 44°K.

It is possible that certain parts of the desert terrain, along the flight track, consisted of moist soil. If so, it is worth considering the radiative properties of such a material. Von Hippel presents data at 10 GHz, for sandy soil with a 16.8 percent moisture content, by weight. The dielectric permittivity of this material is, e' = 13.0 and e" = 3.75. Due to an insufficient amount of information on the frequency dependence of moist soil permittivities, it is not possible to extrapolate this data to 19.35 GHz. It will, therefore, be assumed that the above values apply at this frequency. The error in this assumption is considered to be small, due to the fact that a large change in the dielectric permittivity of fresh water produces a rather small change in emissivity. For example, at 10 GHz and a temperature of 290°K, e' = 58.8 and e" = 34.6 for fresh water. At 17 GHz, e' = 39.6 and e" = 37.7. The resultant emissivities, at vertical incidence, are 0.374 and 0.396 at 10 and 17 GHz, respectively. The 0.022 increase in emissivity would represent a brightness temperature increase of approximately 6.5°K in fresh water, at a temperature of 290°K and clear sky conditions. Since the above moist soil contains only 16.8 percent water, the frequency dependence of the emissivity and brightness temperature is expected to be somewhat smaller than is indicated by this example.

Figure 39 shows a plot of theoretical horizontally polarized emissivities for the above moist soil. The moisture has reduced the emissivities by approximately 0.27, referred to dry soil. Thus, a considerable reduction in brightness temperatures will result, compared with those for dry soil.

Vegetation-covered soils should be treated as diffuse surfaces at 19.35 GHz. Since theoretical emissivities are not available on vegetation, this information was derived from independent ground-based measurements. Diffuse emissivities may be derived from measured brightness temperatures by means of the following expression:

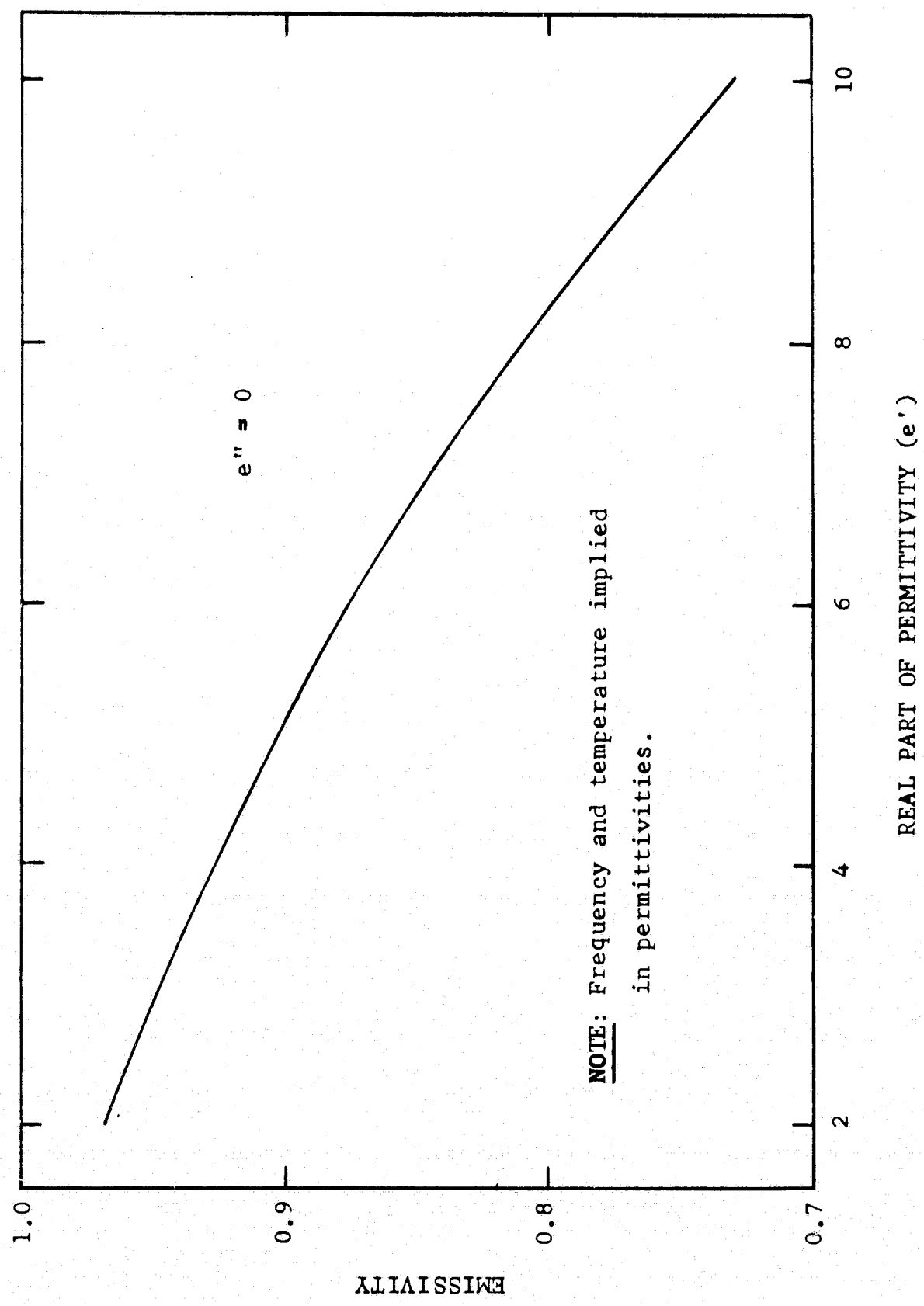

Figure 38 - Variation of Emissivity with Permittivity, For Dry Solid Materials

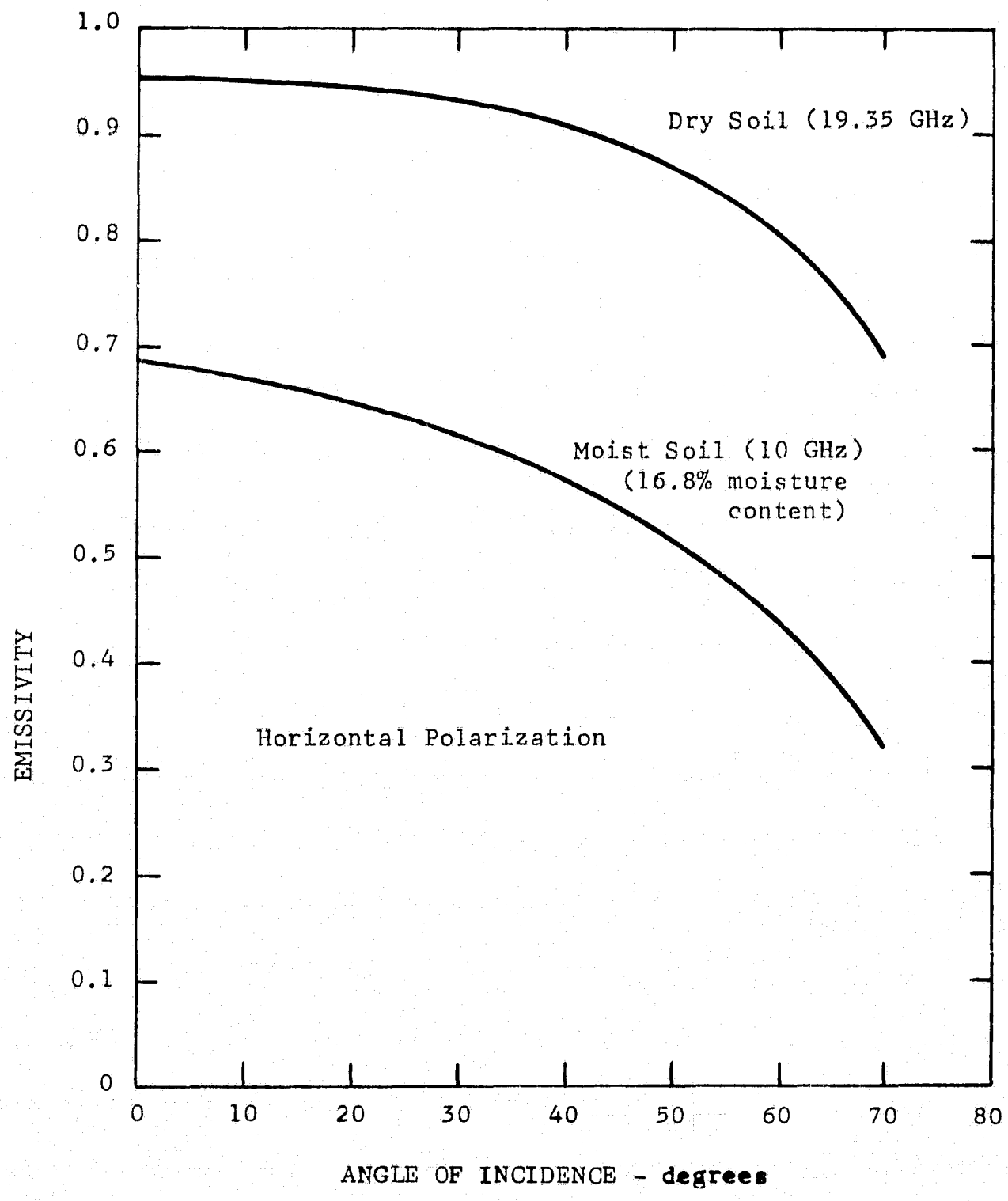

Figure 39 - Theoretical Emissivities of Dry and Moist Soils at Microwave Frequencies.

$$\epsilon_D = \frac{T_B - T_{s,avg.}}{T_G - T_{s,avg.}} \qquad (52)$$

where,

T_B is the observed brightness temperature, ^oK

T_G is the surface temperature, ^oK

and, $T_{s,avg.}$ is the averaged measured sky brightness temperature, from zenith to horizon, ^oK.

Measured brightness temperatures on weed-covered soil were taken from Edgerton (1968). This information is shown reproduced in Figure 40. Referring to the horizontally polarized data near vertical incidence, the average brightness temperature increases from approximately 265^{o}K, at 13.4 GHz, to approximately 283^{o}K at 37 GHz. Thus, an upward shift of approximately 18^{o}K is evident in this frequency interval. Since the change is small compared to the absolute magnitude, linear interpolation is considered reasonable to obtain values at 19.35 GHz. Emissivities derived with the aid of Equation (52) from the interpolated brightness temperatures, are shown plotted in Figure 41. It will be noted that, like the brightness temperatures, the emissivities are essentially independent of viewing angle. The data varies slightly about a mean value of approximately 0.93. Thus, on the average, the emissivities of weed-covered soil are only slightly below those for dry bare soil, over a considerable range of incidence angles.

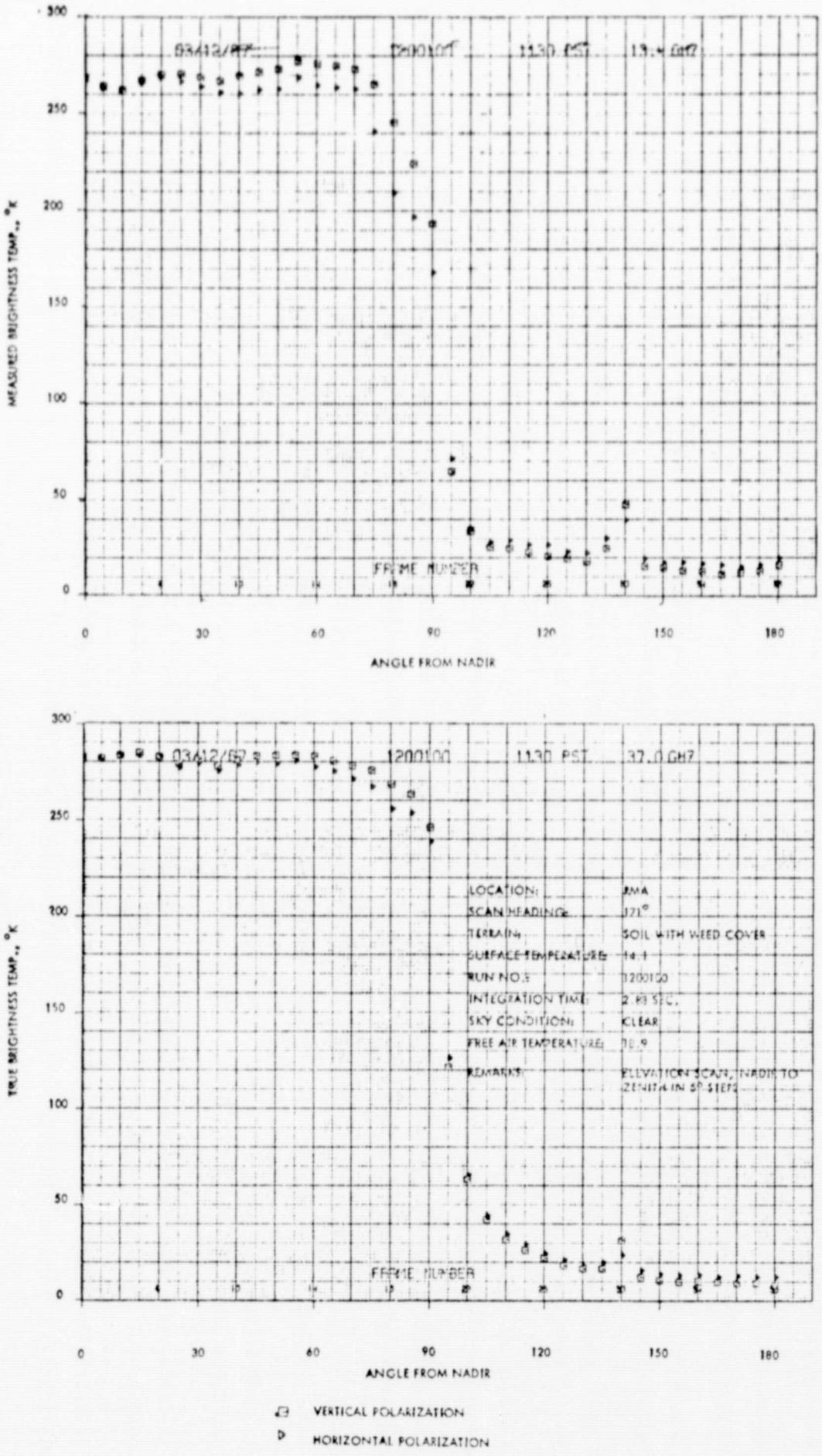

Figure 40 - Measured Brightness Temperatures of Weed-Covered Soil at 13.4 and 37 GHz (after Edgerton et al, 1968).

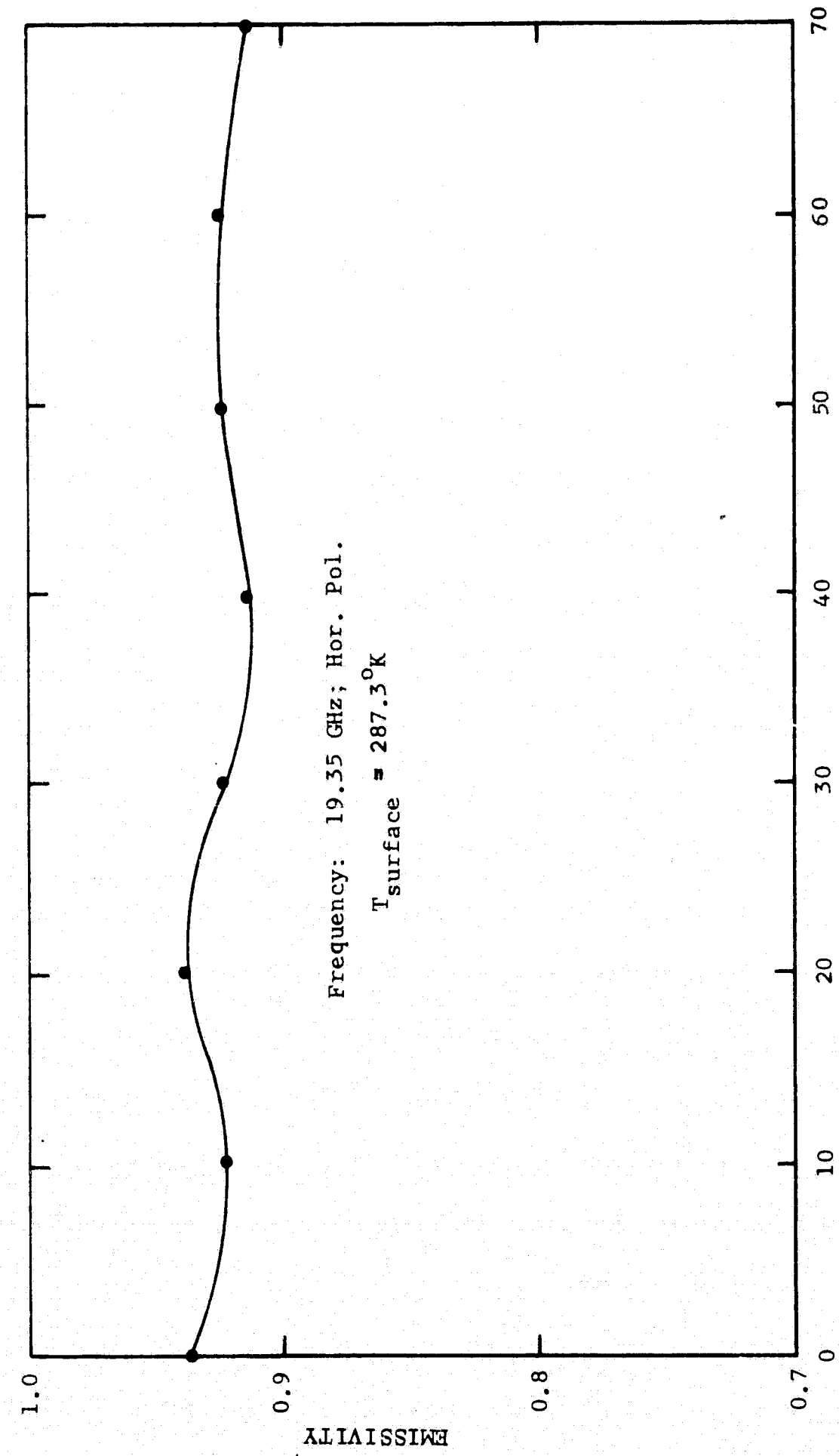

Figure 41 - Diffuse Emissivity Vs. Incidence Angle, Vegetation - Covered Soil.

VI. DETAILED ANALYSIS OF SELECTED DATA CASES

The general procedure used for evaluation of observations of clouds was organized into seven steps. In the order of accomplishment for each case, these steps were as follows:

1) The temperature and water vapor distribution were established.

2) A cloud model was constructed.

3) The ground temperature was determined.

4) Using the above parameters, and an observed brightness temperature for a non-cloudy case, a forced value of surface reflectivity was derived.

5) Using the surface reflectivity of (4), and assuming that the relative humidity reaches 100% in clouds, the cloud density for a given case was varied until the computed brightness temperature matched the observed brightness temperature.

6) If 9.3 GHz information existed, the consistency of the brightness temperature at this frequency was checked using as input the same cloud model as determined in (5).

7) Finally, the RASP program was used to estimate the importance of scattering in the cloud deduced in (5) and (6).

The results of proceeding through the first six steps above, in each of eleven cases in Flights 13, 9 and 8, are summarized in Table VI-1. The observed temperatures at 10-12 μ, 9.35 GHz and 19.35 GHz are listed on the left side; altitudes and surface temperatures are listed next. The latter correspond to temperatures measured by the 10-12 μ channel in the clear case. Derived quantities are recorded on the right side of the Table and include forced values of surface reflectivity as well as theoretical values; computed brightness temperatures for 9.35 and 19.35 GHz; and the integrated water from the vapor and liquid water suspended in the atmosphere.

Table VI-2 lists the results which allow evaluation of the importance of scattering in the clouds deduced from Steps (1) through (6). The Table is

TABLE VI-1 - Summary of Data Simulation Results at Vertical Incidence

FLIGHT and CASE NO.	OBSERVED T_B (^oK)			ALT.	T_G	FORCED REFLECTIVITY VALUES		THEOR. RELECTIV-ITY	COMP. T_B (^oK)		WATER CONTENT		MATERIAL
	MRIR	9.35	19.35	(kFt)	(^oK)	9.35	19.35	19.35	9.35	19.35	VAPOR	CLOUD	
FLIGHT 13-1	282	--	132	36	296.2	--	0.660	0.603	--	132.7	3.51	2.13-03	Sea Water
2	283	--	200	37	296.2	--	0.660	0.603	--	200.5	3.22	6.59-01	
3	262	--	269	37	296.2	--	0.660	0.603	--	270.6	5.17	2.77-00	
4	296	--	120	38	296.2	--	0.660	0.603	--	124.0	2.49	CLEAR	
FLIGHT 9-1	284	--	125	26	284.2	--	0.615	0.590	--	124.9	1.54	CLEAR	Sea Water
2	286	--	145	39	286.2	--	0.600	0.592	--	129.7	1.54	CLEAR	
3	252	--	160	39	284.2	--	0.615	0.590	--	159.4	3.46	1.41-01	
4	246	--	247	39	284.2	--	0.615	0.590	--	247.4	4.06	1.22-00	
FLIGHT 8-1	276	102	120	5.6	276.2	0.650	0.620	0.577	101.2	119.1	1.84	CLEAR	Sea Water
2	259	122	159	13.0	276.2	0.630	0.600	0.577	118.2	164.7	2.13	1.92-01	
3	278	119	156	2.1	278.0	0.650	0.620	0.579	113.3	159.2	2.13	4.00-01	
FLIGHT 2-1	306.7	--	276.3	39.2	300.0	--	--	0.051	--	284.9	0.82	CLEAR	Bare Dry Sandy Soil
2	269.0	--	278.0	39.2	300.0	--	--	0.051	--	285.5	--	STR.CU.	
3	306.7	230.8	276.3	39.2	300.0	--	--	0.320	--	208.0	0.82	CLEAR	Moist Soil
4	269.0	228.0	278.0	39.2	300.0	--	--	0.320	--	218.0	--	STR.CU.	
	--	--	--	39.2	287.3	--	--	0.064	--	269.6	0.82	CLEAR	Vegeta-tion
	268.2	229.5	267.1	39.2	287.3	--	--	0.064	--	271.4	--	STR.CU.	

Table VI-2 Scattering Properties for Derived Cloud Models

CASE	m(max) (gm/m^3)	MODEL PARAMETERS			19.35 GHz		9.35 GHz		SCALE LENGTH (km)
		$r_c(\mu)$	C_1	C_2	$\tilde{\omega}_o$	d_s(km)	$\tilde{\omega}_o$	d_s(km)	
FLIGHT 13-1	0.01	10.0	6.0	1.0	3.46-06	3.13+07	1.58-06	4.81+08	2.0
2	6.00	20.0	5.0	0.8	6.06-05	3.12+03	1.88-05	5.37+04	1.0
3	8.00	400.	5.0	0.6	2.20-01	1.44-01	6.75-02	1.97+00	3.0
FLIGHT 9-3	0.35	15.0	6.0	1.0	1.15-05	2.88+05	5.23-06	4.46+06	4.0
4	2.30	400.	5.0	0.6	2.20-01	5.00-01	6.75-02	6.84+00	4.0
FLIGHT 8-2	0.60	10.0	6.0	1.0	3.46-06	4.17+07	1.58-06	6.41+06	3.2
3	1.25	10.0	6.0	1.0	3.46-06	2.61+05	1.58-06	4.01+06	3.2

the result of accomplishing Step (7).

On the left Table VI-2 is listed the maximum condensed water density that a cloud model exhibits. That is, for Flight 13, Case 1, the maximum cloud water density was 0.01 g/m^3. For Flight 13, Case 3, the maximum was 8.00 g/m^3. All other parts of the cloud in Case 3 were scaled down in proportion to the model depicted in Figure 22. The next three columns give the necessary data to construct the Deirmendjian droplet size distribution which was assumed to represent the cloud in question. The two columns under 19.35 GHz and 9.35 GHz are the scattering albedo ($\tilde{\omega}_o$) and the scattering depth (d_s). On the right side of the Table is listed a scale length applicable to the clouds analyzed, for convenience of comparison to the scattering depth.

Table VI-3 is presented as a further aid for interpretation of data generated by the cloud model computations. This Table contains informaion which, with information already presented, can be used to specify each of the variables in the following equation:

$$T_B\,(\text{aircraft}) = \left[(1-R)T_G + R(T_{atm} + T_{sky}\ t_{atm})_{surf}\right] t_{airc} + (T_{atm})_{airc} \qquad (53)$$

For simplicity, this equation will be expressed as follows:

$$T_B(\text{aircraft}) = \left[\epsilon T_G + (1-\epsilon)\ T_{s,down}\right] t_f + T_{s,up} \qquad (54)$$

in which,

ϵ is the emissivity of the surface.

$(1-\epsilon)$ is the reflectivity of a specular surface, under conditions of thermal equilibrium.

$T_{s,down}$ is the sky brightness temperature, as viewed from the surface, ^oK.

t_f is the atmospheric transmission factor for that part of the atmosphere lying between the surface and the airborne radiometer.

Table VI-3 Summary of Various Contributing Sources of Radiation to Brightness Temperature at the Airborne Radiometer.

FLIGHT and CASE NO.	19.35 GHz T_B(Air) ^oK $T_{s,down}$	19.35 GHz T_B(Air) ^oK $T_{s,up}$	19.35 GHz Transmission Factor	9.3 GHz T_B(Air) ^oK $T_{s,down}$	9.3 GHz T_B(Air) ^oK $T_{s,up}$	9.3 GHz Transmission Factor	Cloud Scale Factor	Surface Material
FLIGHT 13-1	27.0	24.2	0.914	6.6	3.7	0.988	0.01	Sea Water
13-2	91.8	89.5	0.689	19.1	22.3	0.922	6.00	
13-3	260.8	259.7	0.040	148.1	144.5	0.478	8.00	
13-4	19.9	17.1	0.940	6.0	3.1	0.990	Clear	
FLIGHT 9-1	14.6	11.4	0.960	5.7	2.6	0.991	Clear	Sea Water
9-2	14.6	11.7	0.958	5.7	2.8	0.991	Clear	
9-3	45.9	43.3	0.844	11.9	9.0	0.970	0.35	
9-4	166.4	162.6	0.399	53.2	50.6	0.816	2.30	
FLIGHT 8-1	16.4	7.0	Atmosphere: 0.951 Aircraft: 0.977	5.8	1.2	Atmosphere: 0.990 Aircraft: 0.999		Sea Water
8-2	52.4	48.1 From Aircraft	0.816	14.9	11.3	0.958	0.60	
8-3	85.4	2.9	Atmosphere: 0.695 Aircraft: 0.990	24.2	0.4	Atmosphere: 0.899 Aircraft: 0.999	1.25	
FLIGHT 2-1	6.7	6.7	0.976	---	---	---	Clear	Dry Soil
2-2	25.0	25.0	0.911	---	---	---		
2-3	6.7	6.7	0.976	---	---	---	Clear	Moist Soil
2-4	25.0	25.0	0.911	---	---	---		
2-5	6.7	6.7	0.976	---	---	---	Clear	Vegetation-Covered Soil
2-6	25.0	25.0	0.911	---	---	---		

and $T_{s\ up}$ is the sky brightness temperature of that part of the atmosphere between the surface and the radiometer (radiating upward to the radiometer), ^{o}K.

Comparing Equation (54) with (53), $T_{s,down}$ represents the quantity $(T_{atm.} + T_{sky}\ t_{atm})_{surf.}$. The term $T_{s,up}$ represents the quantity $(T_{atm.})_{airc.}$ Finally, the transmission factor, t_f, represents the term $t_{airc.}$

Values of observed brightness temperature, T_B, surface temperatures, T_G, and surface reflectivities are given in Table VI-1. If the effect of changes in any of the environmental variables is desired, Equation ( ) can be readily applied to evaluate them.

A. FLIGHT 13, 1967

Four separate observations were investigated in detail for Flight 13, in 1967. The clear air case is represented by Case 4 and is considered first because the reflectivity used for all other cases of Flight 13 has been determined from this case.

Figure 42 is presented to allow insight into the properties of the clear atmosphere of Flight 13. It provides some indication of the effectiveness of the same density of absorber (water vapor, oxygen, cloud) under different ambient conditions found in the tropical atmosphere of Flight 13. Simple opacity weighting functions are shown for the three important absorbers. They can be written in the following forms:

$$\left(WF_{H_2O}\right)_i = \frac{\left(\gamma_{H_2O}\right)_i}{\rho_i} \quad \text{nepers } m^{-1} \ (g/m^3)^{-1} \tag{55}$$

$$\left(WF_{O_2}\right)_i = \frac{\left(\gamma_{O_2}\right)_i}{P_i} \quad \text{nepers } m^{-1} \ mb^{-1} \tag{56}$$

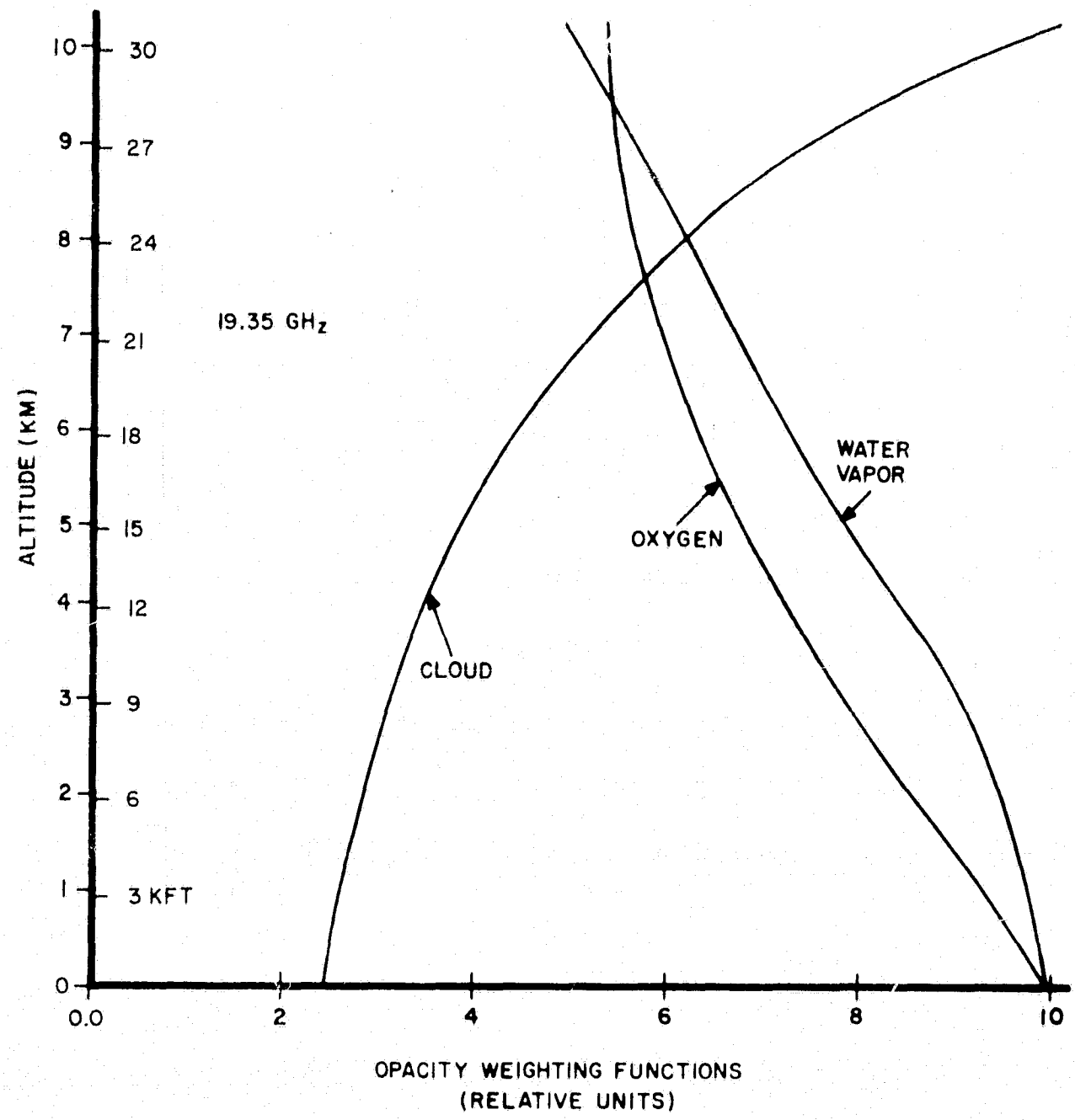

Figure 42 - Opacity Weighting Functions for Water Vapor, Oxygen and Cloud.

$$\left(WF_{CL}\right)_i = \frac{\left(\gamma_{CL}\right)_i}{M_i} \quad \text{nepers } m^{-1} \ (g/m^3)^{-1} \tag{57}$$

in which, the γ's represent absorption coefficients at level i; ρ_i is the water vapor density at level i; P_i is the total atmospheric pressure at level i; and M_i is the liquid water density at level i.

The results of computing Equations (55), (56) and (57) at each level and normalizing the values obtained such that the largest value computed for each absorber is always equal to unity are plotted in Figure 43. The curves clearly show that water vapor has an anomalous region near the surface, in which its effectiveness to absorb radiation does not change much. Above about one (1) kilometer its effectiveness diminishes about 10% of its surface value for every 2 kilometer rise into the atmosphere.

The oxygen curve is more regular than the water vapor curve. The rate of decline in effectiveness with height of a fixed amount of oxygen gradually decreases with height.

Perhaps most interesting of the three curves is the weighting function for cloud absorption. It may be written more completely than in Equation (57), but still in an unnormalized form, as follows:

$$\left(WF_{CL}\right)_i = \frac{10^{[0.0122\ (291-T)\ -4\ ]}}{\lambda^2} \quad \text{nepers } m^{-1} \ (g/m^3)^{-1} \tag{58}$$

The curve in Figure 43 is therefore the result of the temperature change with height alone. The colder the temperature, the more effective clouds are in absorbing radiation.

In order to better understand the origin of the signals computed from the various cloud models, curves have been drawn detailing the origin of the radiation. For Flight 13, Figures, 43, 44 and 45 give the cumulative percentage energy received at the aircraft from water vapor, oxygen, and clouds as a function of height for Cases 1, 2, and 3, respectively.

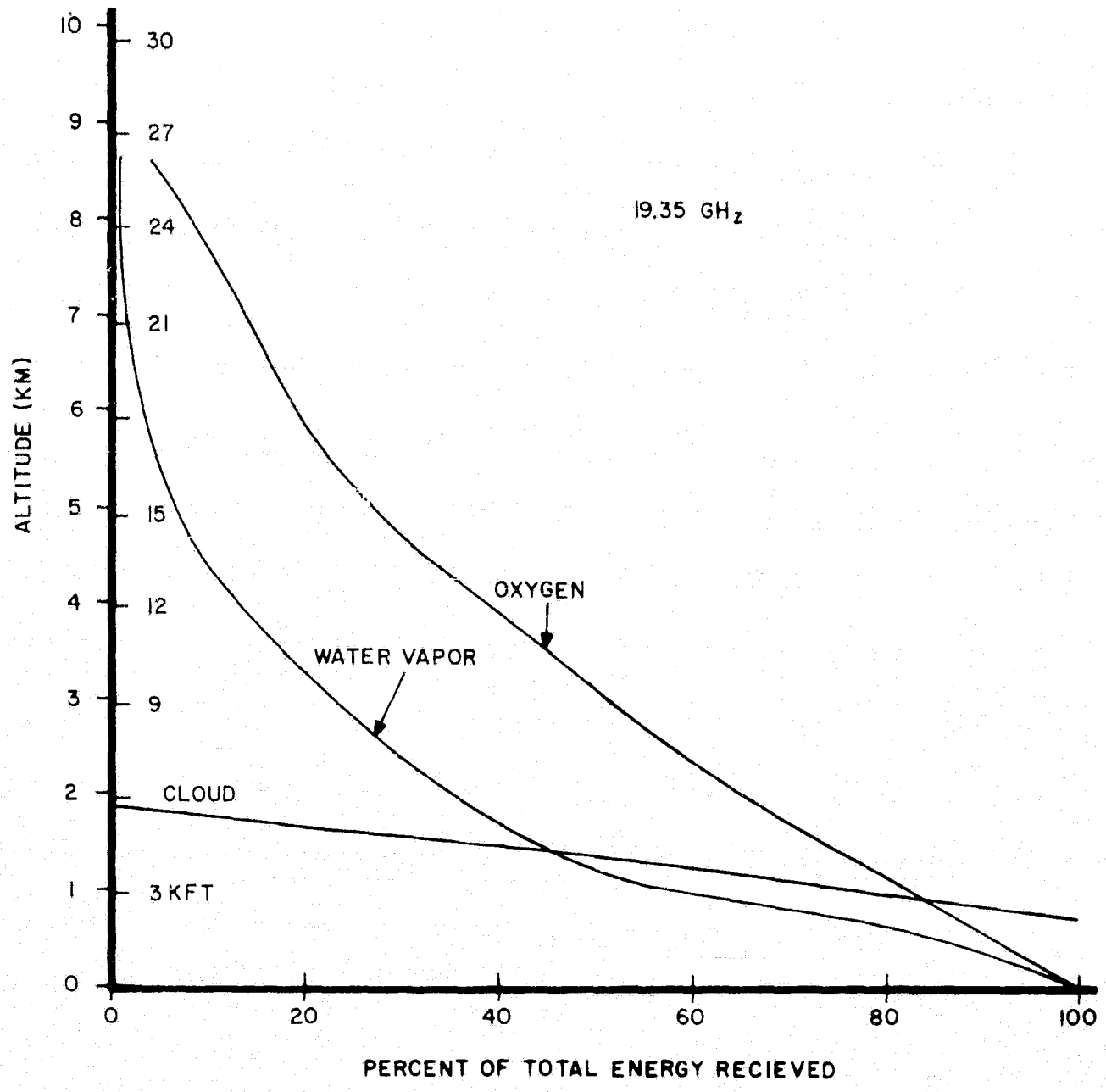

Figure 43 - Percent of Total Energy Received at the Aircraft as a Function of Altitude and Absorber. Flight 13, Case 1.

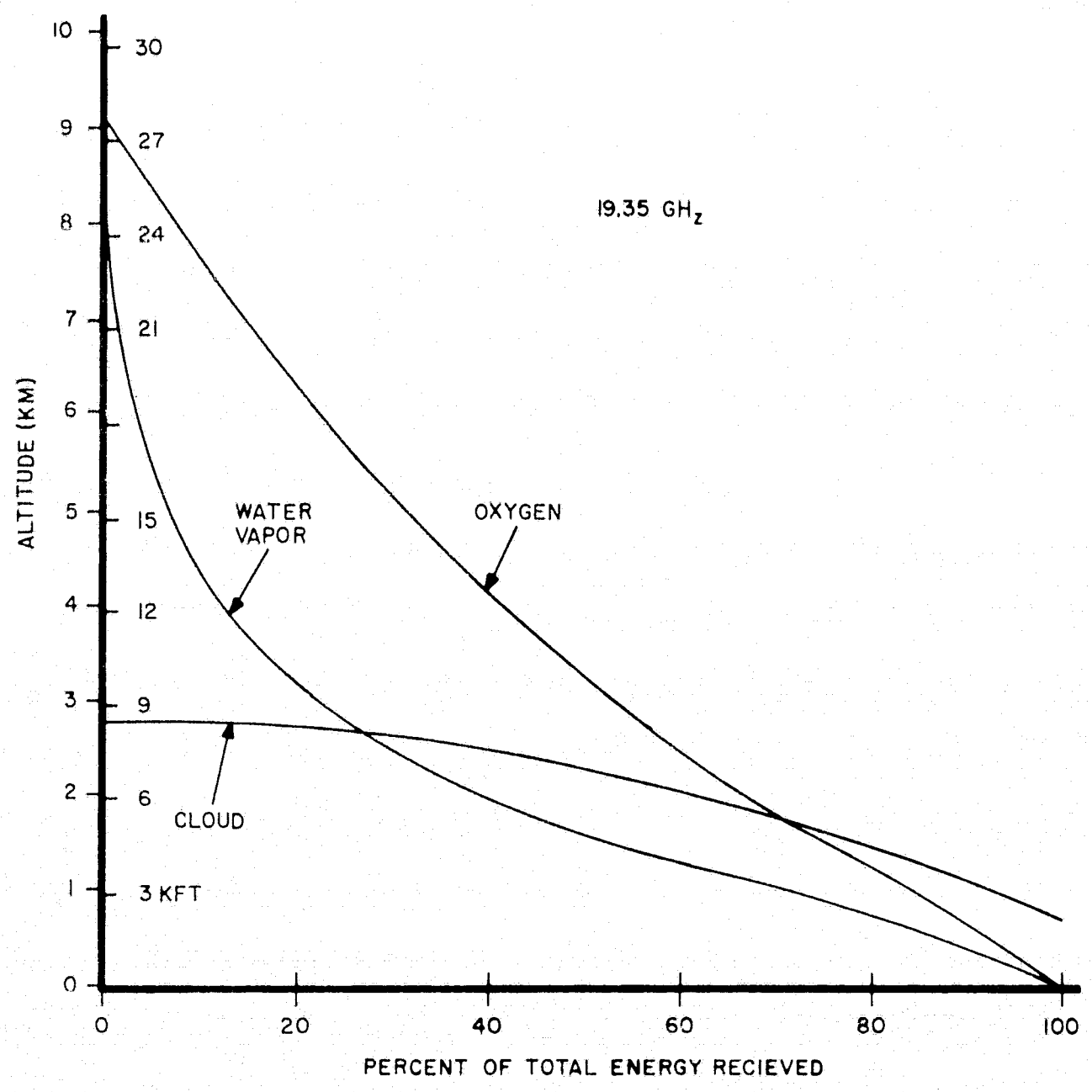

Figure 44 - Percent of Total Energy Received at the Aircraft as a Function of Altitude and Absorber. Flight 13, Case 2.

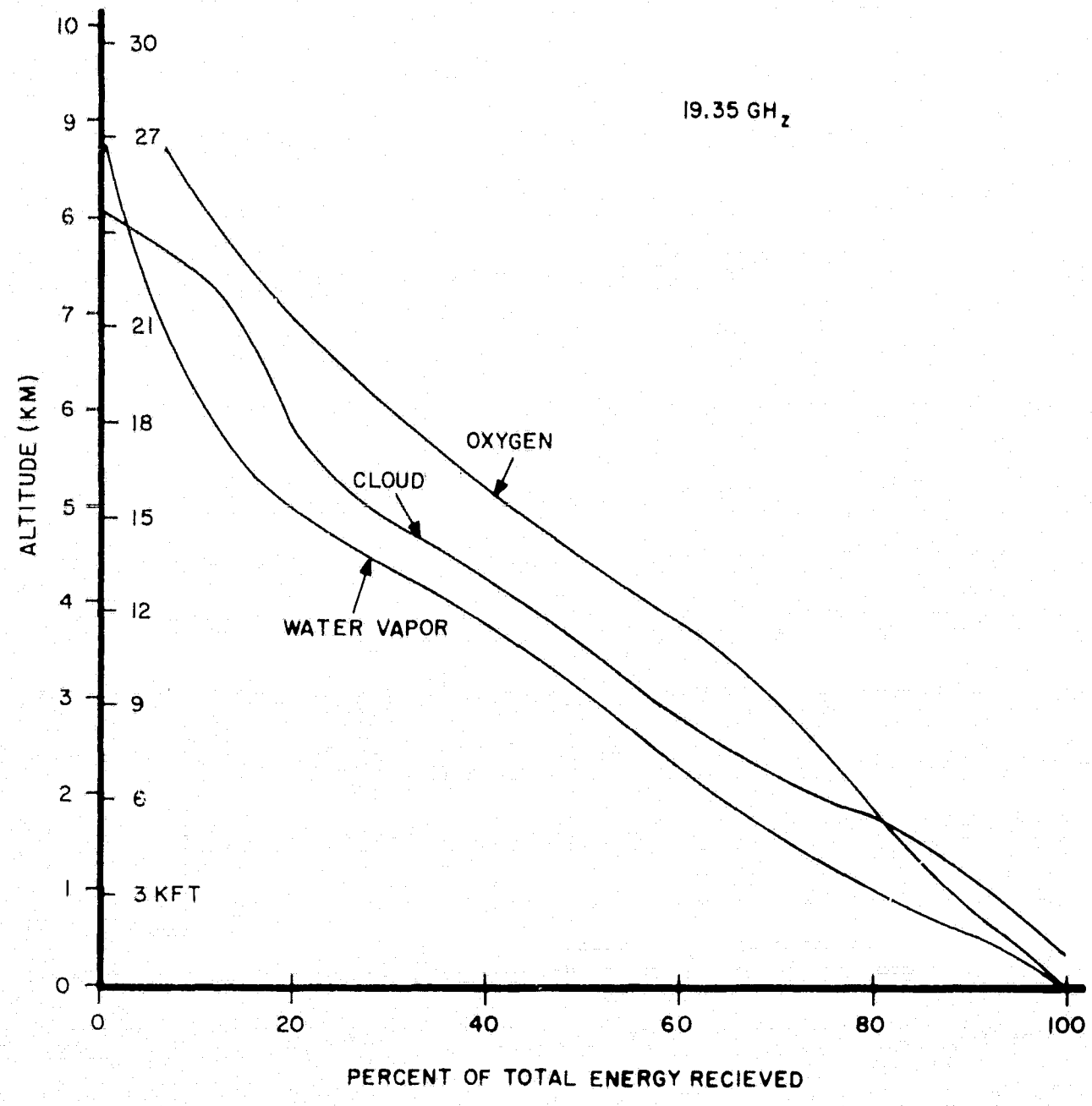

Figure 45 - Percent of Total Energy Received at the Aircraft as a Function of Altitude and Absorber. Flight 13, Case 3.

For Case 1, the cloud was shallow and transparent. Therefore, oxygen, water vapor and the surface dominate the atmospheric contribution and are little affected by the cloud at 800 to 1900 meters. In fact, from Table VI-4, it is evident that the total contribution of the cloud is only 0.4°K, indicating that this frequency is not very sensitive to stratocumulus having the modeled characteristics. Figure 43 furnishes details of Case 1.

It should be pointed out that the contributions included in Table VI-4 have the following meaning: the water vapor and oxygen contributions include all of the energy from these constituents reaching the antenna directly with no reflections, plus energy which has originated in the atmosphere below the aircraft, which has traveled to the surface and has been reflected back to the radiometer. The same is true of the cloud contribution. The surface contribution is the term, ϵT_G, modified by the atmospheric transmission factor, t_f. The contribution from above the radiometer is the energy originating from the galactic background and whatever atmosphere exists above the aircraft. These radiations pass down to the surface and are reflected back to the radiometer.

Information from Case 2, studied from Flight 13, is shown in Figure 44. From Table VI-4, it is evident that the cloud modeled for this case dominates the received radiation. Over 50% of the radiation originates in the cloud and, because of its opacity, the surface term is reduced from the stratocumulus case of 92.1°K to the present 69.3°K. The contribution from water vapor is reduced even though more water vapor is present (See Table VI-1). From Table VI-2, the scattering depth remains safely above the cloud scale length (3.12×10^3 km versus 1 km) but this may be misleading because of the droplet size distribution chosen.

Case 3 of Flight 13 represents the most saturated condition measured at 19.35 GHz. The maximum condensed water density needed to reach 270.6°K was 8.0 g/m^3 (Table VI-2). This is a very dense cloud. It is near the limit of densities seen in any cloud. Further, the scattering depth (See Table VI-2) for our approximate evaluation, indicates that one cannot properly apply the simple absorption theory to this cloud. Significant scattering, no doubt, occurs and its exact effects are unknown.

Nevertheless, Figure 45 is presented as though all of the limitations

Table VI-4 - Contributions From Individual Sources At 19.35 GHz to the Total Brightness Temperature Computed at the Aircraft.

FLIGHT AND CASE NO.	H_2O	O_2	CLOUD	SURFACE	ABOVE AIRC.	TOTAL
Flight 13-1	34.7°K	3.8°K	0.4°K	92.1°K	1.7°K	132.7°K
2	24.6	3.1	102.6	69.3	0.9	200.5
3	15.2	1.4	234.9	19.0	0.1	270.6
4	23.8	3.9	----	94.6	1.7	124.0
Flight 9-1	14.4	3.7	----	104.9	1.9	124.9
2	10.1	2.6	----	131.0	1.3	145.0
3	29.1	3.6	33.0	92.4	1.3	159.4
4	17.9	2.1	183.3	43.8	0.3	247.4
Flight 8-1	9.9	1.3	----	102.3	5.5	119.1
2	15.6	2.3	54.0	90.8	2.0	164.7
3	4.1	0.5	----	104.6	50.1	159.3
Flight 2-1	5.2	2.2	----	263.5	0.3	271.2

noted above did not exist. The contributions of water vapor and oxygen are reduced substantially and the origin of the energy from each is affected by the cloud opacity. The surface contribution is very small, when compared with the clear atmosphere contribution in Case 4.

Case 4 of Flight 13 is a clear atmosphere case. The percentage contribution of water vapor and oxygen are not plotted. Their individual contributions are found, however, in Table VI-4.

Table VI-5 shows a comparison of calculated, derived and observed brightness temperatures for Flights 13, 9 and 8. Only Flight 13 data will be discussed here; the other Flights will be covered in Subsections B and C, respectively. Specular emissivities were calculated for a 0.578 normal NaCl solution, at the surface temperature recorded by the MRIR. Atmospheric radiation temperatures and transmission factors, listed in Table VI-5 were calculated for the atmospheric conditions described above. The "Derived" brightness temperatures are those listed in Table VI-1, in the column headed "COMP. T_B". Perhaps the most interesting columns in Table VI-5 are the final two, since they furnish a comparison of theoretical and observed T_B's. Referring to the second-last column, it will be noted that the best agreement between calculated and observed data is represented by Case 3 - the heavy cloud situation. Since, in general, theoretical T_B's tend to be lower than measured values, due to the assumption of a specular surface, the theoretical value is considered to be high - an observation which applies equally well to the remaining three cases. Thus, it is likely that the atmospheric models are on the heavy side.

Figure 46 shows a comparison of theoretical and observed sea water brightness temperatures, for Flight 13, Cases 1 and 4. The plotted data substantiates the comments made above, concerning the somewhat high atmospheric radiation temperatures. In quantitative terms, the theoretical T_B's would be expected to lie approximately $10^{o}K$ below the observed values, instead of $15^{o}K$ above them, for a calm sea. This is brought out in Porter (1969) at a frequency of 16.5 GHz.

Table VI-5 Comparison of Calculated, Derived and Observed Brightness Temperatures over Ocean Surfaces

Frequency: 19.35 GHz Hor. Pol. Vert. Incidence

Flight and Case No.	T (°K)	Emissivity (Specular)	$T_{s,down}$ (°K)	$T_{s,up}$ (°K)	t_f	T_B(°K) (calculated)	T_B(°K) (Derived)	T_B(°K) (Observed)	$T_{B(calc.)}-T_{B(obs.)}$ (°K)	Deviation* (%)
Flight 13-1	296.2	0.397	27.0	24.2	0.914	146.6	132.7	132	14.6	11.1
2	296.2	0.397	91.8	89.5	0.689	208.7	200.5	200	8.7	4.4
3	296.2	0.397	260.8	259.7	0.040	271.8	270.6	269	2.8	1.0
4	296.2	0.397	19.9	17.1	0.940	138.9	124.0	120	18.9	15.8
Flight 9-1	284.2	0.410	14.6	11.4	0.960	131.5	124.9	125	6.5	5.2
2	286.2	0.441	14.6	11.7	0.958	140.4	129.7	145	-3.6	-2.5
3	284.2	0.410	45.9	43.3	0.844	164.5	159.4	160	4.5	2.8
4	284.2	0.410	166.4	162.6	0.399	248.2	247.4	247	1.2	0.5
Flight 8-1	276.2	0.420	16.4	7.0	0.977	129.6	119.1	120	9.6	8.0
2	276.2	0.420	52.4	48.1	0.816	167.6	164.7	159	8.6	5.4
3	278.0	0.421	85.4	2.9	0.990	168.3	159.2	156	12.3	7.9

*Calculated as follows: $\text{Deviation (\%)} = \frac{T_{B(calc.)}-T_{B(obs.)}}{T_{B(obs.)}} \times 100$

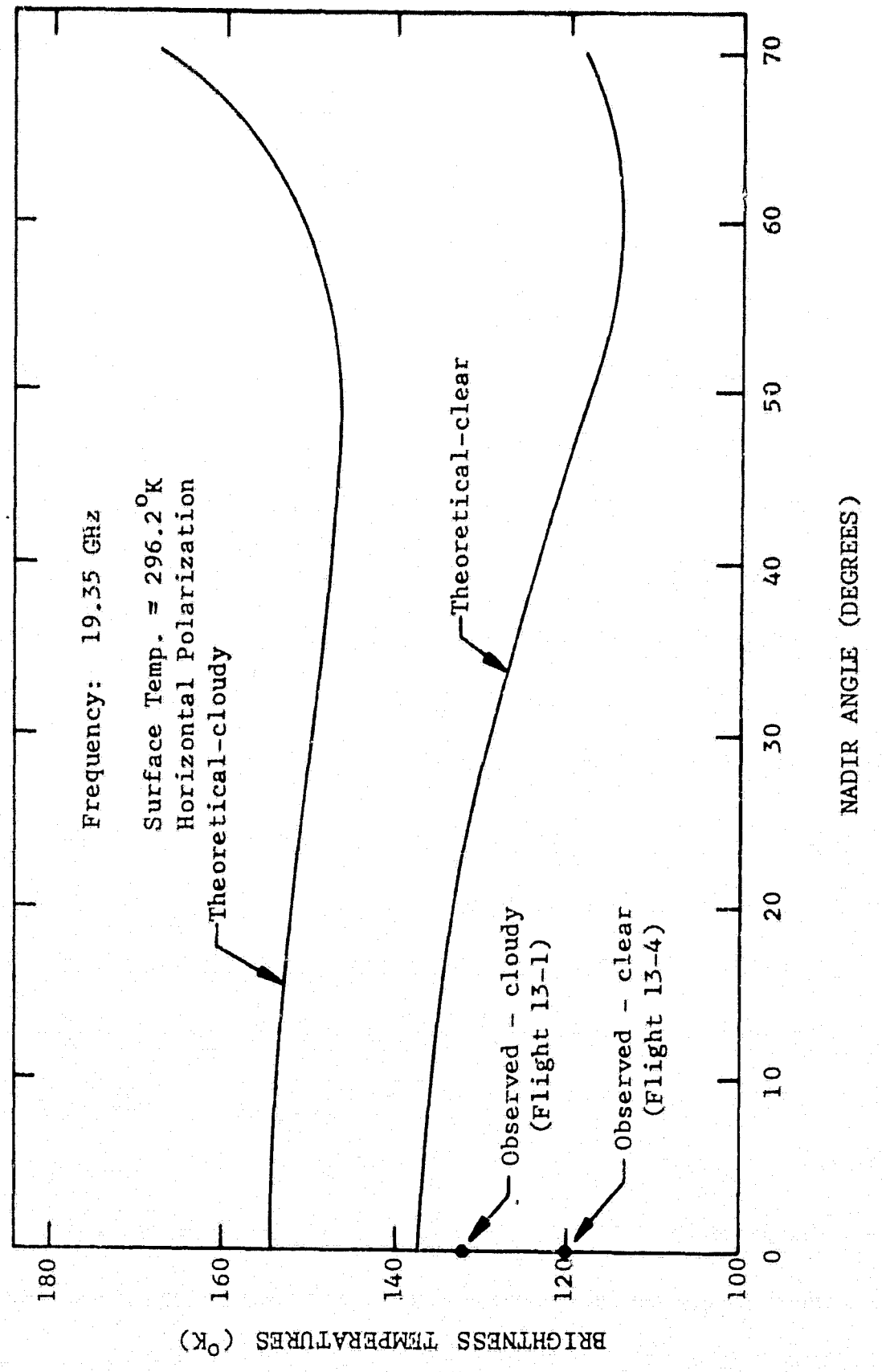

Figure 46 - Comparison of Theoretical and Observed Sea Water Brightness Temperatures at 19.35 GHz.

B. FLIGHT 9, 1968

Four cases were studied from Flight 9 of 1968. The opacity weighting functions for the atmosphere, assumed to represent this flight, show only slight modifications from the Flight 13 weighting functions. Oxygen and cloud weighting functions are essentially similar to the Flight 13 curves. The anomalous behavior of the water vapor weighting function near the surface is slightly reduced.

Cases 1 and 2, from Flight 9, are included for two reasons: (1) Case 1 is used to establish the surface reflectivity used in Cases 3 and 4; and (2), Case 2 is supposedly derived from observational conditions similar to those of Case 1, but shows a considerably higher brightness temperature. To match the temperature observed ($\sim 145^{o}K$) in Case 2 it was necessary to postulate that the reflectivity was reduced from 0.615, as deduced in Case 1, to 0.522. The exact reasons for the difference in observed temperatures between Cases 1 and 2 are not understood.

The contributions from various sources of radiation, tabulated in Table VI-4, show that the change in reflectivity from Case 1 and Case 2 substantially increases the surface term and slightly reduce all others. The latter are reduced because the reflected energy from each is reduced.

Case 3 represents the effects of a moderately sized, moderately opaque cloud with cirrus above it. Figure 47 shows clearly that the cirrus cap, even though half as dense as the main cloud but much less thick, does not contribute significant amounts of energy - less than 3% to the total cloud contribution. Of significance is the effect of the cloud on energy contributed by water vapor from various levels. The significant increase in water vapor density inside the cloud causes most of the energy from water vapor to arise inside the cloud. Between the upper and lower sections of the cloud model and between the lower section and the surface, not much emitted water vapor energy reaches the aircraft. Substantial contributions from water vapor, the cloud and the surface make up the total brightness temperature.

Case 4 of Flight 9 is a massive cloud, probably on the order of the

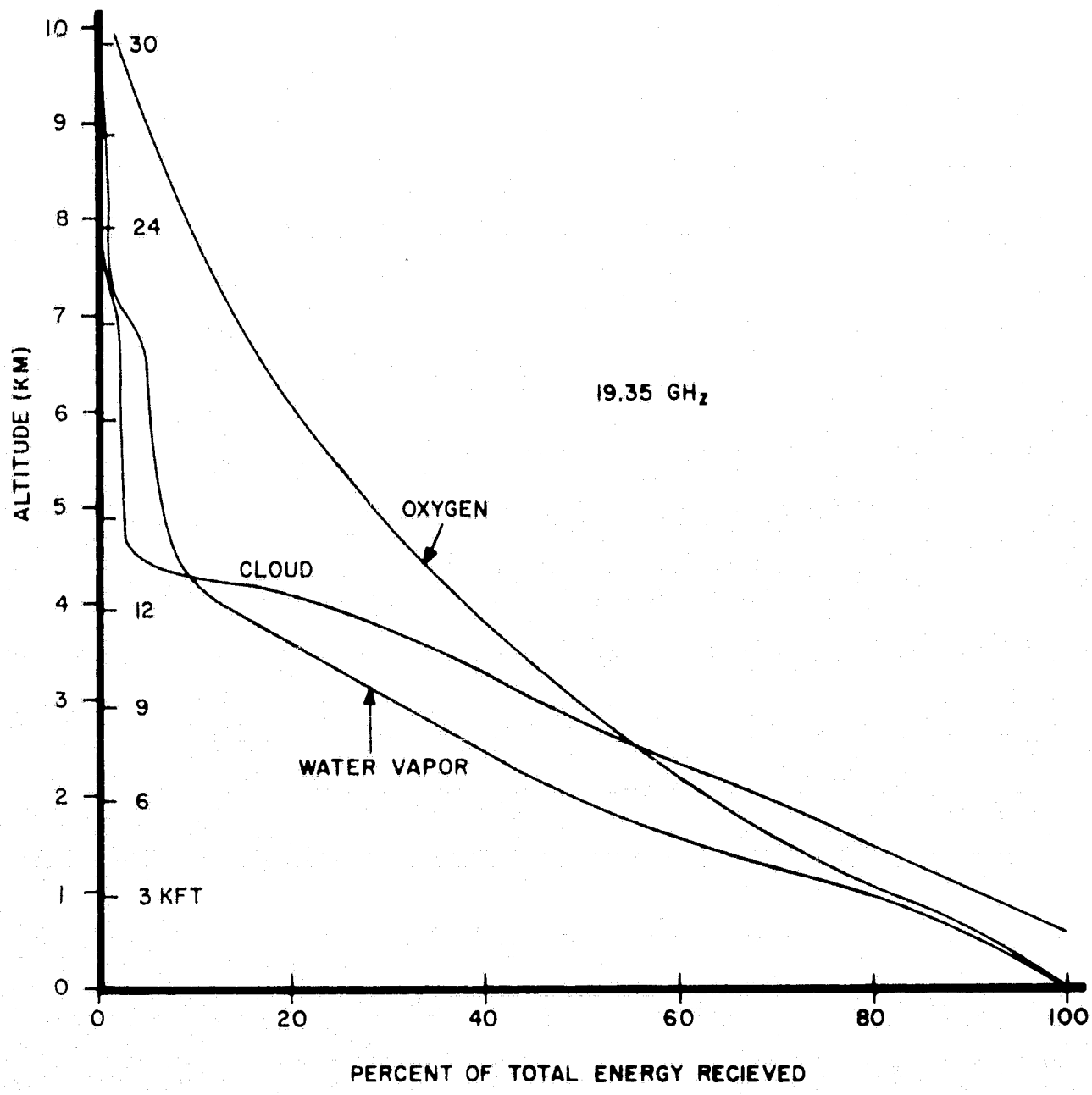

Figure 47 - Percent of Total Energy Received at The Aircraft as a Function of Altitude and Absorber. Flight 9, Case 3.

cloud studied in Case 3 of Flight 13. The observed temperature for this cloud is reached, however, by using a maximum condensed water density of only 2.30 g/m^3; this is considerably more reasonable than the 8.0 g/m^3 used in Case 3, Flight 13. The density is sustained through a greater depth, which is probably more realistic than the cloud model used for the Flight 13 cumulonimbus. Even so, application of RASP to this cloud indicates that scattering is probably very important. The scattering depth is only 0.5 km for 19.35 GHz. The percentage of total energy received from individual absorbers is shown in Figure 48.

Referring to Table VI-5, the differences between calculated and observed brightness temperatures are generally smaller in Flight 9 than in Flight 13. In Case 2, in particular, the observed T_B is 3.6°K higher than the calculated value. Although this is considered to be too small an increase, it is the only case in Table VI-5 showing this relationship with theoretical data.

C. FLIGHT 8, 1969

The most significant data of this flight was that obtained by flying over and under the same cloud. These two points are analyzed as Cases 2 and 3. Case 1 is the clear air case and is reported in Tables VI-1, VI-3 and VI-4.

Case 2 analyzed data taken as the aircraft flew over the cloud. Points to notice are: (1) the maximum condensed water density established is 0.60 g/m^3; (2) the reflectivity used is 0.600; (3) the cloud contribution is 54.0°K; (4) the observed brightness temperature, at 9.3 GHz, is recorded to be 122°K and computed to be 118.2°; and (5), the precipitable water derived from vapor is 2.13 g/cm^2.

The same data for Case 3 show that the matching process was unsuccessful: (1) the maximum condensed water density is 1.25 g/m^3; (2) the reflectivity used is 0.620; (3) the contribution of the clouds below the aircraft is zero; (4) the observed brightness temperature at 9.3 GHz is 119°K and computed to be 113°K; and (5), the precipitable water derived from vapor is 2.13 g/cm^2.

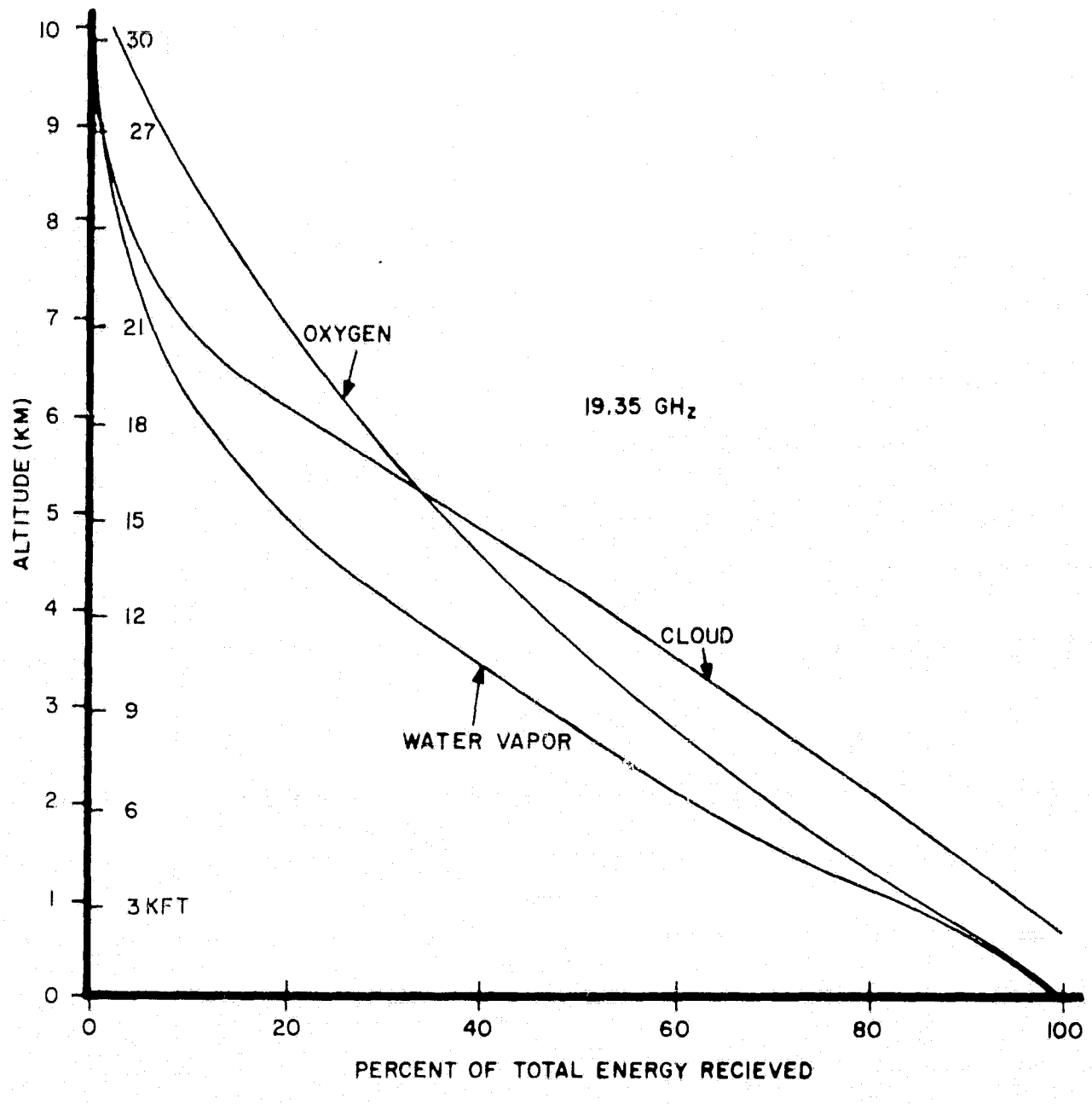

Figure 48 - Percent of Total Energy Received at the Aircraft as a Function of Altitude and Absorber. Flight 9, Case 4.

The match failed with the cloud density and the surface reflectivity. Later information illuminated the primary reason for the failure. The analysis, as it is presented, assumes no condensed water below the aircraft when it was supposedly flying below the clouds. This may be seen from the cloud model in Figure 25 and from Figure 49 which gives the percentage total energy received as a function of height from water vapor, oxygen and clouds from Case 2, Flight 8. It was later learned that rain was falling from the cloud, which means that the cloud model was unrepresentative.

Referring to Table VI-5, the calculated T_B's are higher than the observed values by about the same amount as in Flight 13. Thus, it appears that the atmospheric models established for Flight 8 were also too heavy.

D. ANALYSIS OF CONTRIBUTION OF CLEAR ATMOSPHERE AND CLOUD TO BRIGHTNESS TEMPERATURES

An attempt has been made to determine the contributions of both clear atmosphere and cloud to ocean brightness temperatures, by selecting appropriate segments of Flights 8 and 9. Ideally, this type of analysis should be performed on data taken in the same Flight, over constant surface conditions. Since these requirements could not be satisfied with the available data, portions of Flights 8 and 9 were employed, i.e., Flight 8, Case 1 represented a low altitude clear air situation; Flight 9, Case 2 represented a high altitude clear air case; and Flight 9, Case 4 involved a high altitude heavy cloud situation.

For each case, the surface temperature was noted and sea water emissivity calculated for vertical incidence, in accordance with expressions appearing in Section V-C. Following this, theoretical brightness temperatures were determined using atmospheric data given in Table VI-3. The resultant T_B's are shown in Table VI-6. The observed T_B's, listed in the Table, were obtained over the times listed below:

Flight 8, Case 1: Average from 1248:05 to 1251:04
Flight 9, Case 2: Average from 2349:00 to 2352:50
Flight 9, Case 4: 2311:40.

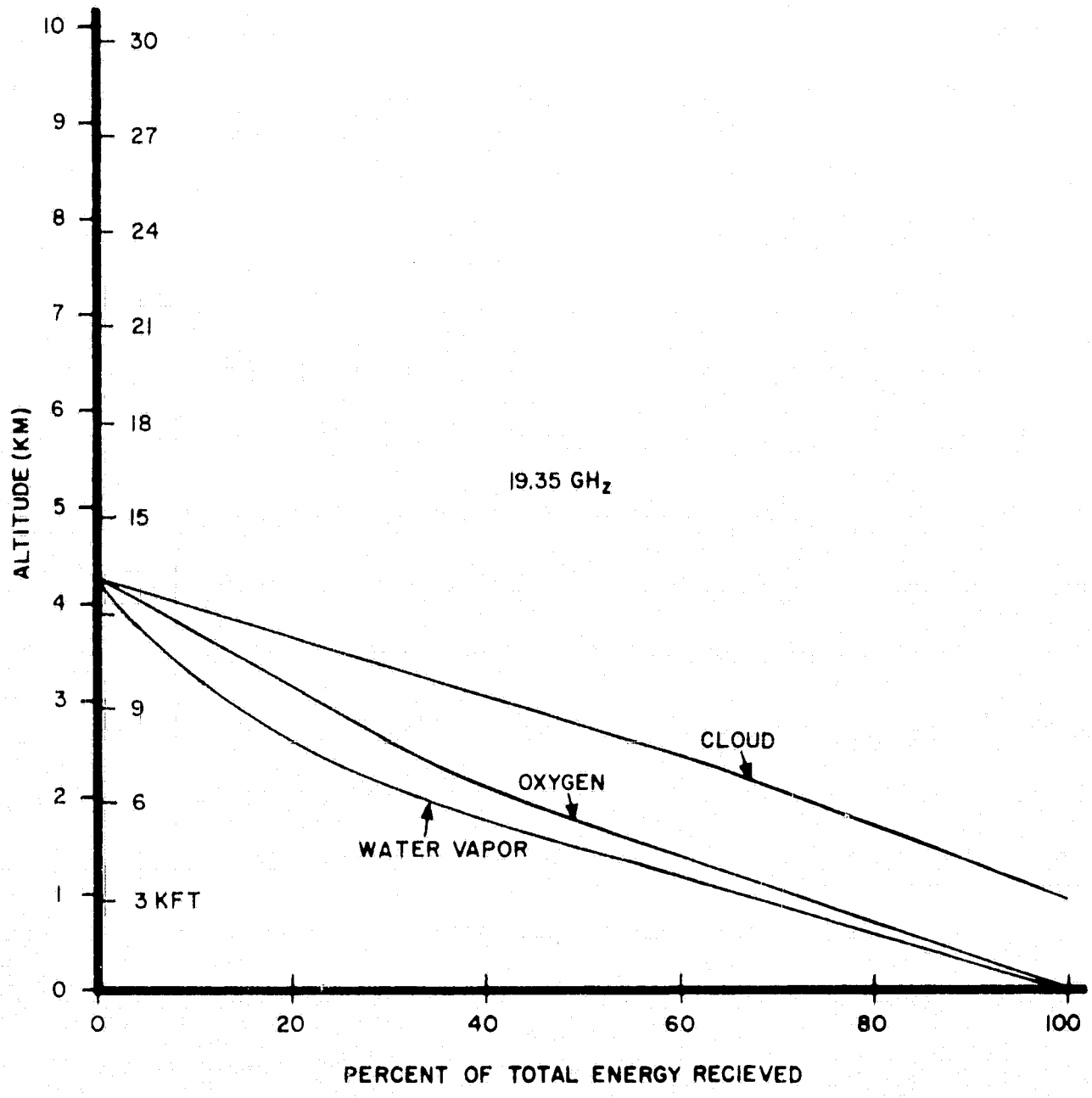

Figure 49 - Percent of Total Energy Received at the Aircraft as a Function of Altitude and Absorber. Flight 8, Case 2.

TABLE VI-6

CONTRIBUTION OF CLEAR ATMOSPHERE AND CLOUD TO OCEAN BRIGHTNESS TEMPERATURES

19.35 GHz Hor. Pol. Vert. Incidence

Flight and Case No.	Altitude (kft.)	Surface Temperature (^oK)	Observed T_B (^oK)	Calculated			Theor. T_B (^oK)	Difference: Theor.—Obs. (^oK)	Contribution By Clear Atmos. (^oK)	Contribution By Cloud (^oK)
				$T_{s,down}$ (^oK)	$T_{s,up}$ (^oK)	t_f				
Flight 8 Case 1	5.6	276.2	121.2	16.4	7.0	0.977	129.6	8.4	12.0	
Flight 9 Case 2	39.3	286.2	144.0	14.6	11.7	0.958	140.4	-3.6		107.8
Flight 9 Case 4	39.0	286.2	247.0	166.4	162.6	0.399	248.2	1.2		

Assuming similar sea conditions, the difference of 12.0°K in calculated brightness temperatures, for Flights 9-2 and 8-1, is due to 32,000 feet of clear atmosphere. The observed T_B difference is somewhat greater, being 22.8°K; however, this represents the difference between two averages and does not provide the desired near-instantaneous information. Of course, even without averaging the observed T_B's, it is impossible to obtain near-instantaneous differences in many cases due to wide fluctuations in the observed data. In Flight 9, Case 2, for example, the observed T_B's varied approximately 12°K; in Flight 8, Case 1, they varied approximately 9°K.

The cloud contribution, represented by the difference in calculated T_B's for Flights 9-4 and 9-2, is 107.8°K. This is quite close to the difference between observed T_B's, i.e., 103.0°K, and implies a satisfactory atmospheric model, if calm sea conditions prevailed in both cases. This is somewhat surprising since the forced value of reflectivity is 0.025 higher than the theoretical value - 0.615 versus 0.590, respectively. When the forced value of reflectivity is on the high side, it means that the chosen values of $T_{s,down}$, t_f and $T_{s,up}$ were all higher than they ought to be. This follows from the expression below, which is an inversion of Equation (54).

$$\rho = \frac{T - \dfrac{T_B - T_{s,up}}{t_f}}{T - T_{s,down}} \qquad (59)$$

E. FLIGHT 2, 1968

There are six Cases in this Flight, as shown in Table II-1. Cases 1 and 2 involve bare dry sandy soil, overflown in the latter part of the Flight (see Del Sur quadrangle in Figures 6 and 9) treating clear air and stratocumulus, respectively. Cases 3 and 4 represent moist soil which may have been present in the same area. Finally, Case 5 is a theoretical one, involving vegetation under clear skies, in the Cabazon quadrangle (Figures 6 and 8); stratocumulus conditions, over vegetation, are covered in Case 6.

Table VI-1 provides a summary of data simulation results, including values of theoretical reflectivities and brightness temperatures, at vertical

incidence. In the case of both dry sandy soil and vegetation there is practically no difference in T_B's between the stratocumulus and clear conditions, at vertical incidence. This is due to the high emissivities of these materials, which dominate the contributions to the total brightness temperature.

Figure 50 shows a comparison of theoretical and observed T_B's for dry sandy soil, as a function of antenna beam nadir angle. An interesting effect is exhibited by the observed data, in that the cloudy values are almost all lower than the clear values. This results from the fact that the surface material exhibits a high emissivity and temperature and, hence, the surface brightness temperature is markedly higher than the temperature of the cloud. The cloud, therefore, depresses the total brightness temperature below that for clear conditions. This effect is similar to the effect observed over clouds with infrared radiometers. The theoretical curves show an opposite relationship although the difference between cloudy and clear conditions is rather small, ranging from $1.5^{o}K$ to $6^{o}K$ over the angular range 0^{o} - 50^{o}. The reason for the discrepancy between the theoretical and observed sets of data is not clear, except that the expressions used in the theoretical portion may not represent the physical situation with sufficient accuracy.

Table VI-1 also shows theoretical data on the effect of clouds over moist soil (Cases 3 and 4). At vertical incidence, there is an increase of $10^{o}K$ due to the stratocumulus cloud, compared with the brightness temperature for clear conditions. If the surface temperature were reduced to $285^{o}K$, the effect of the cloud would be approximately $1^{o}K$ higher.

Figure 51 shows a comparison of theoretical and observed T_B's for vegetation-covered soil as a function of antenna beam nadir angle. It will be noted that, with the exception of a dip at an angle of 0^{o}, the observed cloudy curve lies above the theoretical cloudy curve over most of the angular range. Also, both the observed and theoretical curves show relatively constant T_B's with nadir angle; the bumps in the theoretical curves, at an angle of 20^{o}, should be ignored since they merely reflect the wavey nature of the emissivity curve in this region (see Figure 41). Finally, the observed cloudy data has an average value of approximately $277^{o}K$; the average value for cloud

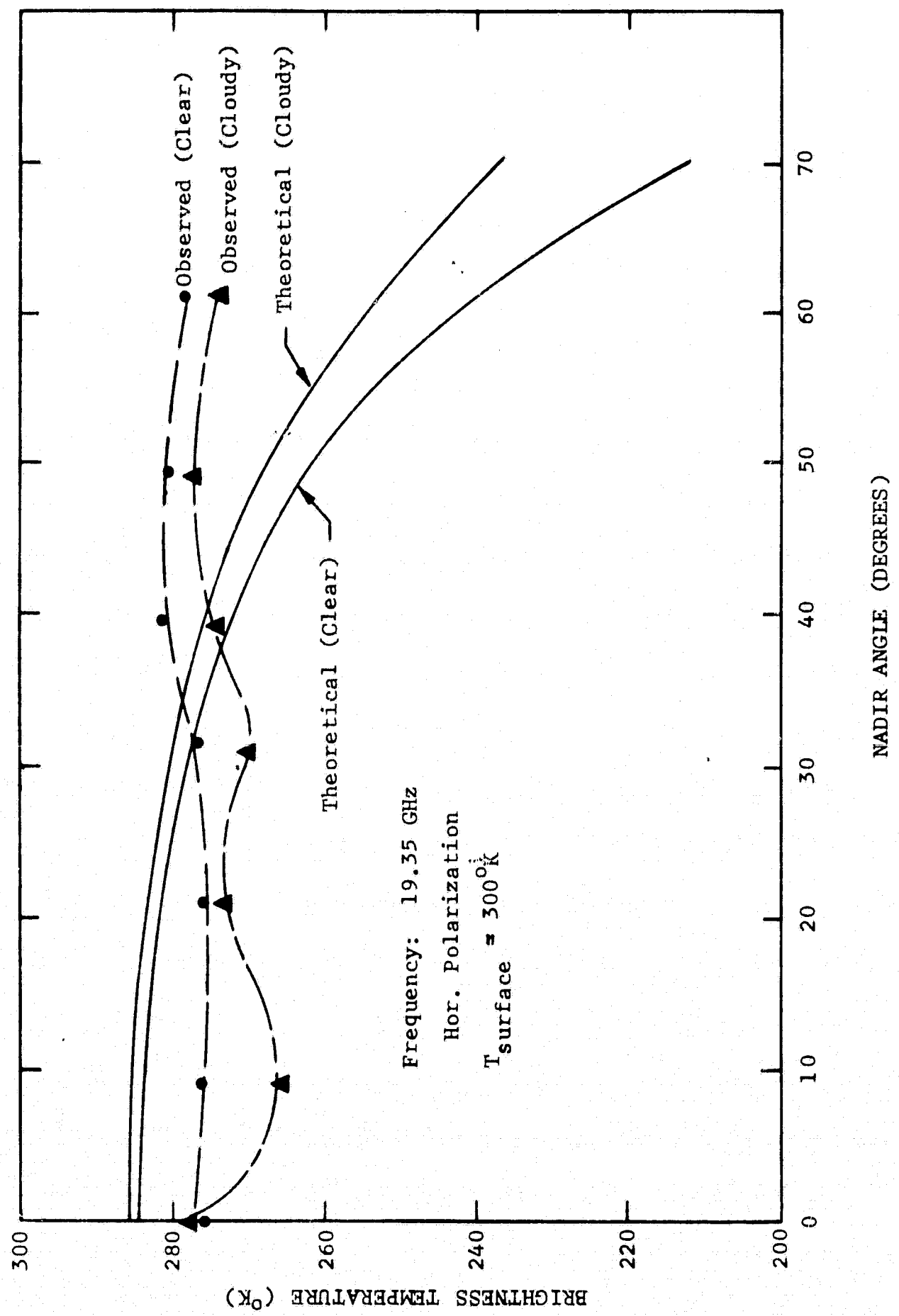

Figure 50 - Comparison of Theoretical and Observed Brightness Temperatures - Bare Dry Sandy Soil

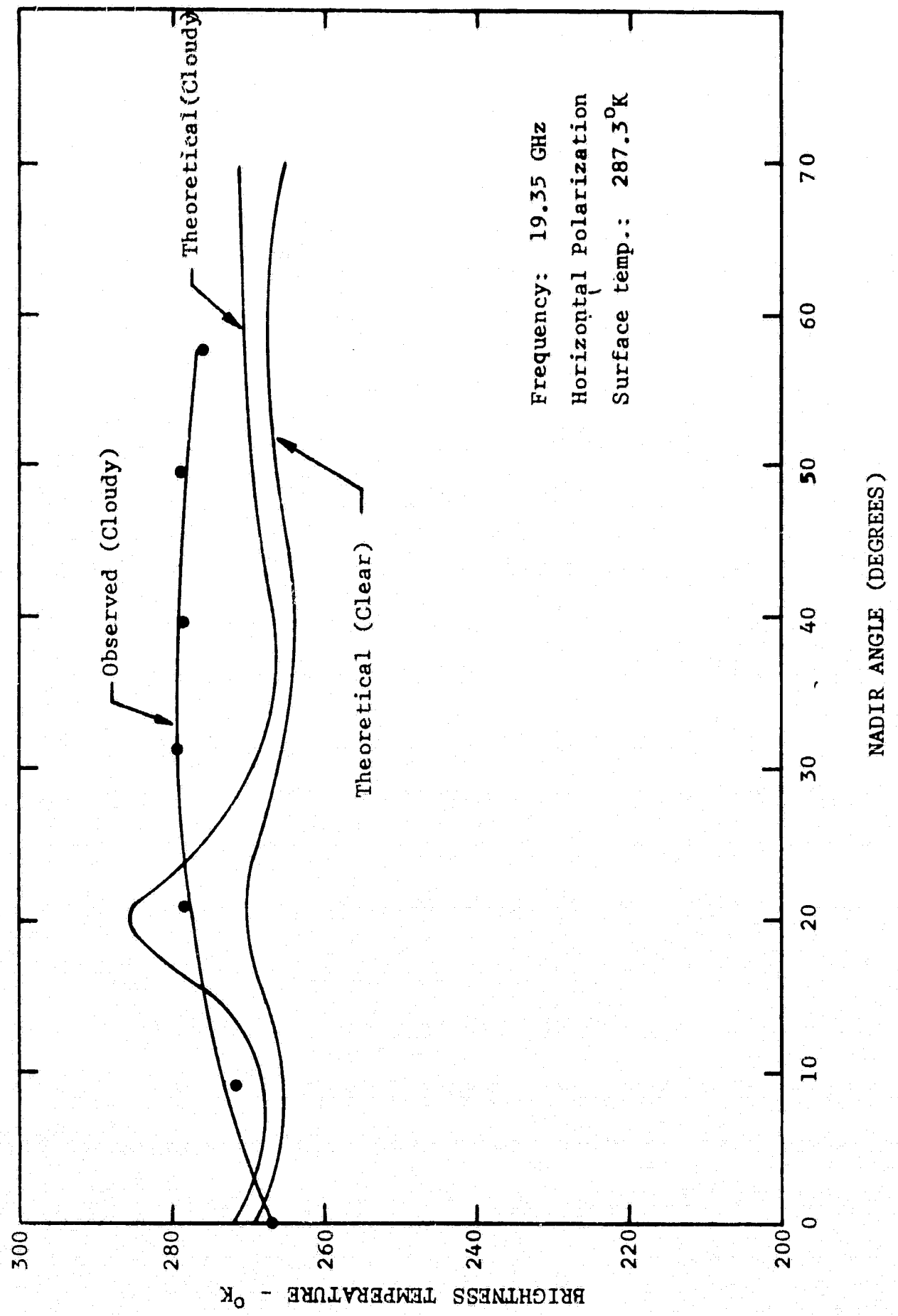

Figure 51 - Comparison of Theoretical and Observed Brightness Temperatures - Vegetation - Covered Soil

over dry soil is approximately 273°K, for the full angular range. This relationship is difficult to reconcile, particularly since the MRIR surface temperature of the dry soil, under clear conditions, was considerably higher than the measured temperature of the weed-covered soil - 306.7°K versus 287.3°K, respectively. In addition, it is likely that the emissivities of weed-covered soil are slightly lower than those for dry soil, over the angular range 0° - 30° (see Figures 41 and 37, respectively). These interpretive difficulties emphasize the need for ground truth information for this type of analysis.

VII. CONDENSED WATER INVERSION SCHEME

The analysis of cloud water content has been given in Section VI using the computed solutions of the equation of radiative transfer with detailed atmosphere and cloud models based upon a priori knowledge and support information provided with the experimental data. These solutions have involved the use of a computer program which takes into account the contribution of the three major constituents of the atmosphere: water vapor, oxygen, and clouds, at all levels. It is of interest to ask whether there exist simple algorithms which enable one to use the observed data directly to obtain an estimate of the condensed water content.

Figure 52 shows a flow chart which symbolizes the approach taken in validating the simple inversion scheme presented in this report. GABTAWF and detailed atmospheric information represents the left hand column in the Figure. The simple one-layer inversion scheme presented below represents the right-hand column.

A. SINGLE LAYER SINGLE FREQUENCY INVERSION SCHEME

To simplify the inversion procedure, a single layer atmosphere has been investigated. The question of how accurately one can specify the brightness temperature at the aircraft, when using such an approximation, has been explored. The simple one-layer model was postulated to have: (1) a uniform isothermal layer containing water vapor and oxygen only; or (2), a uniform isothermal cloud layer containing water vapor, oxygen, and cloud droplets. It is assumed that scattering may be neglected and that the cloud absorption coefficient is given by the Rayleigh approximation formula (Section IV).

The clear air case for the model configuration consists of an isothermal layer at temperature T_1 with optical depth τ_1. The sky temperature is T_{sky}, and the surface, at temperature T_G, has a reflectivity, R. As observed from above the atmosphere, the brightness temperature is given by

$$T_{B1} = T_G (1 - R) e^{-\tau_1} + T_1 (1 - e^{-\tau_1}) + Re^{-\tau_1} \left[T_1 (1 - e^{-\tau_1}) + T_{sky} e^{-\tau_1} \right] \qquad (60)$$

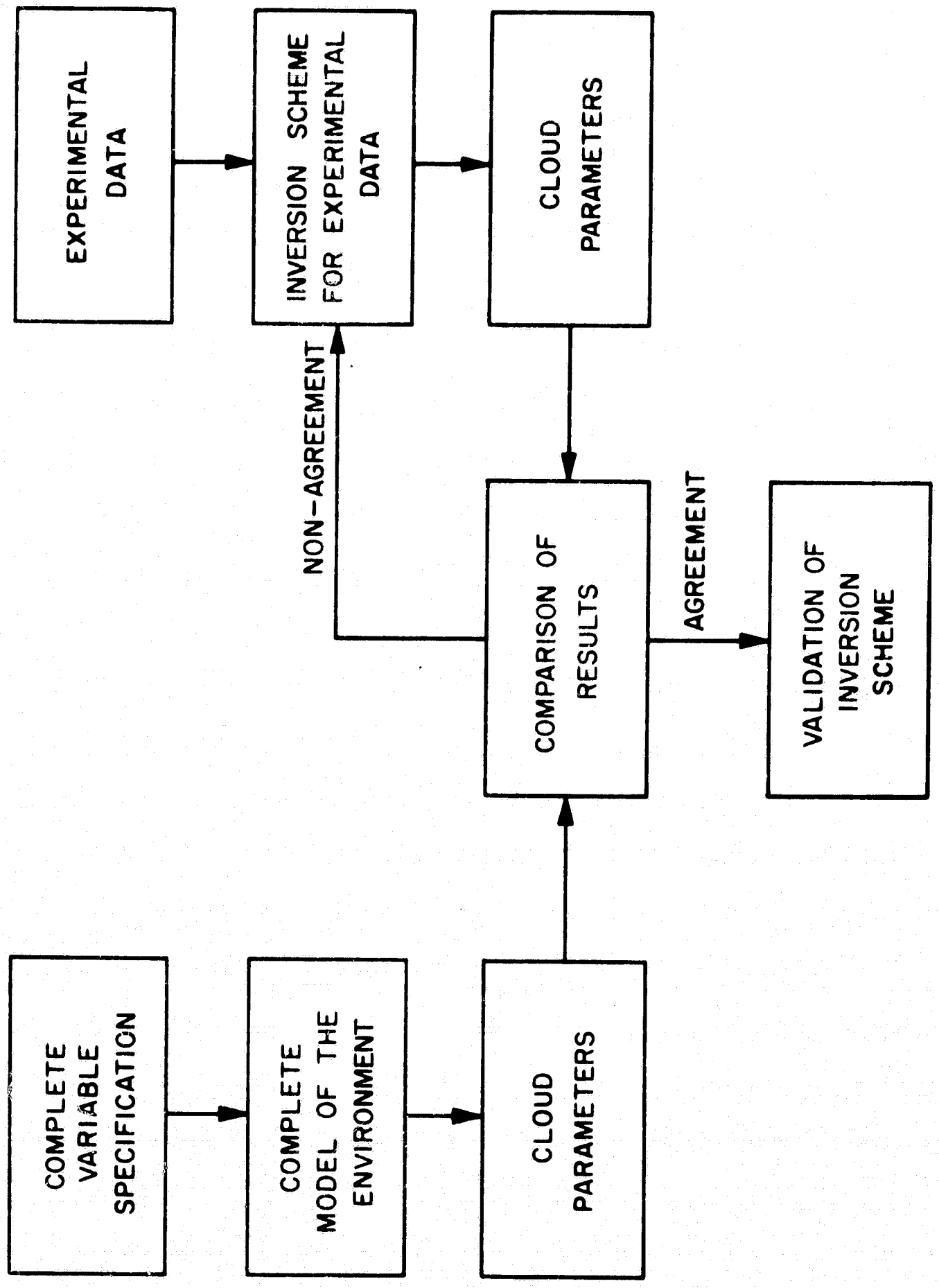

Figure 52 - Validation of Inversion Schemes

The variables, together with their values and sources, are given in Table VII-1 as they were extracted from Flight 9, Case 1 at 19.35 GHz.

TABLE VII-1

VARIABLES USED IN TWO-LAYER MODEL FOR CLEAR ATMOSPHERE FLIGHT 9, CASE 1.

VARIABLE	SYMBOL	VALUE	SOURCE
Sky Temperature	T_{sky}	3.0°K	a priori
Ground Temperature	T_G	284.2°K	MRIR data
Reflectivity	R	0.615	Matching procedure
Air Temperature	T_1	280°K	Support data
Total optical depth	τ_1	0.041	GABTAWF

When the values from Table VII-1 are substituted into Equation (60) T_B is computed to be 124.6°K. This compares with 124.9°K determined from GABTAWF. The choice of T_G and R are critical to the accuracy, but not particularly T_1.

The solution for the "cloudy" case is obtained in an identical fashion, with the optical depth, τ_2, for the cloudy case being, in this instance, that due to liquid water plus vapor. A value of 0.170 neper has been used for τ_2, based on an assumed cloud density of 0.35 gm/m^3, as obtained in the data simulation process for Flight 9, Case 3. The value of T_B obtained is 158.7°K, which is to be compared with 159.4°K obtained by the computer program.

From these results it can be seen that the one-layer model provides a reasonable estimate of the observed brightness temperature, even at 19.35 GHz, where the contribution due to water vapor absorption represents a significant unknown which must be determined from a priori knowledge of the climatological conditions. At 9.35 GHz, however, the water vapor contribution is negligible, and the residual atmospheric term, due to oxygen

absorption, sufficiently small so that the method could be used with substantially greater accuracy for estimation of cloud water content, provided of course that clouds of sufficient density are present.

Having established the applicability of the one-layer model, consider now the problem of inverting the measured data. The data consist of brightness temperature for the clear and cloudy cases, together with the support data, which enable the determination of a mean air temperature, $\overline{T}_{air}$, and an effective cloud temperature, $\overline{T}_{CL}$. We assume that R, T_G and T_{sky} are known, but not the optical depths. The following steps constitute the algorithm by which an estimate of the water content may be made:

(1) For the clear air case, use the measured brightness temperature, T_B, the estimated mean air temperature, $\overline{T}_{air}$, and the ground term, T_G (1-R), to obtain a first guess for the total opacity of the atmosphere, τ_1. Do this by substituting the values into the following equation for an isothermal single-layered atmosphere:

$$T_B = (1 - R)\, T_G\, e^{-\tau_1} + \overline{T}_{air}\, [1 - e^{-\tau_1}] \tag{61}$$

which may be solved for τ_1 in the form,

$$\tau_1 = \ln \left[\frac{\overline{T}_{air} - T_s}{\overline{T}_{air} - T_B} \right] \tag{62}$$

where,

$$T_s = (1 - R)\, T_G \tag{63}$$

The value of τ_1 from Equation (62) does not include the reflected downward component.

(2) Solve for the reflected component from the following equation:

$$T_r = R\, \overline{T}_{air}\, (1 - e^{-\tau_g}) + T_{sky}\, e^{-\tau_g} \tag{64}$$

compute τ_g from

$$\tau_g = 1/2 \left(\tau_1^i + \tau_1^{i-1} \right) \tag{65}$$

in which τ_1^i and τ_1^{i-1} are the two previous computed values for τ_1.

(3) Using the value of T_r from Equation (64) solve for τ_1 again, but now include the reflected downward component.

$$\tau_1' = \ln \left[\frac{\overline{T}_{air} - T_s - T_r}{\overline{T}_{air} - T_B} \right] \tag{66}$$

Steps (1) through (3) are repeated until an acceptably stable value of τ_1 is determined. Two iterations are usually enough to bring τ_1 well within 10% of its final value.

(4) To compute τ_2, the opacity when clouds are included, first repeat steps (1) through (3) using T_B measured for the cloudy condition and $\overline{T}_{CL}$ appropriate to the cloudy case. The value so obtained includes the absorption of several components related as follows:

$$\tau_2 = \tau_{CL} + \tau_{wv} + \tau_{O_2} \tag{67}$$

in which

$$\tau_{wv} = \left(\tau_{H_2O}\right)_{CL} + \left(\tau_{H_2O}\right)_{air} \tag{68}$$

$\left(\tau_{H_2O}\right)_{CL}$ = absorption due to excess water vapor found in clouds over the clear air mount.

$\left(\tau_{H_2O}\right)_{air}$ = absorption by water vapor in the clear air case.

(5) Estimate τ_{wv} by making the approximation that $\tau_{O_2} = 0.010$ nepers and that

$$\tau_{wv} \cong (\tau_1 - \tau_{O_2}) \left[1 + D \left(100/H - 1\right)\right] \tag{69}$$

D is a number less than one; it is an estimate of the fraction of water vapor in the atmosphere which is affected by saturated conditions in clouds. D can be well approximated for most regions by using Figure 53, to estimate its value. H is an estimate of the mean relative humidity in the clear atmosphere. This could be accurately estimated from τ_1 and the saturated water vapor associated with the temperature profile.

(6) Estimate τ_{CL} by solving the equation,

$$\tau_{CL} = \tau_2 - \tau_{wv} - \tau_{O_2} \tag{70}$$

(7) Using the Rayleigh approximation formula, solve for the integrated water density as follows:

$$L = (\tau_{CL} \cdot \lambda^2)/10^{[0.0122(291-\bar{T}_{CL})]} \tag{71}$$

L = integrated liquid water in the beam of the antenna, in g/cm^{-2}

τ_{CL} = absorption of the clouds, in nepers

λ = wavelength, in centimeters

$\bar{T}_{CL}$ = mean temperature of the cloud, in degrees Kelvin.

(8) If the vertical extent of the cloud can be inferred from adjunctive data, then the average water density is given by

$$M = \frac{L \cdot 10^4}{A} \text{ gm}^{-3} \tag{72}$$

where,

M = average condensed water density, in g/m^3

A = estimated vertical extent of the clouds, in meters.

An example of using the above procedure can be given by using Cases 1 and 3 of Flight 9 and the information from Figure 53. Pertinent information

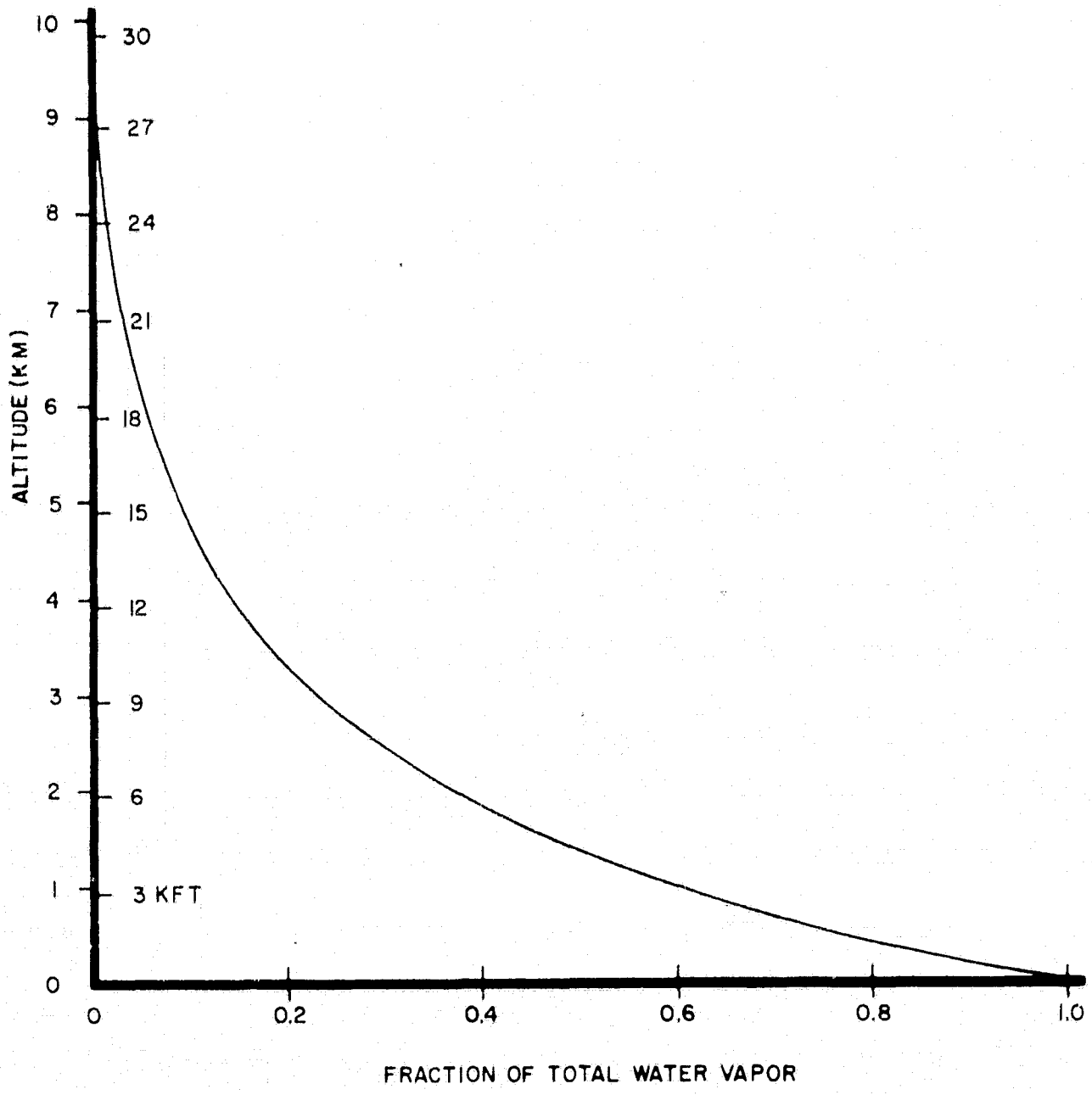

Figure 53 - General Curve From Which D May Be Computed

to derive cloud information for each case is listed in Table VII-2.

TABLE VII-2

VALUES OF PARAMETERS NEEDED TO INFER CLOUD WATER CONTENT

ITEM	FLIGHT 9 CASE 1	FLIGHT 9 CASE 3
1. T_{sky}	3.0°K	3.0°K
2. T_G	284.2°K	284.2°K
3. $\overline{T}_{air}$	280.0°K	----
4. $\overline{T}_{CL}$	----	278.0°K
5. R	0.615	0.615
6. Observed T_B	125.0°K	160.0°K

STEP 1: Clear air case; first estimate of τ_1:

$$\tau_1 = \ln \frac{(T_{air} - T_s)}{(T_{air} - T_B)}$$

$$= \ln \frac{(280 - 109.4)}{(280 - 125\ )}$$

$$= 0.0953 \text{ nepers.}$$

STEP 2: Solve for the reflected term T_r using a guess for τ_1 based on the following formula:

$$\tau_g = 1/2\ (\tau_1^i + \tau_1^{i-1})$$

For the first iteration $\tau_1^{i-1} = 0$. Therefore $\tau_g = 0.0477$ and

$$T_r = R\ [T_G\ (1 - e^{-\tau_g}) + T_{sky}\ e^{-\tau_g}]$$

STEP 3: Use T_r to solve for a new τ_1. Iterate until a stable value of τ_1 is achieved.

$\tau_1' = 0.0276 \rightarrow \tau_g = 1/2\ (0.0276 + 0.0477) = 0.0377$

$T_r' = 9.27^\circ K$

$\tau_1'' = 0.0402 \rightarrow \tau_g = 1/2\ (0.0402 + 0.0377) = 0.0389$

$T_r'' = 9.67^\circ K$

$\tau_1''' = 0.0373$

Final: $\tau_1 = 1/2\ (0.0373 + 0.0389)$

$= 0.038$ nepers.

STEP 4: Compute τ_2 for the cloudy situation, repeating Steps 1-3 but using $\overline{T}_{CL}$ and T_B observed for the cloudy case. The values computed are

$\tau_2 = 0.170$ nepers

$T_r = 29.4^\circ K$

STEP 5: Estimate τ_{wv} using $\tau_{O_2} = 0.010$ nepers

$$\tau_{wv} = (\tau_1 - \tau_{O_2}) \left[1 + D \left(\frac{100}{H} - 1\right)\right]$$

$$= (0.038 - 0.010) \left[1 + 0.75 \left(\frac{100}{10} - 1\right)\right]$$

$$= 0.060$$

$$\tau_{wv} + \tau_{O_2} = 0.070$$

STEP 6: Estimate τ_{CL}.

$$\tau_{CL} = \tau_2 - \tau_{wv} + \tau_{O_2}$$

$$= 0.170 - 0.060 - 0.010$$

$$= 0.100 \text{ nepers.}$$

STEP 7: Solve for integrated water density.

$$L = \frac{\tau_{Cl} \cdot \lambda^2}{10^{[0.0122(291-\overline{T}_{CL})]}}$$

$$= 0.167 \text{ g/cm}^2$$

STEP 8: Solve for average water density.

$$\overline{M} = \frac{L \cdot 10^4}{A} \text{ g/m}^3$$

$$= 0.38 \text{ g/m}^3$$

Table VII-3 below compares the above approximate results with those computed from GABTAWF.

TABLE VII-3

COMPARATIVE VALUES FROM GABTAWF AND THE ONE-LAYER MODEL

QUANTITY	GABTAWF VALUE	ONE-LAYER VALUE
τ_{CL}	0.085 nepers	0.100 nepers
$(\tau_{wv} + \tau_{O_2})_{cloud}$	0.085	0.070
τ_{total}	0.170	0.170
$(\tau_{wv} + \tau_{O_2})_{clear}$	0.041	0.038
L	0.141 g/cm^2	0.167 g/cm^2
$\overline{M}$	0.035 g/cm^3	0.038 g/m^3

It is apparent that the estimate of τ_{total} for the cloudy case was good. The problem of accuracy is in the determination of $\tau_{wv} + \tau_{O_2}$. This is a sensitive quantity and would most likely have been more accurately determined if better than slide rule accuracy had been employed. Still, in real cases, the values of T_G, R and $(T_B)_{clear}$ will, no doubt, have errors or be

non-available. Then, it is most probable that the best estimate for $(\tau_{wv} + \tau_{O2})_{clear}$ will be made by statistical procedures using climatological information. Further, it is quite obvious that $(\tau_{wv})_{cloud}$ is correlated with the brightness temperature observed in the cloudy case.

Many approaches to improve estimates of τ_{CL} and therefore L and $\bar{M}$ suggest themselves. Probably one of the best, as it will turn out, will be application of the optimum Linear Estimator technique as employed by Gaut (1967, 1968) and Waters and Staelin (1969).

VIII. CONCLUSIONS AND RECOMMENDATIONS

A. CONCLUSIONS

Several conclusions of importance can be drawn from the results of this work:

1. Liquid water, in the beam of a radiometer antenna, can be inferred from single frequency measurements at 19.35 GHz, with reasonable accuracy. Inherent errors, in the technique utilized in this study, can be reduced if independent data were available on the emissivities of rough sea surfaces. Such data could be used as a check on forced values of reflectivities, derived from observed brightness temperatures, and permit refinement of cloud contributions to total brightness temperatures.

2. The effect of liquid water, on brightness temperatures observed over dry bare soil and vegetation, is considered to be too small to permit inferring this constituent from recorded data. However, since the emissivities and, hence, brightness temperatures of moist soils are relatively low, it may be possible to infer liquid water over such materials, particularly in the case of heavier clouds. A dual-frequency technique, in which one of the frequencies is unaffected by cloud attenuation and radiation, may be required over moist land areas where lighter clouds are concerned.

3. Some cloud structure can be inferred from measurements of brightness temperature at 19.35 GHz and in the IR band covering 10-12 μ.

The inversion procedure, as outlined in the report, was crude yet a fairly satisfactory determination of the liquid water content was obtained. Three statements should be made about the inversion scheme:

1) It is not clear how representative it is, since it involved only one case.
2) The accuracy of the GABTAWF results are uncertain because no simultaneous measurements of cloud properties were made during the course of microwave observations.
3) The degree of improvement possible in the inversion scheme, with a more sophisticated procedure, is somewhat uncertain unless a controlled type of experiment is performed.

B. RECOMMENDATIONS

A number of avenues for further research and experimental work are evident from the study. These are discussed below:

1. An Experimental Program Which Brings Together In A Single Flight Microwave Measurements And Cloud Property Measurements.

If possible, the cloud cases chosen should be very uniform and constant in time so that the cloud measurements are stable and representative over the period of the microwave measurements. A most obvious set of desirable conditions would occur in a classical advancing warm front. The cirrus shield, followed by altostratus, followed by stratus and nimbostratus, would offer in one flight many sets of clouds of fairly uniform properties. It is imperative that water vapor and temperature measurements be taken. Preferably, the temperature and the water vapor measurements would be taken by using, both, *in situ* measurements by on-board sensors and by microwave techniques. Sea surface temperatures, roughness, and wind velocities should be recorded to permit proper treatment of surface emissivities and reflectivities. Such a program would offer the data necessary to check some of the basic techniques now employed to model and invert cloud data.

2. A Research Effort Designed To Establish The Complete Solutions To The Radiative Transfer Characteristics of Clouds.

At present, approximations and procedures, not wholly satisfactory, are being used to compute the radiative properties of clouds. Eventually, the complete modeling procedure should be carried as far as the state of the art allows.

3. An Investigation Of Liquid Water Over Moist Soils

An experiment should be performed, with suitable ground truth observations, to explore techniques of inferring cloud liquid water over moist soils. Measurements of soil moisture and laboratory determinations of dielectric permittivities would be required in such an investigation.

4. Inversion Procedures For Cloud Properties Should Be Explored.

Many sophisticated techniques exist which will, no doubt, greatly improve the accuracy of inferring cloud properties from microwave and adjunctive data. Optimum procedures, frequencies and adjunctive data should be identified.

5. The Use Of Other Microwave Data Available From NIMBUS Should Be Explored To Improve Observed Cloud Data.

This constitutes a portion of (4) above; it is imperative that the possible cross-benefits from experiments performed to determine water vapor and temperature by microwave techniques be coupled to the cloud property determinations.

By carrying out experiments and supporting theoretical studies, it is not inconceivable that procedures will be developed to give simultaneously excellent data on the temperature structure, water vapor distribution, and clouds in the atmosphere over the oceanic regions and, possibly, moist land areas of the earth.

REFERENCES

1. Barrett, A.H., and V.K. Chung (1962): A method for the determination of high-altitude water-vapor abundance from ground-based microwave observations. J. Geo. Res., 67, p. 4259.
2. Bauer, E. (1964): Applied Optics, Vol. 3, p. 197.
3. Chandrasekhar, S. (1950): Radiative Transfer, Dover, New York.
4. Crane, R.K. (1969): private communication.
5. Deirmendjian, D. (1964): Applied Optics, Vol. 3, p. 187.
6. Gaut, N.E. (1967): Studies of Atmospheric Water Vapor by Means of Passive Microwave Techniques. Ph.D. Thesis, M.I.T., Cambridge, Mass.
7. Gaut, N.E. (1968): Studies of Atmospheric Water Vapor by Means of Passive Microwave Techniques. Tech. Rep. 467, Res. Lab. of Elect., Mass. Inst. of Technology, Cambridge, Mass.
8. Samuelson. R.E. (1967): The Transfer of Thermal Radiation in Cloudy Planetary Atmospheres; Applications to Venus. Ph.D. Thesis, Georgetown University, Washington, D.C.
9. Staelin, D.H. (1966): Measurement and interpretation of the microwave spectrum of the terrestrial atmosphere near 1 cm wavelength. J. Geo. Res., 71, p. 2875.
10. Waters, J.W., and E.H. Staelin (1968): Statistical inversion of radiometric data, M.I.T. Res. Lab of Electronics, Cambridge, Mass., Quart. Prog. Rep. 89.
11. von Hippel, A.R., "Dielectric Materials and Applications", 1954 John Wiley (New York).
12. Porter, R.A., "An Analytical Study of Measured Radiometric Data", Jet Propulsion Laboratory Contract No. 952397, December 1969.
13. Paris, J.F., 'Microwave Radiometry and Its Application to Marine Meteorology and Oceanography", Texas A.& M University, January 1969.
14. Hasted, J.B., D.M. Ritson and C.H. Collie, "Dielectric Properties of Aqueous Ionic Solutions, Parts I and II", J. Chem. Physics, Vol. 16, No. 1, January 1948.
15. Edgerton, A.T., et al., "Passive Microwave Measurements of Snow, Soils, and Snow-Ice-Water Systems", Technical Report No. 4 SGD 829-6, February 1968.